UNIVERSIDAD POLITÉCNICA DE MADRID

ESCUELA TÉCNICA SUPERIOR DE INGENIEROS DE TELECOMUNICACIÓN



TESIS DOCTORAL

ESTIMATE OF THE TOTAL ICE VOLUME OF SVALBARD GLACIERS AND THEIR POTENTIAL CONTRIBUTION TO SEA-LEVEL RISE

ESTIMACIÓN DEL VOLUMEN DE HIELO DE SVALBARD Y SU CONTRIBUCIÓN POTENCIAL A LA SUBIDA DEL NIVEL DEL MAR

Alba Martín Español

Licenciada en Ciencias Ambientales

Madrid, 2013

UNIVERSIDAD POLITÉCNICA DE MADRID

ESCUELA TÉCNICA SUPERIOR DE INGENIEROS DE TELECOMUNICACIÓN

DEPARTAMENTO DE MATEMÁTICA APLICADA A LAS TECNOLOGÍAS DE LA INFORMACIÓN

TESIS DOCTORAL

ESTIMATE OF THE TOTAL ICE VOLUME OF SVALBARD GLACIERS AND THEIR POTENTIAL CONTRIBUTION TO SEA-LEVEL RISE

ESTIMACIÓN DEL VOLUMEN DE HIELO DE SVALBARD Y SU CONTRIBUCIÓN POTENCIAL A LA SUBIDA DEL NIVEL DEL MAR

Autor:

Alba Martín Español

Licenciada en Ciencias Ambientales

Directores:

Francisco José Navarro Valero

Doctor en Ciencias Físicas

Jaime Otero García

Doctor por la Universidad Complutense

Madrid, 2013



Tribunal nombrado por el Mgfco. y Excemo. Sr. Rector de la Universidad Politécnica de Madrid, el día _____ de _____ de 2013.

Presidente	D. _____
Vocal	D. _____
Vocal	D. _____
Vocal	D. _____
Vocal Secretario	D. _____

Realizado el acto de defensa y lectura de la Tesis el día _____ de _____ de 2013, en la E.T.S.I. _____.

Calificación:_____

EL PRESIDENTE LOS VOCALES

EL VOCAL SECRETARIO

Resumen

El objetivo final de las investigaciones recogidas en esta tesis doctoral es la estimación del volumen de hielo total de los ms de 1600 glaciares de Svalbard, en el Ártico, y, con ello, su contribución potencial a la subida del nivel medio del mar en un escenario de calentamiento global. Los cálculos más exactos del volumen de un glaciar se efectúan a partir de medidas del espesor de hielo obtenidas con georradar. Sin embargo, estas medidas no son viables para conjuntos grandes de glaciares, debido al coste, dificultades logísticas y tiempo requerido por ellas, especialmente en las regiones polares o de montaña. Frente a ello, la determinación de áreas de glaciares a partir de imágenes de satélite sí es viable a escalas global y regional, por lo que las relaciones de escala volumen-área constituyen el mecanismo más adecuado para las estimaciones de volúmenes globales y regionales, como las realizadas para Svalbard en esta tesis. Como parte del trabajo de tesis, hemos elaborado un inventario de los glaciares de Svalbard en los que se han efectuado radioecosondeos, y hemos realizado los cálculos del volumen de hielo de más de 80 cuencas glaciares de Svalbard a partir de datos de georradar. Estos volúmenes han sido utilizados para calibrar las relaciones volumen-área desarrolladas en la tesis. Los datos de georradar han sido obtenidos en diversas campañas llevadas a cabo por grupos de investigación internacionales, gran parte de ellas lideradas por el Grupo de Simulación Numérica en Ciencias e Ingeniería de la Universidad Politécnica de Madrid, del que forman parte la doctoranda y los directores de tesis. Además, se ha desarrollado una metodología para la estimación del error en el cálculo de volumen, que aporta una novedosa técnica de cálculo del error de interpolación para conjuntos de datos del tipo de los obtenidos con perfiles de georradar, que presentan distribuciones espaciales con unos patrones muy característicos pero con una densidad de datos muy irregular. Hemos obtenido en este trabajo de tesis relaciones de escala específicas para los glaciares de Svalbard, explorando la sensibilidad de los parámetros a diferentes morfologías glaciares, e incorporando nuevas variables. En particular, hemos efectuado experimentos orientados a verificar si las relaciones de escala obtenidas caracterizando los glaciares individuales por su tamaño, pendiente o forma

implican diferencias significativas en el volumen total estimado para los glaciares de Svalbard, y si esta partición implica algún patrón significativo en los parámetros de las relaciones de escala. Nuestros resultados indican que, para un valor constante del factor multiplicativo de la relacin de escala, el exponente que afecta al área en la relación volumen-área decrece según aumentan la pendiente y el factor de forma, mientras que las clasificaciones basadas en tamaño no muestran un patrón significativo. Esto significa que los glaciares con mayores pendientes y de tipo circo son menos sensibles a los cambios de área. Además, los volúmenes de la población total de los glaciares de Svalbard calculados con fraccionamiento en grupos por tamaño y pendiente son un 1-4% menores que los obtenidas usando la totalidad de glaciares sin fraccionamiento en grupos, mientras que los volúmenes calculados fraccionando por forma son un 3-5% mayores. También realizamos experimentos multivariable para obtener estimaciones óptimas del volumen total mediante una combinación de distintos predictores. Nuestros resultados muestran que un modelo potencial simple volumen-área explica el 98.6% de la varianza. Sólo el predictor longitud del glaciar proporciona significación estadística cuando se usa además del área del glaciar, aunque el coeficiente de determinación disminuye en comparación con el modelo más simple V-A. El predictor intervalo de altitud no proporciona información adicional cuando se usa además del área del glaciar. Nuestras estimaciones del volumen de la totalidad de glaciares de Svalbard usando las diferentes relaciones de escala obtenidas en esta tesis oscilan entre 6890 y 8106 km^3, con errores relativos del orden de 6.6-8.1%. El valor medio de nuestras estimaciones, que puede ser considerado como nuestra mejor estimación del volumen, es de 7.504 km^3. En términos de equivalente en nivel del mar (SLE), nuestras estimaciones corresponden a una subida potencial del nivel del mar de 17-20 mm SLE, promediando 19 ± 2 mm SLE, donde el error corresponde al error en volumen antes indicado. En comparación, las estimaciones usando las relaciones V-A de otros autores son de 13-26 mm SLE, promediando 20 ± 2 mm SLE, donde el error representa la desviación estándar de las distintas estimaciones.

Abstract

The final aim of the research involved in this doctoral thesis is the estimation of the total ice volume of the more than 1600 glaciers of Svalbard, in the Arctic region, and thus their potential contribution to sea-level rise under a global warming scenario. The most accurate calculations of glacier volumes are those based on ice-thicknesses measured by ground-penetrating radar (GPR). However, such measurements are not viable for very large sets of glaciers, due to their cost, logistic difficulties and time requirements, especially in polar or mountain regions. On the contrary, the calculation of glacier areas from satellite images is perfectly viable at global and regional scales, so the volume-area scaling relationships are the most useful tool to determine glacier volumes at global and regional scales, as done for Svalbard in this PhD thesis. As part of the PhD work, we have compiled an inventory of the radio-echo sounded glaciers in Svalbard, and we have performed the volume calculations for more than 80 glacier basins in Svalbard from GPR data. These volumes have been used to calibrate the volume-area relationships derived in this dissertation. Such GPR data have been obtained during fieldwork campaigns carried out by international teams, often lead by the Group of Numerical Simulation in Science and Engineering of the Technical University of Madrid, to which the PhD candidate and her supervisors belong. Furthermore, we have developed a methodology to estimate the error in the volume calculation, which includes a novel technique to calculate the interpolation error for data sets of the type produced by GPR profiling, which show very characteristic data distribution patterns but with very irregular data density. We have derived in this dissertation scaling relationships specific for Svalbard glaciers, exploring the sensitivity of the scaling parameters to different glacier morphologies and adding new variables. In particular, we did experiments aimed to verify whether scaling relationships obtained through characterization of individual glacier shape, slope and size imply significant differences in the estimated volume of the total population of Svalbard glaciers, and whether this partitioning implies any noticeable pattern in the scaling relationship parameters. Our results indicate that, for a fixed value of the factor in the scaling relationship,

the exponent of the area in the volume-area relationship decreases as slope and shape increase, whereas size-based classifications do not reveal any clear trend. This means that steep slopes and cirque-type glaciers are less sensitive to changes in glacier area. Moreover, the volumes of the total population of Svalbard glaciers calculated according to partitioning in subgroups by size and slope are smaller (by 1-4%) than that obtained considering all glaciers without partitioning into subgroups, whereas the volumes calculated according to partitioning in subgroups by shape are 3-5% larger. We also did multivariate experiments attempting to optimally predict the volume of Svalbard glaciers from a combination of different predictors. Our results show that a simple power-type V-A model explains 98.6% of the variance. Only the predictor glacier length provides statistical significance when used in addition to the predictor glacier area, though the coefficient of determination decreases as compared with the simpler V-A model. The predictor elevation range did not provide any additional information when used in addition to glacier area. Our estimates of the volume of the entire population of Svalbard glaciers using the different scaling relationships that we have derived along this thesis range within 6890-8106 km^3, with estimated relative errors in total volume of the order of 6.6-8.1% The average value of all of our estimates, which could be used as a best estimate for the volume, is 7,504 km^3. In terms of sea-level equivalent (SLE), our volume estimates correspond to a potential contribution to sea-level rise within 17-20 mm SLE, averaging 19 ± 2 mm SLE, where the quoted error corresponds to our estimated relative error in volume. For comparison, the estimates using the V-A scaling relations found in the literature range within 13-26 mm SLE, averaging 20 ± 2 mm SLE, where the quoted error represents the standard deviation of the different estimates.

Contents

Contents v

List of Figures ix

List of Tables xi

1 Introduction 1

1.1 Motivation . . . 1

1.2 State of the art at a glance . . . 5

1.3 Goals . . . 6

1.4 Thesis Organization . . . 7

2 Global and regional estimates of glacier volume 9

2.1 Outline . . . 9

2.2 Estimation techniques . . . 10

2.3 Scaling relationships . . . 10

2.3.1 Physical basis of scaling analysis for glacier volume estimates . . . 11

2.3.2 Some studies following the volume-area approach . . . 12

2.3.3 Some glacier volume projections using V-A scaling . . . 15

2.3.4 Summary of the available volume-area scaling laws . . . 16

2.4 Physically-based approaches . . . 18

2.4.1 An example of physically-based method . . . 18

2.4.2 Some studies following the physically-based approach . . . 21

2.5 Strengths and weaknesses . . . 22

2.6 Overview of the results . . . 22

3 Methodology to calculate glacier volumes from GPR measurements 25

3.1 Outline . . . 25

3.2 GPR: a radar for glaciological studies . . . 25
3.3 Data coherence and assimilation . . . 28
3.4 Radio-wave velocity . . . 29
3.5 Ice thickness estimation of non-surveyed tributary glaciers . . . 33
3.6 Constructing ice-thickness maps and estimating glacier volumes . . . 35
3.6.1 Spatial interpolation . . . 36
3.6.2 Ordinary kriging . . . 40
3.7 Error estimates . . . 44
3.7.1 Preliminars . . . 45
3.7.2 Ice-thickness error . . . 45
3.7.3 Error in volume . . . 51
3.7.4 Tests performed on synthetic glaciers . . . 56

4 Inventory of Svalbard radio-echo sounded glaciers and volume estimates 59
4.1 Outline . . . 59
4.2 History of echo soundings in Svalbard aimed to ice-thickness measurements . 60
4.3 Inventory of radio-echo sounded glaciers in Svalbard . . . 62
4.3.1 Available GPR data . . . 64
4.4 Ice-thickness maps and glacier volumes . . . 70
4.4.1 Comparison with other volume estimates in the literature . . . 81
4.4.2 Review of the thermal structure of the analysed glaciers . . . 82

5 Volume-area relationship for Svalbard glaciers and associated volume 89
5.1 Outline . . . 89
5.2 Establishing a basis data set for a volume-area relationship . . . 90
5.3 Estimating accuracy from cross-validation . . . 99
5.4 Selecting a fitting strategy: *logmse* versus *absdev* misfit functions . . . 100
5.5 Comparison between inventories . . . 101
5.6 Scaling-law parameters for different glacier settings . . . 101
5.7 Multivariate analysis . . . 104
5.8 The case of Austfonna and Vestfonna ice caps . . . 107
5.9 Comparison with other V-A relationships . . . 109
5.10 An error estimate of the total volume . . . 113
5.11 Potential contribution of Svalbard glaciers to SLR . . . 114

6 Conclusions and outlook **115**

6.1 Conclusions 116

6.2 Outlook 122

7 APPENDIX **125**

Bibliography **141**

List of Figures

3.1 VIRL 7 and RAMAC GPR systems 27
3.2 Thermal regime distribution of Hansbreen 30
3.3 Assumptions for volume estimates of unmeasured tributary glaciers 35
3.4 Influence of error containing data in the interpolation 38
3.5 Ice thickness deviation from the real measurements 38
3.6 Profiles display Nye Vialov ice cap 39
3.7 GPR profiles a synthetic parabolic model 39
3.8 Variogram function 42
3.9 Blanking circumferences and discrepancies against distances 49
3.10 Distance-Bias function (DBF) and Distance-Error function (DEF) 49
3.11 Distance-Bias function, example of its frequency distribution 50
3.12 Ice thickness error map 52
3.13 Volume error induced by boundary uncertainty 54

4.1 Radio-echo sounded glaciers in Svalbard 63
4.2 Radio-echo sounded glaciers in Svalbard: Islands 64
4.3 West Nordenkiöld Land glaciers: GPR profiles 75
4.4 West Nordenkiöld Land glaciers: ice thickness map 76
4.5 Central Nordenkiöld Land glaciers: ice thickness map and GPR profiles . . . 77
4.6 Dickson Land glaciers: ice thickness map and GPR profiles 78
4.7 Wedel Jarlsberg Land glaciers: GPR profiles 79
4.8 Wedel Jarlsberg Land glaciers: ice thickness map 80
4.9 Heerland glaciers: ice thickness map and GPR profiles 85
4.10 Brøggerhalvøya area: ice thickness map and GPR profiles 86
4.11 Reindalen area: ice thickness map and GPR profiles 87
4.12 Nordaustlandet glaciers: ice thickness map and GPR profiles 88

5.1 Accuracy of true volume estimation for different measurement uncertainties . 92
5.2 Area distribution histograms 98

List of Tables

2.1 Volume scaling relationships for different types of ice bodies 17
2.2 Global ice volume estimates 24
2.3 Estimates of Total Ice Volume stored in Svalbard Glaciers 24

3.1 Sensitivity of volume estimates to RWV 30
3.2 Compilation of common mid-point (CMP) measurements on Svalbard glaciers. 32
3.3 Comparison of errors using Gridfit and Kriging interpolation 40
3.4 Volume error computation on synthetic glaciers 57

4.1 Meta data compiled in the Inventory of radio-echo sounded glaciers in Svalbard. 65
4.2 GPR surveys, radar equipment and km of radar profiles 66
4.2 GPR surveys, radar equipment and km of radar profiles 67
4.2 GPR surveys, radar equipment and km of radar profiles 68
4.2 GPR surveys, radar equipment and km of radar profiles 69
4.2 GPR surveys, radar equipment and km of radar profiles 70
4.3 Glacier areas, volumes, mean and maximum ice thickness and accuracy (I) . . 73
4.3 Glacier areas, volumes, mean and maximum ice thickness and accuracy (II) . 74

5.1 Sensitivity Test 1 94
5.2 Sample of glaciers to obtain the scaling coefficients (I) 95
5.2 Sample of glaciers to obtain the scaling coefficients (II) 96
5.2 Sample of glaciers to obtain the scaling coefficients (III) 97
5.3 Cross-validation Test 99
5.4 Sensitivity Test 2 100
5.5 Comparing results using different glacier inventories 101
5.6 Sensitivity Test 3 103
5.7 ANOVA test: Model 1, Volume-Area. 105

5.8 ANOVA test: Model 2, Volume-Area-Length. 105
5.9 ANOVA test: Model 3, Volume-Area-Elevation Range. 105
5.10 ANOVA test: Model 4, Volume-Area-Length-Elevation Range. 106
5.11 Sensitivity Test 4 107
5.12 Ice caps vs. Glacier scaling laws 109
5.13 Svalbard volume estimate from the literature 112
5.14 Potential contribution to SLR 114

Chapter 1

Introduction

1.1 Motivation

Global sea level is currently rising at an increased rate and models indicate that it will continue to rise during this century (Bindoff et al., 2007). The two major contributors to global sea-level rise are the thermal expansion caused by the warming of the oceans and the loss of land-based ice, such as glaciers and polar ice caps and ice sheets, due to increased melting and accelerated ice discharge into the ocean. Thermal expansion is projected to contribute more than half of the average rise, but it is expected that land ice will lose mass increasingly rapidly as the century progresses. The contributions of glaciers and ice caps (GICs), on one hand, and the large ice sheets of Antarctica and Greenland, on the other, are usually evaluated separately because of their different response times, both in mass balance and dynamic aspects, to changes in climate. These response times are generally much faster in the case of GICs. The evaluation by the Fourth Assessment Report of the Intergovernmental Panel on Climate Change (IPCC 2007) of the contributions (referred to the period 1993-2003) to sea-level rise by thermal expansion of the oceans, GICs mass losses and ice-sheet mass losses assigned to each of them roughly 1/2, 1/3-1/4 and 1/7 of the contributions, respectively (Lemke et al., 2007). The IPCC 2007 projected only one third of the global sea-level rise during the twenty-first-century to be caused by the wastage of GICs. Later on, further studies suggested an increased contribution to sea-level rise by the ice-sheets of Antarctica and Greenland (Rignot et al., 2011). However, a recent publication, which has reconciled the results of ice-sheet mass-balance studies performed using different techniques (laser and radar altimetry, input-output method, and gravimetry), has led to a downward revision of the current contribution of the ice-sheets to sea-level rise (Shepherd and others,

2012), thereby suggesting and increased contribution by GICs. Surprisingly, a yet more recent estimate of the current (referred to the period 2003-2009) contribution to sea-level rise by GICs (Gardner et al., 2013) has also made a downward revision of the latter, pointing to a contribution to the observed changes in sea-level rise very similar (though slightly lower) to that of the ice-sheets (Hanna et al., 2013). No matter whether the ice sheets or the GICs are currently contributing more to sea-level rise, and for how long this will continue to be so, it is clear that there is a renewed interest in the role of the glaciers and ice caps as concerns to their response to climate changes and their current and projected contributions to sea-level rise, matters that have received much attention by the scientific community during recent years (Radić and Hock, 2011; Cogley, 2012; Radić et al., 2013).

One of the main goals of the Fifth Assessment Report of the IPCC is to get an updated estimation of how much the glaciers and ice caps will shrink during the 21st century. One of the the major uncertainties in volume projections is the model calibration and initialization step (Radić et al., 2013), for which an estimation of the initial glacier volume is needed. Moreover, for how long can the glaciers and ice caps sustain a given contribution to sea-level rise depends on their total volume, which provides their *potential* contribution to sea-level rise. These two facts motivate the interest of the subject addressed by this thesis.

The final aim of this dissertation is to derive volume-area (V-A) scaling relationships specific for Svalbard glaciers and estimating, from them, the total ice volume stored on Svalbard glaciers, and thus their potential contribution to sea-level rise. The ice masses of Svalbard cover an area of ca. 36,600 km^2, and are thus among the largest *glacierized* (i.e. currently glaciated) areas in the Arctic. The environment of the Atlantic sector of the Arctic, where Svalbard is located, is highly vulnerable to climate change (ACIA, 2005). Even if Svalbard is one of the best studied regions in the Arctic, crucial glacier data such as the ice-thickness distribution are only available for a few selected glaciers and thus the ice volume is only known for a small sample of glaciers. The information on ice-thickness distribution and glacier volumes is important for quantifying the impacts of glacier changes on global sea level, for implementing thermo-dynamical glacier models to predict their evolution and for managing water resources. Hence, it is of great interest to explore indirect methods to approximate glacier volumes from other known parameters such as glacier area, length or slope.

The volume of the entire population of Svalbard glaciers has recently been derived from global scaling relationships (i.e. Grinsted (2013), Radić et al. (2013)) and by physically-based methods as in Huss and Farinotti (2012). However, figures vary greatly among the different

estimations. There are older estimations derived from Svalbard-specific scaling relationships (Hagen et al., 1993; Macheret and Zhuravlev, 1982) that have lead to more consistent results. However, the latter relationships are mostly based in old echo-sounding flights which, in many cases, included only a single flight along the centre line of each glacier, and the volume was estimated assuming parabolic cross-sections was used, and then, a parabolic cross-sections was assumed, possibly leading to substantial errors in the volume computation. Nowadays, we rely on a greater number of radio-echo sounding studies, with improved positioning and recording systems, that extensively cover the majority of the glacier surface leading to refined volume estimates.

This dissertation has been developed within the Group of Numerical Simulation in Science and Engineering (GSNCI, in the Spanish acronym) of the Technical University of Madrid (UPM), to which the author and both supervisors of this thesis belong. GSNCI is focused, among other research subjects, on ground-penetrating radar (GPR) studies of glaciers, aimed to determine the glacier ice thickness and the physical properties of glacier ice, which have a profound influence on glacier dynamics and thermal regime. GSNCI participated in two International Polar Year 2007-2008 (IPY) projects focused on the Arctic cryosphere, including Svalbard: Glaciodyn (The Dynamic response of Arctic glaciers to global warming) and Kinnvika (Change and Variability of the Arctic Systems). These two projects set the basis for a later project, currently close to completion, within the European Science Foundation PolarCLIMATE programme: the SvalGlac project (Sensitivity of Svalbard glaciers to climate change; http://svalglac.eu/). This dissertation arises within the framework of this latter project, aiming to cover the first declared objective of SvalGlac: 'To obtain a reliable estimate of the total ice volume stored in Svalbard'. Within the frames of SvalGlac and its predecessor projects Glaciodyn and Kinnvika, GSNCI, since 1999, has undertaken, together with Russian, Polish and occasionally Norwegian colleagues, numerous radio-echo sounding campaigns on Svalbard glaciers and ice caps. They have focused on western Nordenskiöld Land (central Spitsbergen) and Wedel Jarlsberg Land (southern Spitsbergen), as well as Austfonna, the largest ice-cap in Svalbard, situated in the island of Nordaustlandet. These fieldwork campaigns have covered 21 glaciers and ice caps, and have included GPR profiling and common-midpoint measurements that have allowed to retrieve the ice-thickness distribution and calculate the associated glacier volume, the hydrothermal structure, the internal structure (layering, crevassing, englacial water conduits, etc.) and, in the locations of CMP measurements, physical properties such as the liquid water content of temperate

ice. Results for individual glaciers can be found e.g. in Navarro et al. (2005), Jania et al. (2005), Vasilenko et al. (2006), Glazovsky et al. (2006) or Lapazaran et al. (2013), whereas studies covering entire sub-regions of Svalbard can be found in Martín-Español et al. (2013), for western Nordenskiöld Land, and Navarro et al. (2013), for Wedel Jarlsberg Land.

Therefore it is timely to make the effort of bringing together all the available GPR data sets for Svalbard and calculating their associated glacier ice volumes and associated error estimates using a homogeneous methodology, in order to derive a new Svalbard-specific scaling relationship. This new scaling law will be used to refine the estimates of the total volume of Svalbard glaciers, and hence their potential contribution to sea-level rise.

A crucial preliminary task is the preparation of an updated Inventory of Radio-Echo Sounded Glaciers of Svalbard. This task has been undertaken as part of this thesis work, and developed under the umbrella of SvalGlac project. In fact, SvalGlac settled the frames to promote the data flow among the different research groups working in Svalbard.

A secondary aim of this work is to complement the recently released Digital Database of Svalbard Glaciers developed by the Norwegian Polar Institute (Köning et al., 2013) with the information of the available glacier volumes. Therefore we were encouraged to use their same glacier outlines with the aim of making a coherent work. It is important to note that the glacier inventory made by the Norwegian Polar Institute follows the original H93 Glacier Atlas of Svalbard and Jan Mayen (Hagen et al., 1993), whose definitions of individual glaciers, drainage basins and identification codes are slightly different from those used by the GLIMS project in the new version of the Randolph Glacier Inventory V3 (Arendt et al., 2012). These differences, however, are indeed very small, as we will show when calculating and comparing the total ice volume of Svalbard using both data bases.

Knowing the accuracy of our individual glacier volume computations is fundamental to estimate the error of the total volume of Svalbard glaciers calculated using V-A relationships, either in the form of an error estimate calculated using standard error propagation techniques, as in Radić and Hock (2010), or as an upper bound for it derived from statistical experiments on large sets of randomly generated synthetic glaciers, as done in Farinotti and Huss (2013). However, error estimates for the individual volumes of radio-echo sounded Svalbard glaciers are often not properly described, or even quantified, in the literature. For instance, none of the estimated glacier volumes from the Soviet flights in the seventies (Macheret and Zhuravlev, 1982), nor those from the Norwegian-British campaigns in the eighties (Dowdeswell et al., 1984a) were accompanied by an estimate of its accuracy. More recent studies such as those

by Bælum and Benn (2010), Pettersson et al. (2011), Grabiec et al. (2012) or Saintenoy et al. (2013), although reporting about some of the most significant error sources independently, do not detail how to combine these errors to derive an error in volume. We have made a great effort on understanding and computing the main components intervening in the error in glacier volume. We have developed in this thesis a methodology which first focuses on calculating the error of a digital ice-thickness model derived from GPR measurements, then analyses the error produced when deriving a glacier volume from such a digital ice-thickness model, delimited by a given boundary, and finally uses a novel methodology, based on the degree of statistical dependence among the errors at the grid points, to combine all the errors intervening in the calculation of the glacier volume. Additionally, we have created a new algorithm to estimate the spatial interpolation error, specifically designed to work with unevenly distributed data, such as those provided by GPR measurements.

1.2 State of the art at a glance

In the previous section we have sketched the scientific reasons that motivate the aims of the present dissertation, including a brief outline of the main efforts that have been undertaken on this research subject. Rather than including in this introductory chapter a complete account of the state-of-art on the subject, we have preferred to split it into the main chapters dealing with the different matters. In particular:

- The state-of-art referred to global and regional volume estimates is discussed in Chapter 2. Section 2.1 includes the general references, while those referred to volume-area scaling and physically-based methods are presented in sections 2.2. and 2.3 respectively. The main contributions including the actual global and regional -including Svalbard- glacier volume computations are presented in Chapter 5, in particular in Section 5.9.

- The main references concerning the calculation of volumes of individual glaciers, and its associated error estimates, are given in Chapter 3. Sections 3.2 to 3.5 deal with the GPR measurements from which the ice-thickness data, an associated errors, are derived. Section 3.6 includes the main references regarding the volume calculation, and Section 3.7 those referred to estimates of the error in volume.

- Finally, the state-of-art regarding the GPR measurements done on Svalbard glaciers is presented in Chapter 4. In particular, section 4.2 focuses on the history of radio-echo sounding studies in Svalbard.

1.3 Goals

As stated previously, the final objective of this thesis is to obtain a reliable estimate of the total ice volume stored in Svalbard glaciers. The fulfilment of this final objective requires the achievement of several intermediate goals, which are summarized below:

1. Building an updated inventory of the radio-echo sounded glaciers and ice caps of Svalbard, and collecting and bringing together the GPR data sets from the different research groups operating in Svalbard, to calculate the corresponding glacier ice volumes using a homogeneous methodology.

2. Developing techniques for accurately estimating all the errors involved in the volume calculation, using a novel methodology for computing the interpolation error, as well as for combining all of the errors intervening at the grid-node level using a statistical approach that considers the degree of correlation among the nodal data.

3. Undertaking the additional radio-echo sounding campaigns necessary to complete the available set of volume-area pairs, and producing the corresponding ice-thickness maps and glacier volume calculations and associated error estimates.

4. Deriving from all available ice volume estimates new volume-area relationships appropriate for Svalbard glaciers. Different relationships will be considered because distinct approaches can be followed for deriving a V-A relationship, which differ in the fitting methodology, whether a single relationship is applied to the entire population of glaciers or the population is divided into subgroups according to parameters such as size, shape or slope or whether only area enters into the relationship or other variables such as glacier length or elevation range can enter it. Particularly in the case of different V-A relationships for different subsets of glaciers according to their morphology, and given the limited number of Svalbard glaciers for which accurate volume estimates are available, a fundamental aspect to be elucidated is whether a volume-area relationship based on such a limited number of glaciers (even if these share a common morphology) will perform better than a general relationship based upon a larger number of glaciers.

5. Using such relationships, together with updated remote sensing images and maps, producing an updated estimate of the ice volume and mass stored in Svalbard glaciers and, thereby, its total potential contribution to sea-level rise. Comparing such estimates with those found in the literature.

1.4 Thesis Organization

This dissertation is organized as follows: Chapter 2 presents a state-of-art of the indirect methods for approximating glacier volumes which are widely used for regional and global ice volume estimates and projections. Here we describe the physical basis of the methods based on scaling relationships, and of those relating the ice-thickness distributions with the glacier geometry and dynamics, and climatic factors. We also present a review of the global ice volume estimates and, in particular, those for Svalbard. As stated above, this thesis relies on scaling methods to estimate the ice volume stored in Svalbard glaciers. To derive a volume-area scaling relationship specific for Svalbard, it is necessary to establish a dataset of glacier volume-area pairs from the study region. How we calculate, from ground-penetrating radar measurements, the individual volumes of the glaciers of such a sample data set is presented in Chapter 3. Here we also explain techniques for combining, avoiding biases, GPR data sets for a given glacier corresponding to different campaigns and/or seasons, and how we overcome the problems associated with non-surveyed tributary glaciers. We also introduce a novel method for estimating the accuracy of the volume calculations which takes into account both the measurement errors and the errors introduced by the interpolation method, and how they are combined when computing the volume of the glacier as a summation of the volume of the individual grid cells. The complete inventory of echo-sounded glaciers in Svalbard is introduced in Chapter 4. From this inventory, we have calculated the volumes of the 103 individual glacier basins which made up our reference dataset. We provide the GPR profile layouts and the ice-thickness maps for each glacier of our dataset in Chapter 4, and the inventory of echo-sounded glaciers is given as an Appendix. From this set of volume-area pairs, we derive in Chapter 5 the scaling relationships specific for Svalbard glaciers. We first explore our data set, comparing the histograms of area distribution of our sample data set with that of the complete population of Svalbard glaciers, to detect the existence of any possible bias. We also make a sensitivity analysis to elucidate if the inclusion of previously published data (Grinsted, 2013; Cogley, 2012) into our data set would lead to substantially different results. We then compare different methods to estimate the predictive skills of distinct V-A scaling relationships, with the aim of establishing a model selection criterion. We also compare different regression techniques, to find the most suitable fitting strategy. Afterwards, we study the sensitivity of scaling parameters to different glacier settings. This is followed by a multivariate analysis, aimed to ascertain whether the inclusion in the scaling relationship of further variables leads to improved results. Finally, we present our total volume estimate

for Svalbard glaciers and compare it with those available in the literature, and conclude the chapter presenting our best estimate of the potential contribution of Svalbard glaciers to sea-level rise. Chapter 6 summarizes the main conclusions of this thesis, and outlines some lines for future research.

Chapter 2

Global and regional estimates of glacier volume

2.1 Outline

Glacier volumes are very important for quantifying impacts of glacier changes on global sea level, for implementing thermo-dynamical glacier models to predict their evolution and for managing water resources. The downward revision of the current contribution of the ice-sheets to sea-level rise. (Shepherd and others, 2012) has renewed the interest on the contribution by glaciers and ice caps (GICs), though, as pointed out by Hanna et al. (2013), the most recent estimates for the latter (Jacob et al., 2012) also show values lower than previous estimates (Cogley, 2012). The potential contribution of GICs to SLR depends on their total volume, and therefore the estimation of the total ice volume stored by GICs has recently received much attention (Radić and Hock, 2010; Huss and Farinotti, 2012; Grinsted, 2013). However, glacier volume determined from ice thickness measurements by methods such as ground-penetrating radar or seismic soundings, or deep ice drilling, are known for less than 0.1% of the global population of glaciers (Bahr et al., 1997). This highlights the importance of exploring indirect methods to approximate glacier volumes from other known parameters. The two main indirect methods available are volume-area (V-A) scaling, which has theoretical support in Bahr et al. (1997) from the scaling analysis of the driving equations of glacier dynamics, and physically based simple models relating ice-thickness distribution to glacier geometry and dynamics, mass balance and thinning rates (e.g. Rasmussen (1988)). The most recent global estimates of the volume of GICs (Radić and Hock, 2010; Huss and Farinotti, 2012; Grinsted, 2013) are based on either of these approaches, and their substantial

differences suggest that further research on the subject is still needed.

This chapter presents the physical basis and reviews the state-of-art of the above methods, including their estimates of the global ice volume and, in particular, those for Svalbard. The most recent of such estimates use the recently released Randolph Glacier Inventory (RGI) V2 (Arendt et al., 2012), developed as a GLIMS initiative.

2.2 Estimation techniques

There are two main approaches in the literature to calculate ice volume not requiring direct ice thickness measurements. Volume-area scaling Bahr et al. (1997); Radić and Hock (2010); Grinsted (2013) is easily implemented and has proved to be useful when dealing with large ensembles of glaciers, being global and regional ice volume characterizations its major achievements. The required information for this method are the glacier areas and sometimes other glaciological parameters such as glacier length or glacier aspect ratio (length to width ratio), which can be extensively determined from satellite images and digital elevation models, and nowadays are gathered and freely available in global inventories such as the Randolph Glacier Inventory (Arendt et al., 2012), or can be easily derived from them.

Alternatively to scaling methods, physically-based methods allow for the calculation of ice thickness distribution and subglacial topography but are generally restricted to the analysis of unique (e.g. Mcnabb et al. (2012)) or small sets of glaciers (e.g. Farinotti et al. (2009)) due to the large amount of information usually required (e.g. surface topography, thinning rates, surface mass balance and surface velocity field in Mcnabb et al. (2012)). However, Huss and Farinotti (2012) recently presented a a new physically-based approach that reduces the required input information, making possible the ice-thickness distribution and volume estimate at a global scale. The main drawback of this method is the fact that it is based on general assumptions such as surface mass balance and calving flux whose parameterisations have been calibrated on small empirical data sets, and thus are susceptible to be biased.

2.3 Scaling relationships

Scale analysis is very widely used in Earth sciences to justify various approximations that can aid in the solution of the governing equations. The techniques of scaling analysis pursue the reduction of the number of model parameters by analysing their intervening dimensions. As opposed to dimensional analysis techniques, scaling procedures take the governing equations

of the model as the starting point.

2.3.1 Physical basis of scaling analysis for glacier volume estimates

Volume-Area scaling is based on the fact that, because the characteristic volume $[V]$ of a glacier is proportional to the product of its characteristic length $[x]$, width $[w]$ and thickness $[h]$, and its characteristic area $[S]$ is proportional to the product of $[x]$ and $[w]$, the characteristic glacier volume can be determined by statistically valid relationships to other known quantities.

Glacier volume-area relationships have been derived theoretically through an scaling analysis of the partial differential equations describing glacier dynamics (Hutter, 1983). Bahr et al. (1997) contributed with a detailed explanation of the physical basis for the choice of the scaling parameters, resulting in a fairly good agreement with those derived from observations. Bahr's reasoning is as follows:
From mass conservation (continuity) equation

$$\left[\dot{b}\right] \propto \frac{[u_x]\,[h]}{[x]} \tag{2.1}$$

and from momentum conservation (mass flow)

$$[u_x] \propto [A]\,[\rho]^n\,[g_x]^n\,[h]^{n+1}\,[F]^n \tag{2.2}$$

Considering shear deformation as the main form of glacier flow (Paterson, 1994), small non-shear terms can be neglected from the flow equations.
Combining Equations (2.1) and (2.2) we find the relation between $[x]$ and $[h]$:

$$[h]^{n+2} \propto [x]^{\frac{1+m+n(f+r)}{n+2}} \tag{2.3}$$

where m, f and r are scaling exponents for the mass balance profile $\left[\dot{b}\right]$, the side drag $[F]$ and the slope $[sin\alpha]$, whose values are given below (n is the flow law exponent), the brackets indicating characteristic quantities.
Combining equations (2.1),(2.2) and (2.3), the volume-area relationship can now be constructed:

$$[V] \propto [x]\,[w]\,[h] \tag{2.4}$$

$$[V] \propto [x]^{1+q+\frac{1+m+n(f+r)}{n+2}} \tag{2.5}$$

$$[V] \propto [S]^{1+\frac{1+m+n(f+r)}{(q+1)(n+2)}} \tag{2.6}$$

Bahr et al. (1997) suggests the following closure choices: For valley glaciers, $q = 0.6$ (width exponent), and $m = 2$ (mass balance exponent) and $f = 2$ (side drag) were proposed from an analysis of width-length-area data from 24,000 Eurasian and 5,400 Alpine glaciers (Bahr, 1997). Reasonable slope closures found were $r = 0$ for steep slopes and $r = \frac{(1-m+n-nf)}{2(n+1)}$ for shallow slopes. For ice caps and ice sheets, $q = 1$ and $f = 0$ because of theoretical requirements. Shallow slope is reasonable in this case, so $r = (4-m)/8$, and assuming roughly "square root" shaped surface profiles, then $r \approx 1/2$ and $m \approx 0$ are frequently assumed. The resulting scaling equation is expressed as

$$[V] = c\,[S]^{\gamma} \tag{2.7}$$

Substituting these values into (2.6), the exponents $\gamma = 1.375$ for valley glaciers and $\gamma = 1.25$ for ice caps are predicted (Bahr et al., 1997), which show a good agreement with the value empirically obtained by Chen and Ohmura (1990) from Alpine glacier data, $\gamma = 1.36$. Empirical values for the proportionality constant c have been suggested by Chen and Ohmura (1990), $c = 0.2055m^{3-2\gamma}$, and by Bahr et al. (1997), $\mathbf{c} = 0.191m^{3-2\gamma}$. However, the coefficient c remains beyond the reach of dimensional analysis and must be treated as a fitting parameter that can differ from region to region (Clarke et al., 2009).

2.3.2 Some studies following the volume-area approach

We here summarize the main studies based on volume-area scaling, starting with those focused on Svalbard glaciers.

- Macheret and Zhuravlev (1982) performed the first attempt to establish a dependence correlation between logarithmic areas and volumes of Svalbard glaciers obtained from helicopter-borne radio-echo soundings. Subsequent studies by Dowdeswell et al. (1984b) manifested that the results from the radio-echo soundings by Macheret (1981) and Macheret and Zhuravlev (1982) using 440 and 620 MHz radar systems had underestimated ice thickness by two to three times, and consequently their empirical relationship based on the measured volumes is biased in a similar way. This underestimation was due to misinterpreting the reflections from the cold-temperate transition surface (CTS) of polythermal glaciers as reflections from the glacier bedrock.

- Hagen et al. (1993) provided an empirical formula to estimate the mean depths and volumes of most of the Svalbard glaciers based on the available radio-echo soundings. As it is partly based on the results obtained by the Soviet echo soundings, it might underestimate the actual volume.

- Chen and Ohmura (1990) derived an empirical power law relation between glacier volume and area based on statistical regression of data from 63 echo sounded Alpine glaciers.

- Bahr et al. (1997) showed the physical basis of the power law relation, derived from dimensional analysis of glacier dynamics and glacier geometry.

- Meier and Bahr (1996) and Bahr and Meier (2000) used scaling methods to estimate the number and glacier/area distribution of glaciers in the world, to overcome the incompleteness of glacier inventories. They found empirical distribution functions for regions with good coverage, and applied them to other regions where coverage was sparse. The only requirements to assess the glacier-area distributions for each region were the knowledge of the approximate total glaciated area and the area of the largest glacier. The total ice volume of all the mountain glaciers and ice caps (including those in peripheral Greenland and Antarctica) was estimated to be $0.5 \pm 0.1m$ sea level equivalent (SLE).

- Dyurgerov and Meier (2005), following the same methodology but using an updated inventory, derived a global glacier volume of 0.65 ± 0.16 m SLE, and 0.33 ± 0.05 m SLE when glaciers in peripheral Greenland and Antarctica were excluded.

- Raper and Braithwhite (2005) suggested an alternative approach to estimate glacier-area distributions of incompletely inventoried glaciers. The lack of reliable glacier size distributions was addressed by relating the size distribution of several regions, using the grid of glacierized data for the globe at 1 x 1 degree resolution by Graham and McIntyre (2003), with their topographic roughness, obtained from a digital elevation model with 30 seconds of arc horizontal resolution. Excluding glaciers in peripheral Greenland and Antarctica, they estimated a global glacier volume of 0.241 ± 0.026 m SLE.

- Radić and Hock (2010) used the World Glacier Inventory extended format (WGI-XF) (J.G., 2009) to get regional volume estimates. Due to the incompleteness of the in-

ventory, they upscaled the glacier volumes as a function of the glacierized area missing in the inventory to match the total glacierized area. Through sensitivity analysis performed on regions with complete inventories, they found that their upscaling method overestimated the glacier volumes, especially when inventories were poor. Their global glacier volume estimate amounted to 0.6 ± 0.07m SLE and, excluding the peripheral glaciers in Greenland and Antarctica, to 0.41 ± 0.03m SLE.

- Farinotti et al. (2009) provided an estimate of the glacier ice volume in the Swiss Alps from a scaling relationship derived from volume data of 62 glaciers obtained by a method based on the mass conservation and principles of ice flow dynamics.

- Huss and Farinotti (2012) provided specific regional V-A relationships based on the results of a new physically-based approach for calculating glacier ice thickness distribution.

- Adhikari and Marshall (2012) calibrated scaling laws using synthetic 3-D valley glaciers. They determined how different glaciological parameters impact on the V-A scaling relation and how the V-A scaling relations change with climatic perturbations as glaciers evolve from a steady to a transient state.

- Grinsted (2013) presented a new estimate of global glacier volume using the most recent Randolph Glacier Inventory (RGI) V2 (Arendt et al., 2012). He calibrated a multivariate scaling relationship by minimizing the absolute volume deviation and applied it individually to each record in the RGI, getting a global glacier volume estimate of 0.35 ± 0.07 m SLE. This differs significantly from the estimate by Radić and Hock (2010), though is in the range of the estimate by Raper and Braithwhite (2005).

- Macheret et al. (2013) test the accuracy of volume-area scaling methods on 121 glaciers in Altay Mountains where volumes are known from direct measurements. They conclude that to improve the accuracy of scaling methods, scaling coefficients should be calculated for dominant morphological glacier types in the region, estimating an error less than 20% for a sample of 10-15 glaciers.

- Farinotti and Huss (2013) derived an upper-bound estimate for the accuracy of volume-area scaling approaches through a series of resampling experiments based on different sets of synthetic data. They quantified the maximum accuracy expected when scaling

is used for determining the glacier volume, and the volume and area changes, of a given glacier population.

2.3.3 Some glacier volume projections using V-A scaling

We now highlight some of the main studies analysing the volume projections (usually to the end of the XXI century) by means of volume-area scaling combined with climate models.

- Radić et al. (2007) compared the volume evolution of a set of synthetic glaciers obtained using scaling relationships with those produced using a 1-D flux model. The simulations were forced by different climate scenarios. The sensitivity analyses showed that the model with feedback between geometry adjustment of the glacier and mass balance update had a better performance for the 100-year prediction, both for glaciers in equilibrium and for glaciers in non-steady state. Another outcome from this study was the relative insensitivity of the volume prediction to the exponent chosen for the scaling method.

- Radić et al. (2008) compared the suitability of different scaling methods (V-A, V-L, V-A-L) to predict the evolution of the volumes of six glaciers perturbed with different mass balance forcings. The three methods underestimated the volume loss, although the highest accuracy was reached by the volume-length scaling approach.

- Möller and Schneider (2010) introduced an advantageous method to calibrate the parameters and constants of the scaling relationships that does not require a priori knowledge of an initial volume. Therefore it can make V-A scaling extensive to areas where the ice volume is unknown.

- Radić and Hock (2011) project the contribution to sea-level rise from mountain glaciers and ice caps (excluding Greenland and Antarctica) for the twenty first century to amount to 0.0124 ± 0.037 m. They calculate mass balance explicitly for each of the roughly 122,000 glaciers and ice caps available in the World Glacier Inventory (WGI-XF)5. They then applied the projections from ten different global climate models to a macroscopic glacier response model that explicitly considers the shrinking area of glaciers and ice caps in the future. For model calibration, they used measured seasonal mass-balance records from different parts of the world and linked them statistically to a number of climate parameters. The resulting set of regression equations, expressing

a relationship between glacier mass balance and climate, can be applied worldwide and also to future climate conditions.

- Radić et al. (2013) modelled volume change for every glacier in response to transient spatially-differentiated temperature and precipitation projections from 14 global climate models with two emission scenarios (RCP4.5 and RCP8.5) prepared for the Fifth Assessment Report of the Intergovernmental Panel on Climate Change. They used volume-length scaling to account for the feedback between glacier mass balance and changes in glacier hypsometry, allowing receding glaciers to approach a new equilibrium under a warming climate.

2.3.4 Summary of the available volume-area scaling laws

A summary of the different scaling relationships appearing in the literature to derive glacier ice volume is shown in Table 2.1.

Table 2.1: Volume scaling relationships for different types of ice bodies. A is assumed to be given in km^2 to get V in km^3.

Source	Ice body	Scaling Law
***Macheret and Zhuravlev*[1982]**	Valley glaciers[a]	$log_{10}V = 1.724 + 1.180 log_{10}A$
From Svalbard echo soundings	Ice caps [b]	$log_{10}V = 1.232 + 1.248 log_{10}A$
***Macheret and others*[1984]**	Valley glaciers	$V = 0.0371A^{1.357}$
***Hagen*[1993][c]**	Glaciers $A > 1km^2$	$D = 33ln(A) + 25$
From Svalbard echo soundings	Ice caps	$D = 28ln(A) + 10$
	$A < 1km^2$	D = 25
***Chen and Ohmura*[1990]**	Valley glaciers	$V = 0.0285A^{1.357}$
Fit to 64 Alpine glaciers		
***Bahr*[1997]**	Glaciers	$V = kA^{1.375}$
Physically based	Ice caps	$V = kA^{1.25}$
***Bahr et al.*[1997]**	Glaciers	$V = 0.0276A^{1.36}$
Fit to 144 glaciers		
***Van der Wal and Wild*[2001]**	Glaciers	$V = 0.0213A^{1.375}$
Scaling constant tuned to total sea level from Warrick (1996)		
***Radić and Hock*[2010]**	Valley glaciers	$V = 0.0365A^{1.375}$
Based on earlier studies	Ice caps	$V = 0.0538A^{1.25}$
***Farinotti et al.*[2009]**	Valley glaciers	$V = 0.025A^{1.41}$
***Huss and Farinotti*[2012]**	Glaciers	$V = [0.024 - 0.042]A^{[1.26-1.355]}$
From a physically based model Relationships specific for each RGI region		
***Adhikari and Marshall*[2012]**	Glaciers	$V = 0.027A^{[1.458]}$
From a sample of 280 synthetic steady state glaciers		
***Grinsted*[2013]**	Ice caps (RGI)	$V = 0.0432A^{1.23}$
Fit to 254 glaciers and ice caps	Glaciers(RGI)	$V = 0.0433A^{1.29}$
	$A > 25\ km^2$ (WGI/GLIMS)	$V = 0.0540A^{1.20}$
	$A < 25\ km^2$(WGI/GLIMS)	$V = 0.0435A^{1.23}$

[a] : In *Macheret and Zhuravlev* they refer to them as type 1 and type 2. Specific for Svalbard glaciers.
[b] : In *Macheret and Zhuravlev* they refer to them as type 3 and type 4. Specific for Svalbard glaciers.
[c] : Empirical relationship for determining the mean ice thickness. Specific for Svalbard glaciers.

2.4 Physically-based approaches

Although the volume-area scaling laws have also a physical basis, we will here refer to physically-based approaches as those deriving the ice thickness, and hence the volume, from some physical law or combination of laws (such as the mass and momentum conservation equations) relating glacier geometry and dynamics with other variables such as mass balance and thinning rate. There are many of such physical approaches in the literature. The earliest one, by Nye (1952), is based on the parabolic cross-section and the perfect plasticity assumptions. This theoretical line does not require mass balance information, and just assumes that, for actively deforming glaciers, the basal shear stress τ_0 should be close to the plastic yield stress for ice. Driedger and Kennard applied this approach to estimate the volume of glaciers of known thickness and suggested that their volume estimates were accurate to 620%. Li et al. (2011, 2012) presented an improved perfect plasticity method accounting for the effect of side drag on the stress balance.

Many authors have developed methods based on the mass conservation equation, in which the ice flux divergence is balanced by the thickness change rate and the net surface and basal mass balances. Some of the approaches involve steady state or near-steady state assumptions, while others do not. In many cases the ice flux computation is simplified by calculating it between pairs of adjacent flowlines. The main handicap of most of the methods based on the evaluation of the mass conservation equation is that they require much glacier data which is often unavailable for large sets of glaciers, so their application has usually been restricted to individual glaciers or small sets of glaciers. However, Huss and Farinotti (2012) have recently published a simplified method that circumvents this limitation by introducing a set of assumptions and simplifications that have allowed to estimate the ice volume of all glaciers in the world. In what follows we will present an example of physically-based method evaluating the mass conservation equation, and then we will briefly comment on some other similar approaches found in the literature, as well as some physically-based methods not evaluating the mass conservation equation.

2.4.1 An example of physically-based method

As an example of the physically-based methods evaluating the mass conservation equation, we describe here the fundamentals of the method developed by Farinotti et al. (2009) to calculate the ice-thickness distribution and volume of four Alpine glaciers from available information on the glacier surface plus additional environmental and dynamical variable parameterisations,

and its further simplification by Huss and Farinotti (2012), especially suited to cases where little glacier information is available.

According to the principle of mass conservation, the mass-balance integrated over the whole glacier domain should be balanced by the ice flux-divergence and the resulting surface elevation change (under the assumption of no mass losses by basal melting and calving). The ice thickness can then be inferred from the ice fluxes. The theoretical background is as follows. First, consider a vertical column of ice with length dx and heigth H in a longitudinal glacier profile. Assuming a constant ice density, the mass conservation equation is given by

$$\frac{\partial H}{\partial t} = \dot{b} - \nabla_h.\vec{q}, \tag{2.8}$$

where H is the ice thickness, $\nabla_h.\vec{q}$ is the horizontal ice-flux divergence and $\dot{b}$ is the climatic-basal mass balance rate (i.e., the sum of the surface, internal and basal mass balances (Cogley et al., 2011), often approximated by the surface mass balance). Integrating Equation 2.8 over the surface area S of any cell and using the Gauss Theorem leads to:

$$\int_\Omega \nabla_h.\vec{q}d\Omega = \int_{\partial\Omega} \vec{q}.d\vec{n} = 0 \tag{2.9}$$

where $\vec{n}$ is the normal vector to the glacier outline $\partial\Omega$. In general, the spatial distribution of $\dot{b}$ and $\frac{\partial H}{\partial t}$ are unknown. Therefore they introduced a new variable, the apparent mass balance, $\tilde{b}$, to allow the direct calculation of the balancing ice volume flux. It is assumed to vary linearly with elevation and satisfies:

$$\int_\Omega \tilde{b}d\Omega = \int_\Omega \dot{b}d\Omega - \int_\Omega \frac{\partial H}{\partial t}d\Omega = \int_\Omega \left(\dot{b} - \frac{\partial H}{\partial t}\right) d\Omega = 0 \tag{2.10}$$

The method consists of estimating a distribution of the apparent mass balance, from which an ice flux for defined ice flowlines is computed, and then converted to an ice thickness using an integrated form of Glen's flow law and interpolated over the entire glacier. The resulting ice-thickness distribution is adjusted with a factor that accounts for the local surface slope. The result is an estimate of the glacier ice-thickness distribution (Farinotti et al., 2009).

The required inputs in the original formulation by Farinotti et al. (2009) are: (1) a digital elevation model (DEM) of the region; (2) a corresponding glacier outline; (3) a set of ice flowlines which determine the main ice-flow paths through the glacier; (4) a set of borders that confine the ice-flow catchments of the defined ice flowlines; (5) three parameters defining the distribution of the apparent mass balance; and (6) two parameters describing the ice-flow

dynamics.

Huss and Farinotti (2012) applied a simplified version of this methodology to calculate the ice thickness and volume of all glaciers around the globe. This generalization requires to make certain further assumptions. As in Farinotti et al. (2009), altitudinal gradients of the apparent mass balance for the accumulation and ablation areas are required. However, in Huss and Farinotti (2012), accumulation rates are limited to a maximum value in order to prevent unrealistically high accumulation n glaciers with a large elevation range. For glaciers smaller than a certain critical area, the mass balance gradient is decreased linearly with glacier area, down to a given minimum value. Tidewater glaciers are expected to have higher balance gradients. To adapt the reference apparent surface mass balances gradients $\partial d\tilde{b}/\partial z_0$ to local conditions they include a parameter called continentality index which is related to the glacier equilibrium line altitude (ELA) and to an empirically derived parameter f_{cont}, calibrated to observed differences of mass balance between continental and maritime glaciers. Glen's flow law is used for inverting the volume flux due to ice deformation to obtain the ice thickness. This requires taking into account the fraction of flux f_{fl} due to sliding at the glacier base. This is done using a glacier-dependent parameter estimated from the glacier area and its continentality index. Finally, to account for the calving fluxes they make an equivalent lowering of the ELA by an amount that is region-specific but not glacier dependent. Then, the ice flux calculated from the surface mass balance becomes positive at the glacier terminus, simulating calving effects and resulting in an increase of the flux. This change in the ELA due to calving is poorly constrained, with a 50% agreement compared to published values.

Considering all the assumptions above, the ice thickness for each elevation band i is calculated as:

$$H_i = \sqrt[n+2]{\frac{(1-f_{sl})\,q_i}{2A_f(T)}\frac{n+2}{(F_{s,i}\rho\sin\bar{\alpha}_i)^n}} \tag{2.11}$$

where q_i is the ice flux normalized by the glacier width, $n = 3$ is the power of the flow law, ρ is the ice density, g is the acceleration of gravity, α is the glacier slope, $A_f(T)$ is a temperature-dependent rate factor of the flow law and $F_{s,i} = w_i/(2h_i + w_i)$ is a valley-shape factor.

Using this method, Huss and Farinotti (2012) have estimated the volume of all mountain glaciers and ice caps other than the Antarctic and Greenland ice sheets as 0.43 ± 0.06 m SLE.

2.4.2 Some studies following the physically-based approach

We will briefly introduce here some additional physically-based methods that have appeared in the literature to estimate the ice-thickness distribution of glaciers. First, we will present a few methods based on the evaluation of the mass conservation equation, and then a couple of other approaches.

- Probably the earliest of the approaches based on the direct evaluation of the mass conservation equation is that by Rasmussen (1988), who used ice velocities at the surface of Columbia Glacier to infer a spatially consistent map of ice thickness.

- Based on the principles described by Rasmussen (1988), Mcnabb et al. (2012) have developed a method where the ice-flux computation is simplified by calculating it between pairs of adjacent flowlines. Required input data are surface topography, thinning rates, surface mass balance rates and a surface velocity field. They tested their method against Columbia Glacier, whose rapid retreat and thinning has nearly halved the glacier volume over the period 1957-2007.

- The idea of using ice velocity to infer ice thickness has been further developed by Morlighem et al. (2011), who proposed an approach, based on mass conservation, to infer ice thickness onto a high spatial-resolution mesh by combining sparse ice thickness data from radar sounding profilers with dense, high spatial-resolution ice velocity data collected by swath mapping satellites and ancillary data. Note, however, that this method relies on already available (though sparse) ice-thickness data.

Some alternative approaches, not based on the direct evaluation of the mass conservation equation, are:

- Clarke et al. (2009), who used neural networks ,together with simplifications of the mass conservation equation, to estimate ice thickness and glacier volume of entire regions where little more than the surface topography is known.

- Linsbauer et al. (2012), who developed an approach based on an empirical relation between average basal shear stress and elevation range of individual glaciers, calibrated with geometric information from paleoglaciers, and validated with radio echo soundings on contemporary glaciers.

2.5 Strengths and weaknesses

Using the volume-area scaling approach is very weakly dependent on glacier data availability (just glacier outlines are required), and has therefore been widely used to estimate ice volumes at regional and global scales. The main limitation of this method appears when one is interested in individual glacier volumes, because errors as large as to 200% (Grinsted, 2013) can appear when applying V-A relationships to calculate volumes of to individual glaciers. On the other hand, V-A scaling does not provide an ice-thickness distribution (it only gives total volume), which is a requirement to use glacier dynamical models.

Physically-based approaches are able to determinate bedrock topography and ice-thickness distribution for individual glaciers. However, their glacier data requirements are large and therefore its application is often restricted to individual glaciers or small sets of glaciers. As discussed, this limitation has been recently overcome by the method of Huss and Farinotti (2012), though this is achieved at the expense of parameterisations which involve a rather large set of simplifications and assumptions.

Cogley (2012) points out the simplicity of the V-A scaling as one limitation of the method, because glaciers with the same area can vary greatly in ice thickness. He suggests that the new works in this field should look for other ways of parameterising mean thickness, as in Haeberli and Hoelzle (1995), where the ice thickness is related to the surface slope and the basal shear stress, in turn parameterised in terms of the elevation range of the glacier. Adhikari and Marshall (2012) have presented V-A scaling laws which take into account other glacier information (size, slope, aspect ratio), while Grinsted (2013) has carried out an estimate of global glacier ice volume through multivariate scaling methods. This type of studies have become viable only recently, at regional or global level, through the release of updated global glacier inventories such as the Randolph Glacier Inventory (Arendt et al., 2012).

2.6 Overview of the results

Tables 2.2 and 2.3 summarize the available estimations of the global ice volume of worldwide mountain glaciers and ice caps (GIC's) and the estimations of the total ice volume of Svalbard glaciers, respectively.

Values of the global ice volume of GIC's including those in Greenland and Antarctica range from 170-260 x $10^3 km^3$ and from 51-165 x $10^3 km^3$ if those are excluded. The upper-bound estimations are given by Dyurgerov and Meier (2005) and by Radić and Hock (2010)

whereas the smallest by Grinsted (2013) and Ohumura(2004) respectively. The value given by Dyurgerov and Meier (2005) has a large uncertainty up to 25% as reflected in Table 2.2. Estimations by Radić and Hock (2010) have received some critics (ie. Grinsted (2013)) for being positively biased. Grinsted (2013) argued that Radić and Hock's relationship is based in the scaling coefficient of Chen and Ohmura (1990) (whose relationship is expressed in km^2 and km^3 for A and V), but replacing the exponent with 1.375, theoretically derived by Bahr et al. (1997). Here, Bahr et al. (1997) uses the units m^2 and m^3 for A and V respectively. As the units of the scaling-constant depends on the exponent, the Chen and Ohmura constant do not apply for the Bahr's exponent, leading to an overestimation of the volume. In addition, their estimate is based on an incomplete inventory of glaciers. This is overcome in Radić et al. (2013), where they use the new released version of the RGI. Huss and Farinotti (2012) estimate is the only one based on a physically-based method, as explained in Section 2.4. Although the individual ice volume estimates are most likely better than those derived from scaling methods, it does not mean that the total volume is also better if there is a bias. It could happen as the parametrizations have been calibrated from a rather small sample.

The estimations of ice volume in Svalbard range between 4.08-10.26 x $10^3 km^3$. This wide range of values is reduced if we exclude the estimation of Macheret and Zhuravlev (1982), as they acknowledged a misinterpretation of the bedrock reflection in several sampled glaciers (see Section 4.2), leading to a new estimation in Macheret et al. (1984). The upper bound estimate is again given by Radić and Hock (2010), whose high value could be positively biased as explained above. It is important to highlight those estimates which are based on scaling relationships derived from a sample exclusively made with Svalbard glaciers. We refer here to Hagen et al. (2003), Macheret and Zhuravlev (1982) and Macheret et al. (1984).

Table 2.2: Total Areas and Volumes of Mountain Glaciers and Ice Caps Excluding and Including Those in Antarctica and Greenland (Modified from Radić and Hock, 2010)

Source	Area[a]		Volume[b]		Sea Level Equivalent[m][c]	
	Excluding	Including	Excluding	Including	Excluding	Including
Meier and Bahr[1996]	540	680	–	180 ± 4	–	0.5 ± 0.1
Ohmura[2004]	521	–	51	–	0.15	–
Dyurgerov and Meier [2005]	540 ± 30	785 ± 100	133 ± 20	260 ± 65	0.33 ± 0.05	0.65 ± 0.16
Raper and Braithwhite [2006]	522	–	87 ± 10	–	0.241 ± 0.026	–
Radić and Hock [2010]	518 ± 2	741 ± 68	165 ± 10	241 ± 29	0.41 ± 0.03	0.60 ± 0.07
Huss and Farinotti[2012]	514	735 ± 2	114 ± 11	170 ± 21	0.29 ± 0.03	0.43 ± 0.06
Grinsted[2013]	–	735	–	141 ± 28	–	0.35 ± 0.07
Radić et al.[2013]	516	737	144	210	0.36	0.52

[a] : Area values are x $10^3 km^2$
[b] : Volume values are x $10^3 km^3$
[c] : Sea level is calculated assuming oceanic area of 3.62x$10^8 km^2$ and a glacier density of 900 kgm^{-3}

Table 2.3: Estimates of Total Ice Volume stored in Svalbard Glaciers

Source	Area [a]	Volume[b]	Sea Level Equivalent[m][c]
Macheret and Zhuravlev[1982]	38.85	4.08	0.01
Macheret et al.[1984]	38.85	7.567	0.019
Hagen[2003]	36.60	7.00	0.02
Radić and Hock[2010]	36.51 ± 364	10.26 ± 823	0.026 ± 0.002
Huss and Farinotti[2012]	33.93	9.69 ± 922	0.024 ± 0.002
Grinsted[2013]	33.96	5.228	0.013
Radić et al.[2013]	33.84	9.09	0.023

[a] : Area values are x $10^3 km^2$
[b] : Volume values are x $10^3 km^3$
[c] : Sea level is calculated assuming oceanic area of 3.62x$10^8 km^2$ and a glacier density of 900 kgm^{-3}

Chapter 3

Methodology to calculate glacier volumes from GPR measurements

3.1 Outline

Ice thickness of glaciers are directly measured from prospective geophysical methods such as ground penetrating radar (GPR), seismic methods or boreholes. Here we focus on ice thickness data retrieved by means of ground penetrating radar, as it is the most widely used tool in glaciology. This chapter describes the techniques used to estimate the glacier ice volume from GPR measurements and gives a detailed description and quantification of the error sources intervening in the process. The main issues addressed in this chapter are: procedures of data assimilation such as crossover analysis that allow for the combination of data from different years and seasons avoiding biases; a case study to estimate the impact of using a constant radio-wave velocity for time to ice thickness conversion of GPR data; a methodology to estimate the volume of non-surveyed tributary glaciers; an analysis of the advantages and disadvantages of two interpolation methods for generating ice thickness maps and calculating ice volumes; and the description and the assessment of the different error sources intervening in the glacier volume computation.

3.2 GPR: a radar for glaciological studies

A ground penetrating radar (GPR) is an impulse radar system (Navarro and Eisen, 2010) used in glaciological studies to characterise the inner structure of the glaciers and to map the bedrock topography. The primary interest of the ground penetrating radar in the context of

this thesis is its use as a tool to determine the ice thickness of glaciers and, consequently, the ice volume (or mass, assuming that density is known) stored within by the ice masses.

A GPR consists of a transmitter and a receiver, with corresponding antennae, a control unit and a recording system. Transmitter and receiver must be synchronized. As compared to the direct wave synchronization of the former radar systems, modern systems are synchronized either through a dedicated radio-channel or, more often, through an optical fibre link. The transmitter antenna emits electromagnetic waves at frequencies that normally vary between 5 MHz and 1 GHz, depending on the purpose of survey. The reflected electromagnetic energy at these frequencies can be used to determine the ice thickness or the internal structure of the investigated ice body. Such a wide range of frequencies allows the use of GPR for different glaciological purposes: high-resolution (but shallow penetration) snow stratigraphy studies, mid-penetration (at medium resolution) investigation of firn layer thickness, or deep-penetration (but lower resolution) ice thickness measurements (Navarro and Eisen, 2010). Following each transmitted pulse, the received signal is sampled and recorded, with a given sampling frequency, during a certain time window. Each of these records is referred to as a trace. The radar traces should be properly geo-referenced, for instance by means of simultaneous global positioning system (GPS) measurements.

For processing the radar data we used different commercial software packages, namely RadExPro, by GDS Production (Kulnitsky et al., 2000), and ReflexW (http://www.sandmeier-geo.de/), and the main processing steps, whose description is out of the scope of this dissertation, consisted of bandpass filtering, amplitude correction, deconvolution and migration. After processing the radar data and picking the bedrock reflections, the two-way travel times shown in the radargram are converted to ice thickness using the radio-wave velocity (RWV) in ice, either using a standard velocity value appropriate to the glacier under study (depending on whether it is a temperate, polythermal or cold glacier, and the melting conditions) or a RWV determined from in situ common mid-point measurements, as discussed in Section 3.4.

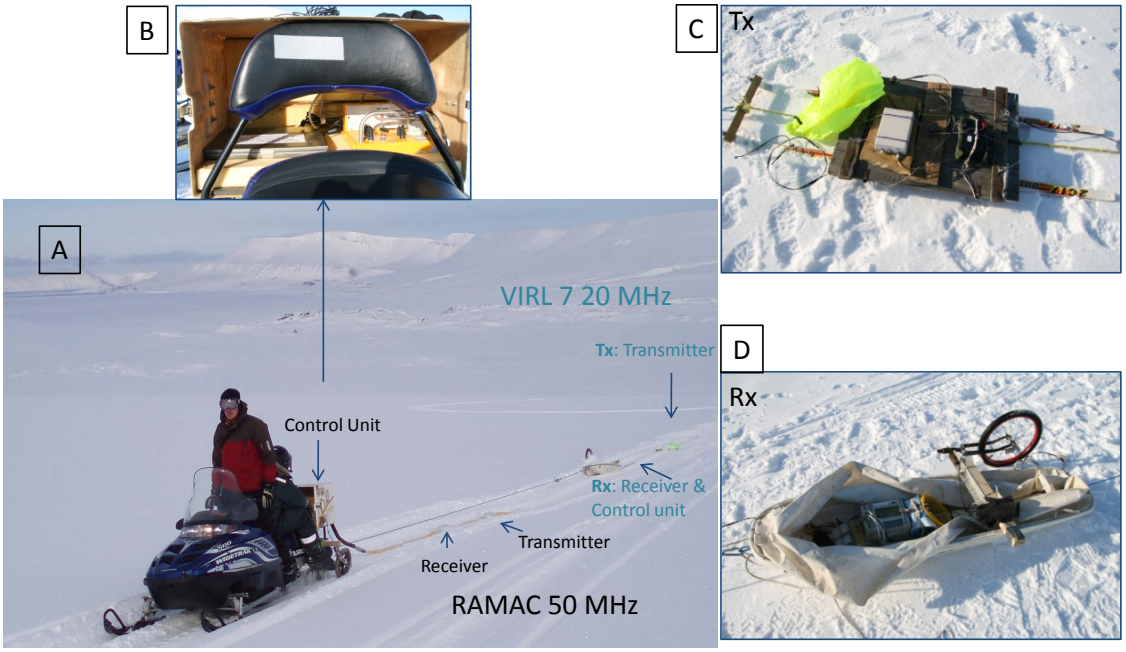


Figure 3.1: VIRL 7 and RAMAC GPR systems. A: A scooter-based convoy carrying two GPR systems, descriptions of RAMAC units shown in black and VIRL units in blue. B: View of the RAMAC control unit. C: View of VIRL7 transmitter unit. D: View of VIRL7 receiver and control units and an odometer wheel used for positioning purposes, in addition to GPS.

3.3 Data coherence and assimilation

In order to construct the ice-thickness map of a glacier, a coherent and self-consistent net of radar profiles should be available. Crossover analysis is a statistical technique used to assess both internal accuracy and consistency between data sets at the crossing points between different profiles e.g. (Bamber et al., 2001; Lingle et al., 1994). Since all measured data contain errors, the ice thickness values measured at any crossover point will in general be different for the two intersecting radar profiles. The values and the spatial distribution of the thickness differences at the crossover points provide insight into the magnitude and source of the errors in the data (Retzlaff et al., 1993). Differences at the crossover points can be caused by inaccurate positioning of the data, picking errors or lack of (or improper) migration of any of the intervening profiles. The mean of the discrepancies found at the crossovers, if different from zero, constitutes a bias that needs to be corrected. In practice, the highest crossover differences are often located in areas with radar profiles taken parallel and close to steep valley side walls. In such cases, the radar often receives reflections from (and perpendicular to) the slopes of the valley walls rather than from the point underneath the radar position. The standard 2D migration procedure only corrects the ice thickness for bed slope along the profiling direction. Consequently, it works properly for profiles perpendicular to the side walls, but not for profiles parallel to them, and hence a large difference often appears at such crossovers. To avoid these problems, we discarded the profiles parallel and close to the side walls.

To combine ice thickness datasets from different years we applied a correction for elevation change rate for each region in Svalbard following Nuth et al. (2010). As a rule, the base year for the correction was that from the campaign with the largest amount of data for each particular glacier. For some glaciers we had to combine measurements from different seasons accounting for differences in snow cover. For instance, we undertook GPR measurements on Ariebreen in summer 2006 and spring 2007. A crossover analysis revealed a 3-m systematic difference between thickness data from both campaigns, with thickness largest for the spring survey due to the snow cover, as confirmed by snow measurements done in the neighbouring Hansbreen in April 2008 (Grabiec et al., 2011). The ice thickness data of Ariebreen were corrected accordingly.

3.4 Radio-wave velocity

It is a widespread practice to convert two-way travel times (TWTT) recorded by the GPR into ice thickness is using a constant radio-wave velocity (RWV) for the entire glacier. However, it is well-known that the RWV of glacier ice depends on many factors (most notably, air and water content fractions) and consequently changes substantially both in space and time. In any glacier, the firn layer has typically a RWV of 190-200 m μs^{-1}, substantially larger than that of the ice (typically 160-170 m μs^{-1}). In polythermal glaciers such as those commonly found in Svalbard, the cold and temperate layers have different velocities, typically about 168-170 m μs^{-1} for cold ice, depending on the air fraction, and 160-165 mμs^{-1} for temperate ice, depending on the water content fraction. Temporal RWV variations are also common, mostly associated to the changing melting conditions and associated amount of water in the glacier body (Jania et al., 2005; Navarro and Eisen, 2010).

A proper glacier volume estimate would therefore require a good knowledge of the glacier internal structure (distribution and thickness of the firn, cold and temperate ice) and the ice and water fractions, which is seldom -if ever- available. With the aim of finding an optimal choice of constant RWV to be used for time-to-depth conversion, we carried out an experiment using information about the hydrothermal structure of Hansbreen, one of the best studied polythermal tidewater glaciers in Svalbard.

The ice thickness data used in this study were acquired during different GPR campaigns between 2008 and 2011 using RAMAC, VIRL6 and VIRL7 equipments with antennae operating at 20-25 MHz. The hydrothermal structure of the glacier, displayed in Figure 3.2, was obtained combining data from Grabiec et al. (2012) and Pälli et al. (2003b).

As the data are only available along the centre line, the thickness of the firn and cold layers were assumed to remain constant, for a given distance to the glacier front, across the glacier transversal section. Considering such a layered structure, our two-way travel time data collected during 2008-2011 were converted into ice thickness using RWV's of 190, 170 and 165 m μ^{-1} for the firn, cold ice and temperate ice layers, respectively. These choices were based on available velocities measured on different regions on Hansbreen (Jania et al., 2005). The total volume resulting for Hansbreen was 10.74±0.68 km^3. We then performed volume estimates using constant RWV's for the entire glacier, between 165 and 170 m μs^{-1}, at 1 m μs^{-1} intervals (see results in Table 3.1), and found that the constant RWV which produces the glacier volume closest to that computed using different velocities for distinct media is 166 m μs^{-1}. This value is within the range of column-averaged RWV's measured on

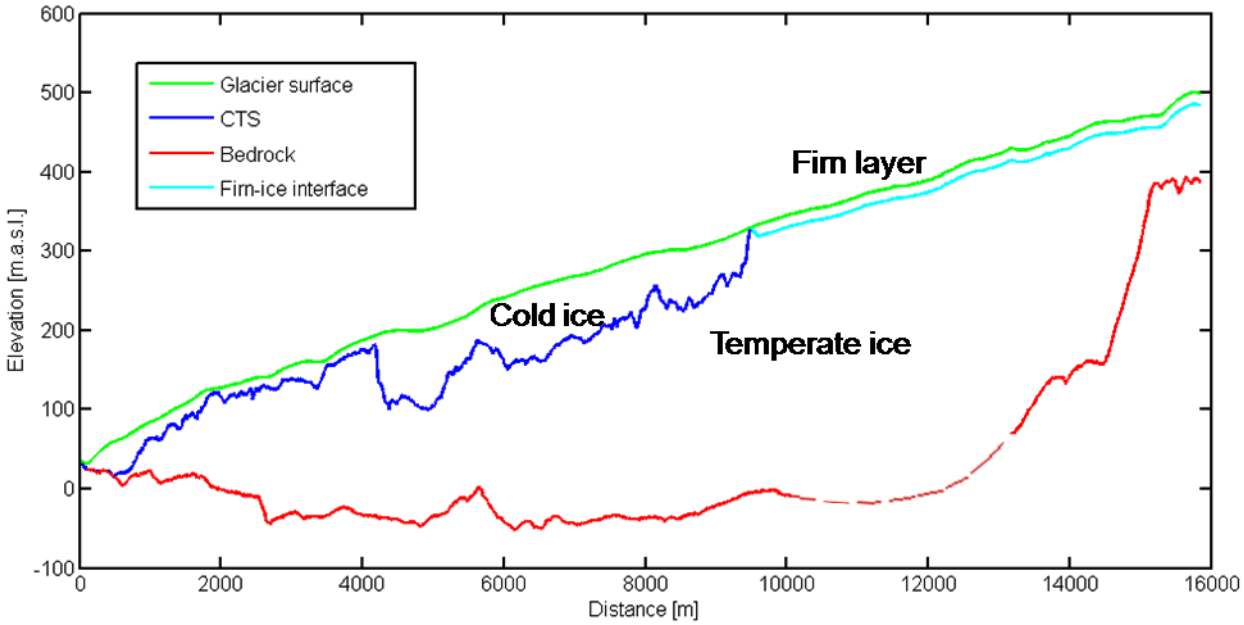


Figure 3.2: Polythermal structure along the centre line of Hansbreen. In the ablation zone, a cold ice layer, with a maximum thickness of ca. 100 m some 5 km from the glacier front, overlies a temperate ice layer. The accumulation zone has a firn layer with average thickness of 15 m. The ice underlying the firn layer is temperate

Table 3.1: Ice volume of Hansbreen and error estimates considering average RWV and using appropriate RWV for each medium

	RWV (m μs^{-1})	Ice volume km^3
Variable RWV		10.74 ± 0.68
Constant RWV	170	11.01 ± 0.70
	168	10.88 ± 0.69
	166	10.75 ± 0.60
	165	10.69 ± 0.58

Hansbreen by the common mid-point method (Jania et al., 2005; Grabiec et al., 2012). The corresponding volume, 10.75±0.73 km^3, is equivalent, within error bounds, to the volume computed used different velocities for the distinct media (in fact, all of the volumes shown in Table 3.1 are equivalent within error bounds).

These results illustrate that, when using the simpler approach of constant RWV, the ice thicknesses overestimated in the firn and cold ice layers (where the real RWVs are higher than the average used as an approximation) are nearly compensated by the underestimation occurring at the temperate ice layer (where the real RWV is slightly lower that the average). A given relative error in RWV produces relative errors in ice thickness and volume of the same magnitude. Consequently, the volume estimate is not extremely sensitive (compared to other error sources) to the choice of a constant RWV for the entire glacier, provided that

the latter is based on local or regional RWV values measured on similar seasons to those of the ice-thickness measurements, to minimize temporal variations of the RWV. Given that, additionally, the necessary data on hydrothermal structure necessary to consider different velocities for distinct media is rarely available, we will use in this thesis the glacier-wide constant RWV approach.

The question remains of what RWV should be use for each glacier or set of glaciers, depending on their geographical settings and the RWV measurements available. The number of published RWV measurements on Svalbard glaciers by the common mid-point method (CMP) (Macheret et al., 1993) is rather limited. The main studies are summarized in Table 3.2. This, together with the fact that existing CMP measurements were done in different seasons (before or after the onset of strong melting at the surface), makes difficult to compare the different results and to decide which is the most suitable RWV to use for each region. The approach that we have taken in this thesis is to select, for each region and type of glacier, a constant RWV consistent with available RWV measurements by the CMP method in the region and/or for glaciers of the same typology (if available), assuming that they will have a similar hydrothermal structure (and consequently similar average RWV), and paying attention to the seasons when both the CMP measurements and the GPR profiling were done, to account for seasonal variations of the RWV due to changes in liquid water content.

In particular, for the largest and thickest glaciers of our dataset of echo-sounded glaciers in Wedel Jarlsberg Land (Hansbreen, Paierlbreen, Recherchebreen and Austre Torellbreen), all of which show a hydrothermal structure similar to that of Hansbreen, and are of tidewater type except Recherchebreen, we took the RWV of 166 m μs^{-1} resulting from our study above. However, for the smaller and thinner glaciers of our dataset in this region (Ariebreen, Renardbreen, Scottbreen, Werenskioldbreen and Finsterwalderbreen), which show a smaller fraction of temperate ice (absent in the case of the smallest glacier, Ariebreen, which is entirely made of cold ice), it seems more realistic to use a higher RWV. We took 168 m μs^{-1}, on the basis of regional RWV measurements (Jania et al., 2005; Grabiec et al., 2012). Similarly, most glaciers of our dataset in West and Central are also smaller and thinner than the large glaciers of Wedel Jarlsberg Land mentioned above, and are therefore expected to have a smaller fraction of temperate ice. This, together with the results from regional CMP measurements (Navarro et al., 2005; Glazovsky et al., 2006), suggested the use for Nordenskiöld Land of a RWV of 170 m μs^{-1}. There are four echo-sounded glaciers in the neighbouring region of Reindalen (eastern Nordenskiöld Land). Due to the proximity, both

Table 3.2: Compilation of common mid-point (CMP) measurements on Svalbard glaciers.

CMP measurements in Svalbard

Subregion[a]	Glacier	RWV[b]	Season and Year	Survey Location	Reference
NW	Aldegondabreen	174	Spring 1999	Glacier snout	Navarro et al. (2005)
NW	Fridtjovbreen	161	Summer 1979	Ice divide	Glazovsky et al. (2006)
NW	Fridtjovbreen	170	Spring 1988	Accumulation zone	Glazovsky et al. (2006)
NW	Fridtjovbreen	165	Summer 2005	Ice divide	Glazovsky et al. (2006)
WN	Fridtjovbreen	174	Summer 2005	Accumulation zone	Glazovsky et al. (2006)
WJ	Hansbreen	168	Summer 2003	Ablation zone	Jania et al. (2005)
WJ	Hansbreen	170	Summer 2004	Ablation zone	Jania et al. (2005)
WJ	Hansbreen	164	Spring 2008	Ablation zone	Grabiec et al. (2012)
BO	Austre Brøggerbreen	166	Summer 1999	NA	Stuart (2003)
BO	Midre Lòvenbreen	168	Spring 2000	Central part	Hambrey (2005)
BO	Austre Lòvenbreen	171.5	Spring 2010	Glacier snout	Saintenoy et al. (2013)
BO	Kongsvegen	168	Summer 1996	Glacier snout	Woodward et al. (2003)
HL	Bakaninbreen	167	Summer 1995	Ablation zone	Murray et al. (1997)

[a] NW: West Nordenskiöld Land, WJ: Wedel Jarlsberg Land, BO: Brøggerhalvøya/Oscar II Land, HL: Heerland.
[b] Radio wave velocities are expressed in m μs^{-1}

geographical and typological, of these glaciers to those in West Nordenskiöld Land, we do not expect the velocity to be very different. Only in the case of Slakbreen, which is the largest and thickest glacier in the area, we can expect a greater fraction of melt water and thus, a slightly smaller velocity. Therefore we use a RWV of 168 m μs^{-1} for Slakbreen and 170 m μs^{-1} for the other three glaciers in this area. The echo-sounded glaciers in the region of Brøggerhalvøya are small mountain glaciers in the north west part of Spitsbergen. There are some CMP measurements in this area which suggest the use of 170 m μs^{-1} as an average RWV for the spring season (see Table 3.2). The echo-sounded glaciers in Dickson Land, located in the central part of Spitsbergen, near the settlement of Pyramirden, are also quite small and thin. As there are not CMP measurement done in this region and because these glaciers are typologically similar to those in Nordenskiöld Land, we use a RWV of 170 m μs^{-1}. For the region of Heerland, south Spitsbergen, we use a RWV of 168 m μs^{-1} as done in the original work (Pälli et al., 2003a). For the ice caps of Austfonna and Vestfonna, we have used 168 m μs^{-1} following Pettersson et al. (2011) and Dowdeswell and Benham (2008).

3.5 Ice thickness estimation of non-surveyed tributary glaciers

We are interested in estimating the volumes of entire glacier basins. However, several of the investigated glaciers have tributaries that, due to time constraints or safety reasons, could not be surveyed. Although they represent a small percentage of the total volume, they have a severe effect on the volume-area ratio, and ignoring them would imply a bias in the volume estimate. If the thickness of the tributaries were interpolated from the closest GPR measurements on the main glacier trunk, plus zero thickness data points at the walls of the tributary glacier, the volume of the tributaries would be systematically underestimated. To get a closer approximation to the volume of such tributary glaciers, we built an empirical function fitting the measured ice thickness along the centre line of a set of 22 tributary glaciers in Svalbard for which GPR ice-thickness measurements were available. Such a function starts from zero thickness at the point of contact of the centre line with the tributary glacier wall, and increases until the zone of confluence with the main glacier trunk. The measured ice thicknesses of each tributary, normalized by that of its deepest point (at the zone of confluence with the main trunk), as a function of the normalized distance to the tributary headwall, is shown in Figure 3.3a), together with its least-square fit to a third-degree polynomial. This "tributary thickness function" provides an estimate of the expected ice thickness along the centre line of the tributary glaciers, but we have to combine it with some estimate of the thickness variations along the transverse direction in order to calculate the volume of the tributary. Once determined the areas of different cross-sections along the tributary, the volume of the slice between two consecutive cross-sections is calculated as product of their average area and the distance between them, and the total volume of the tributary is obtained as sum of the volumes of all of the slices.

There are different approaches in the literature to approximate the cross-section of valley glaciers as power law regressions ($y = \alpha x^{\beta}$) and polynomial regressions (Doornkamp and King, 1971; Wheeler, 1984; James, 1996). However, there is not a definitive method to address this issue (Greenwood and Humphrey, 2002). We explored two different polynomial approaches to approximate the area of the transverse cross sections of the tributaries. The first one integrates over ice thickness, using only the ice thickness at the centre of the cross-section (provided by the tributary thickness function) and the zero-thickness points at both extremes (the contact points with the valley walls). The second approach takes additionally into account the shape of the glacier surface, retrieved from available digital elevation models, and integrates over the difference between the surface and bedrock profiles. Note that the

first approach produces symmetric cross-sections, while the second in general does not. For each of the two approaches we tested polynomials of different degrees, from second to fourth. The parabolic approaches produced significantly more accurate approaches to the real volume of the tributaries. In particular, the parabolic cross-section produced better results than a fourth-degree polynomial, which has sometimes been found to give a better approximation to the cross-section of valley glaciers (Greenwood and Humphrey, 2002). This is not surprising, since we are dealing with tributary glaciers, often small and more confined by the surrounding mountains as compared with the main trunk of the glacier, and are therefore expected to have a bed less flat than that of the main trunk. Hence, the parabolic approach can be expected to work best. Concerning the comparison between the two integration approaches, we did not find any significant improvement when using the second, more complex and demanding approach, so we followed the first, simpler approach. Some exceptions to the parabolic cross-section were used in the present study: Recherchebreen (in Wedel Jarlsberg Land, Spitsbergen) has two large non-surveyed areas to the east which are not typical small tributaries but, instead, rather large valley glaciers (see Figure 4.8). Hornbreen (Heerland, Spitsbergen) also required the use of the tributary function for large non-surveyed areas where a fourth-degree polynomial cross-section is likely to be a better assumption. Consequently, a fourth-degree polynomial approximation was used for calculating their cross-sections.

The standard deviation (non-normalized) of the differences between the entire set of measured thicknesses at the tributaries and the corresponding ones estimated from the tributary thickness function is 32.4 m, which gives and idea of the error in thickness involved when using the tributary thickness function. We assess the error in the estimation of the volume of non-surveyed tributary glaciers as follows. For each tributary with available ice thickness measurements, we compute the standard deviation $\sigma_{\Delta H}$ of the differences between the measured (GPR) and computed (tributary thickness function) ice thickness, and then plot such standard deviations versus the corresponding maximum ice thickness (Figure 3.3b). A linear fit is then performed, which is used to estimate the error in ice thickness along the centre line of the unmeasured tributaries as a function of its maximum ice thickness, the latter being taken as the thickness measured at the closest GPR profile in the main glacier trunk. We still have to propagate this error to the transversal direction and to the volume computation. We do this as illustrated in Figure 3.3c: the tributary parabolic cross-section is incremented and decremented by an amount $\sigma_{\Delta H}$, and the average of the associated volume changes along the entire tributary is taken as an estimate of the error in volume of the tributary.

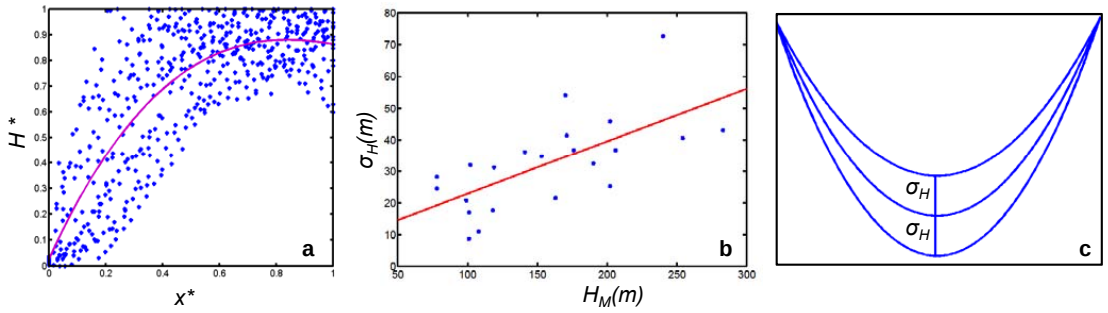


Figure 3.3: a) Normalized ice thickness H* as a function of the distance x* to the headwall, for a collection of 22 Svalbard tributary glaciers. b) Standard deviation σ_H of the differences between the measured (GPR) and computed (tributary thickness function) ice thickness for each tributary glacier, and associated linear fit. c) Tributary glacier cross-section incremented/decremented by an amount equal to σ_H.

3.6 Constructing ice-thickness maps and estimating glacier volumes

A digital elevation model (DEM) is the representation of the spatial distribution of a variable that must be quantitative and continuous. Our aim is to generate ice thickness DEMs from the sparse GPR measurements. We adjusted the available glacier boundaries from the Digital Glacier Database for Svalbard (Köning et al., 2013) to the year when the GPR measurements were recorded using satellite imagery (ASTER and Landsat7). A regular mesh is created within each glacier boundary in order to calculate the ice thickness at each node by means of Ordinary Kriging interpolation, as stated in Section 3.6.1 and therefore the glacier volume. Ice volume estimations are affected by several error sources which are discussed in detail in Section 3.7 and they are calculated for each glacier. The procedure that we have followed for deriving the glacier volumes consisted of the following steps: 1) Collecting a coherent GPR data set; 2) Processing of GPR data following specific methodology methodology; 3) Calculating ice depths along the profile; 4) Adjusting the glacier boundaries (Arendt et al., 2012; Köning et al., 2013) to the year of the radio-echo sounding using satellite images and generating a grid within this boundary (this step is performed using ArgGis v9.3); 5)Interpolating the data into the grid using an own-developed code to obtain the glacier volume an the error estimations.

3.6.1 Spatial interpolation

Spatial interpolation techniques estimate a specific property on non-surveyed locations lying within an area covered by surveyed points. Despite the existence of many different spatial interpolation methods, it does not exist an algorithm superior to others in every situation (Lam, 1983). We are interested in the interpolation of sparse and unevenly distributed ice thickness data and so, first we investigate which is the most appropriate interpolation method to create the glacier ice thickness maps and secondly we show the implementation of the selected interpolation method.

We discuss the advantages and disadvantages of two methods that have retrieved successful results. The first one is the Gridfit method which uses an approximation method closely related to thin plate splines approximation, as opposed to interpolation, so that it is robust against noise and outliers (Bohorquez and Darby, 2008). We chose the triangular interpolation method available within the Gridfit routine, leaving the default values for the remaining parameters. Further details about the algorithms used by Gridfit and its efficiency can be found at MATLAB Central File Exchange (D'Errico, 2006). The second is the widely used Ordinary Kriging method (ie. (Cressie, 1988)) that predicts at unobserved locations from a weighted average from the surrounding measured points. It is a geostatistical method that considers the spatial correlation between points and calculates the optimal weights by minimizing the mean squared deviation between predictions and observations. We focus on the properties of the two methods and its suitability to get an accurate volume estimation. Among these properties, we examine 1) the ability to work with sparse, error containing or duplicate data; 2) the property of delivering a smooth surface without loosing reliability; 3) obtaining accurate ice volumes estimations on synthetic glaciers and ice caps; 4) obtaining low rates of interpolation errors.

Figure 3.4 displays four ice thickness maps of Fridtjovbreen, a tidewater glacier situated in West Nordenskiöld Land, a region located on central-west Spitsbergen. They have been created from two different data sets. Figures 3.4a and 3.4b contain migration-related errors up to 50 meters difference at the crossing profiles (which is quite frequent in GPR data) and Figures 3.4c and 3.4d are error free. Each data set has been interpolated using Gridfit and ordinary Kriging. Figure 3.4a a shows the digital ice thickness map derived from Gridfit from the error-containing dataset and the two red circles mark the locations of the errors in the dataset. The retrieved surface does not show any impact by these errors and therefore it would be difficult to detect them if they are not known in advance. The same two circles

are shown in Figure 3.4b where the surface has been interpolated with ordinary kriging from the same dataset. In this case, the interpolation produces artefacts at the locations where the errors are present. This happens because kriging by definition is an exact interpolation method that honours the data and only deviates from them by an amount set in the variogram model so it can not work so easily with data at the same location and different value (see Section 3.6.2). On the other hand, Gridfit is an approximation method robust to outliers and duplicates, which means that it ignores data that strongly deviate from the mean trend of the data set. Outputs from Gridfit from the error-containing dataset are apparently better, but if errors are not detected and corrected a priori they will propagate unnoticed to our final calculations. Moreover, rough bedrock areas which have not been densely sampled will be seen as outliers and will be wrongly softened. Kriging is much more sensitive to errors in the data as it is reflected in their outputs. But when working with an error-free dataset, it produces a soft surface (Figure 3.4d) comparable to that produced by Gridfit from the same data set (Figure 3.4c).

To quantify the reliability of the interpolated surfaces we calculate their deviance from the real measurements with both algorithms. Figure 3.5 reflects the error statistics from both methods. Mean deviance in both cases is close to zero which means that they are unbiased predictors. However, their standard deviations vary between the two methods, being by far larger in the Gridfit algorithm. Super-smoothing algorithms such as Gridfit put so much effort in creating soft surfaces that field data are sometimes ignored whereas kriging gets reasonably smooth surfaces without losing reliability.

To find out which interpolation method retrieves more accurate ice volume estimations, we have made a test on synthetic glaciers. First we created two synthetic glaciers, a valley model using a parabolic assumption and an ice-cap model following the perfect plasticity assumption (Nye, 1957). Then, we created a set of simulated GPR profiles where the ice thickness values are retrieved from the synthetic models. Finally ice thickness surfaces are retrieved using ordinary Kriging and Gridfit. Figures 3.6 and 3.7 reflect the profiles simulated from the ice-cap model and from the parabolic model respectively, their analytic volume and the volume estimated from the interpolations with the two methods. In the ice-cap model Gridfit yields the best result, mainly due to the quasi-spherical surface of the ice cap, very proper for a smooth interpolation function. On the other hand it should be noted that deviations from the real measurements (synthetic measurements in this case) are still higher in Gridfit than in kriging. The glacier valley model displayed in Figure 3.7 is created from a

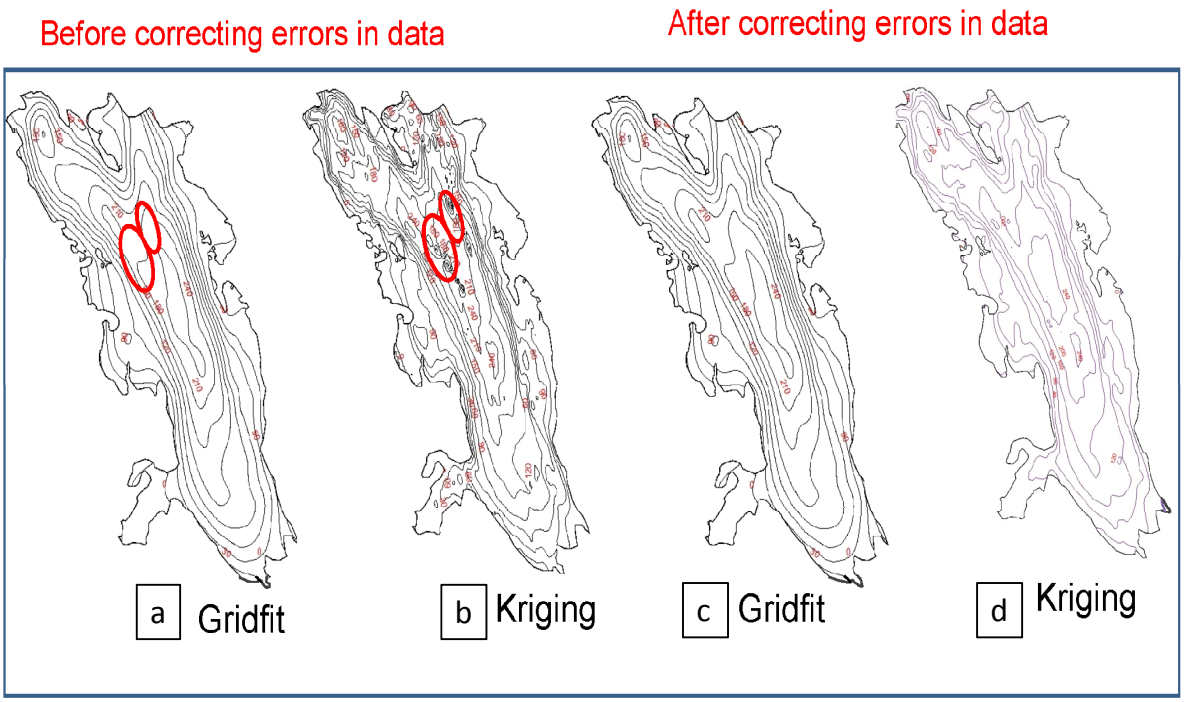


Figure 3.4: Interpolation methods working with error-containing (a and b) error-free (c and d) data

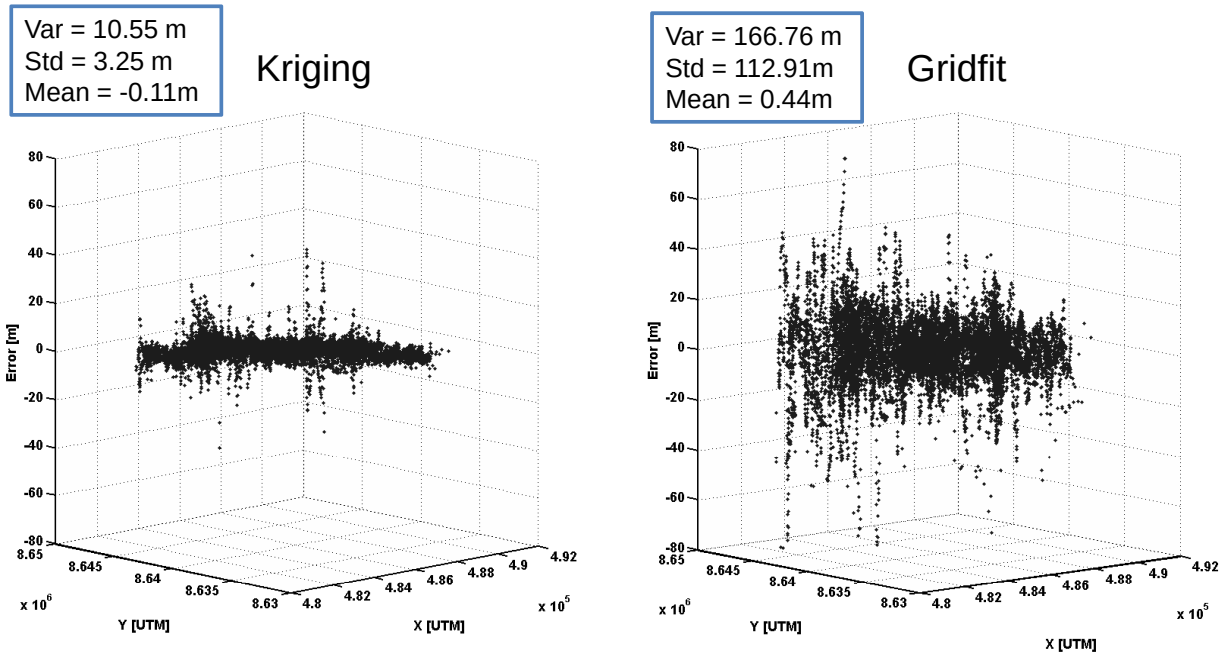


Figure 3.5: Ice thickness deviation from the real measurements

parabolic crossection assumption. Again, Gridfit yields to a good volume estimate although kriging (applying anisotropy) provides the most accurate result. Table 3.3 compares the

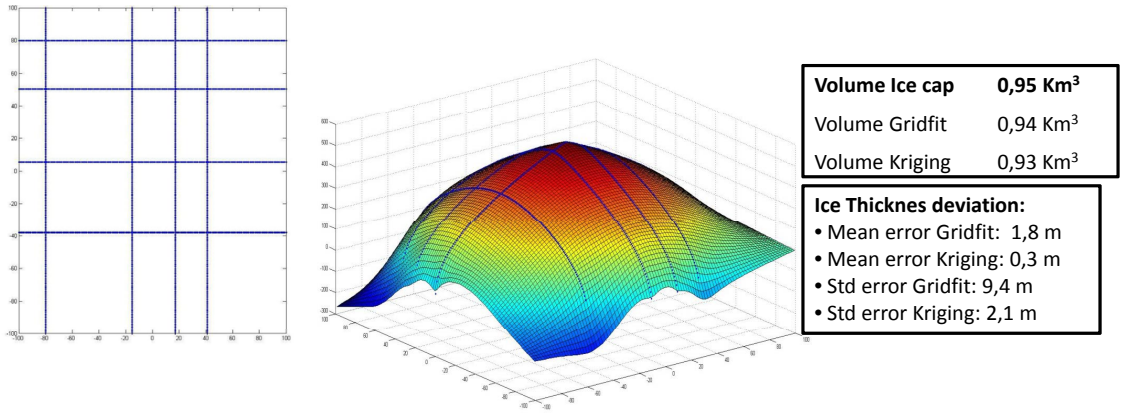


Figure 3.6: Profiles display Nye Vialov ice cap

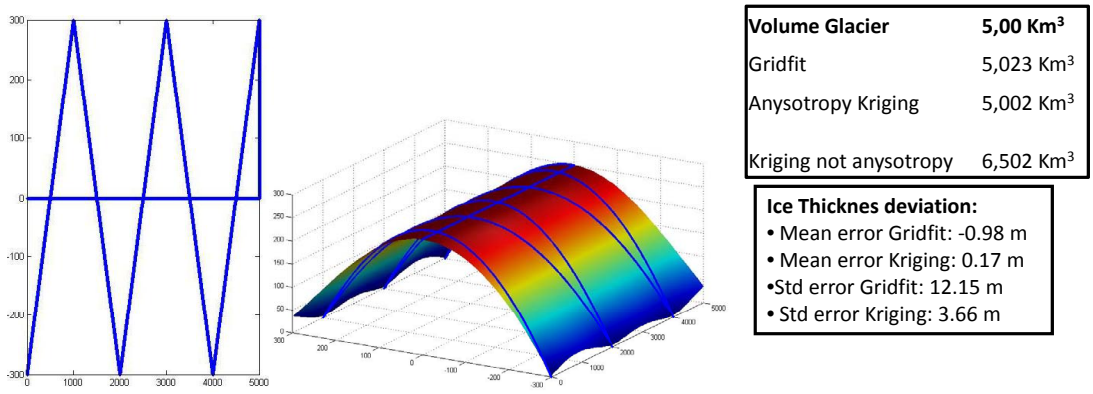


Figure 3.7: GPR profiles a synthetic parabolic model

computational errors in volume (see Section 3.7) yielded by the two interpolation methods. As expected, the glaciers interpolated with Gridfit yield to larger errors. We can conclude that Gridfit yields very good results when dealing with smooth surfaces as the synthetic glaciers presented here. However real glaciers are very much complex and the smooth surface simulated in the synthetic examples is far from reality. Standard deviation errors are large in Gridfit yielding to unrealistic smooth surfaces whereas kriging provides the most accurate ice volume estimations.

Based on the different topics investigated above, we have determined that the most appropriate interpolation method to be used in this thesis for the ice volume calculations is ordinary kriging applying anisotropy if necessary, therefore differing from a former study (Martín-Español et al., 2013), where we used Gridfit. All the glacier volumes shown in this dissertations will be calculated using ordinary kriging, recalculating them from previous works if necessary.

Table 3.3: Comparison of errors using Gridfit and Kriging interpolation in ten Nordenskiöld Land glaciers

Error in Volume (km^3)	Gridfit	Kriging
Aldegondabreen	0.074	0.024
Dalhfonna Austre	0.014	0.009
Dalhfonna Vestre	0.028	0.023
Erdmanbreen	0.039	0.024
Fridtjovbreen	0.339	0.114
Gleditchfonna	0.007	0.004
Grønfjorbreen Austre	0.029	0.027
Grønfjorbreen Vestre	0.149	0.061
Tavlebreen	0.036	0.009
Tungebreen	0.005	0.004

3.6.2 Ordinary kriging

Kriging is a geostatistical method for spatial interpolation, optimized to make inferences of unobserved regionalized variables $z(s_0)$ of the random process Z(s) from observed data $z(s_i)$ (Cressie, 1988). There are different varieties of kriging interpolation methods. Here we focus in ordinary kriging, that assumes a constant mean in the local neighbourhood of each estimation point. The linear kriging estimator $\hat{Z}(s_0)$ is a linear combination of n data point values $Z(s_i)$

$$\hat{Z}(s_0) = \sum_{i=1}^{N} \lambda_i(s) Z(s_i) \tag{3.1}$$

where λ_i are the weights or kriging coefficients that should be estimated in an optimal way. Kriging uses the semivariogram function $\gamma_z(h)$, or equivalently, the associated covariance function $C_Z(h)$ for building this linear estimator $\hat{Z}(s_0)$ minimizing the least square difference between predicted and observed data under the restriction of being unbiased. The choice of a good predictor will depend on the geometry and location of the region of the space where prediction is desired. From actual measures of the correlation between pairs of points (latter defined as the experimental semivariogram), a semivariance function is fitted to the correlation data (also known as the theoretical semivariogram). The semivariance function $\gamma_{(h)}$ is defined by the variance of the increment of Z(s) when moving from location s_i to location s_{i+h}:

$$\gamma_{(h)} = \frac{1}{2}\text{var}\left(Z(s_i) - Z(s_{i+h})\right) \tag{3.2}$$

The kriging predictor solves the following system of (N+1) linear equations to calculate the optimal weights:

$$\hat{\Gamma}(s_0, s_i) = \lambda_s \hat{\Gamma}_(s_i, s_{i+h}) \tag{3.3}$$

$$\begin{vmatrix} \lambda_s \\ \dot{m} \end{vmatrix} = \begin{vmatrix} \hat{\Gamma}(s_i, s_{i+h}) & 1 \\ 1' & 0 \end{vmatrix}^{-1} . \begin{vmatrix} \hat{\Gamma}(s_0, s_i) \\ 1 \end{vmatrix} \tag{3.4}$$

where the term $\hat{\Gamma}(s_i, s_0)$ is a vector containing the semivariances between the prediction points s_o and the measurement points s_i, the term $\hat{\Gamma}(s_i, s_{i+h})$ is a matrix of semivariances between all the pairs of measurement points accounting for s_0 and the kriging weights are the unknown parameters to be solved where the weighting coefficients $\lambda_i(u)$ need to be constrained to have their sum equal to one to honour the unbiased condition:

$$\sum_{i=1}^{N} \lambda_i(s) = 1 \tag{3.5}$$

Among the infinite number of possible weightings $\lambda_i(s)$, ordinary kriging chooses the one that minimizes the so-called estimation variance $\sigma_E^2(s)$

$$\sigma_E^2(s) = E\Big(\hat{Z}(s,.) - Z(s,.)\Big)^2 \tag{3.6}$$

The optimal coefficients minimizing $\sigma_E^2(s)$, while honouring the constrain, can be obtained using the classic Lagrange multipliers technique. According to this technique, the optimal solution should realize the minimum of the function $\lambda(\lambda_1, ..., \lambda_N(u), \mu(u))$ as defined by

$$\lambda = \sigma_E^2(s) + 2\mu(s)\left(\sum_{i=1}^{N} \lambda_i(s) - 1\right) \tag{3.7}$$

where the $\mu(s)$ is the Lagrange multiplier associated with the constraint. Mean expected error will be zero.

The variogram is used to measure the variability of a random process Z(s). It calculates the spatial correlation between pairs of values $Z(s_i)$, $Z(s_{i+h})$. If the data are spatially dependent,

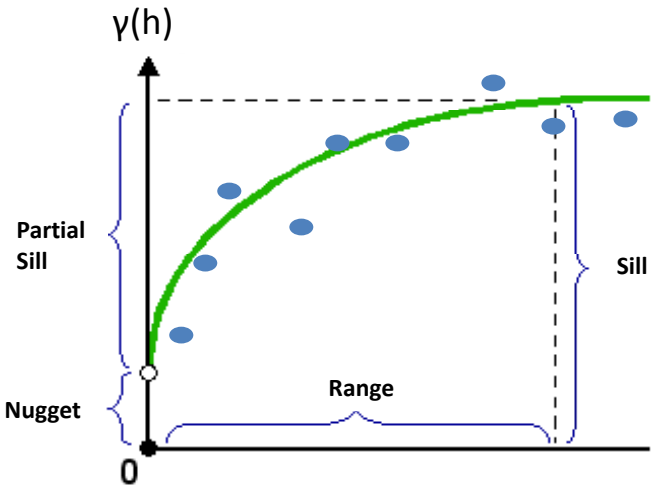


Figure 3.8: Variogram function

pairs of points that are close together (on the far left of the x-axis) should have less difference (be low on the y-axis). As points become farther away from each other (moving right on the x-axis), in general, the squared difference should be greater (moving up on the y-axis). The curve of a theoretical variogram levels out at a certain distance. The distance where the curve first flattens out is known as the range. Sample locations separated by distances closer than the range are considered spatially autocorrelated, whereas locations farther apart than the range are not. The value that the variogram attains at the range (the value on the y-axis) is called the sill. The partial sill is the sill minus the nugget. Theoretically, at zero separation distance (i.e., lag = 0), the variogram value should be zero. However, at an infinitesimally small separation distance, the difference between measurements often does not tend to zero. This is defined as the nugget effect. It reflects the uncertainty (or randomness) which cannot be removed from the phenomenon including all random variation at scales shorter than the inter-sample distances, like measurement errors, reproducibility issues and short scale variations inherent to the variability of the phenomenon being measured.

There are two possible nugget models in the literature (Cressie, 1988; Chils and Delfiner, 2008):

(a) $\gamma(0)$=0: force the model to go through zero at zero distance.

(b) $\gamma(0)$= Measurement Error: allow the model to hit the vertical axis.

Option (a) makes kriging an exact interpolator. If you krige exactly at a sample location, you will get the sample value and a kriging variance of zero. This is originally specified in Matheron (1971). Option (b) means that kriging will not exactly honour the data as it will

allow the surface to deviate from the sample data by the amount determined in the nugget model. This is implemented by including the estimated measurement errors in the main diagonal of the matrix $\hat{\Gamma}(s_i, s_{i+h})$ also known as $\gamma(h)$ within the kriging system (Equations 3.3 and 3.4), corresponding to second case in the nugget model explained above, $\gamma(0) =$ measurement error, and will imply that krigged values at sampled location does not honour the data. It makes sense, as this part of the nugget corresponds to the measurement error. However, it might exist unknown errors which can be taken into account by allowing an additional nugget effect to model unresolved variation (i.e. things happening below the measurement separation distance). The aim is to estimate the nugget effect, but keeping fixed the known observation errors. The intersection of the theoretical variogram with y axis will give a value for the nugget (the expected variance for values in the same location). So the combination of both will be:

$$\begin{cases} \gamma(0) = \text{measurement error} \\ \\ \lim h \to 0 = \text{nugget} \end{cases} \tag{3.8}$$

under the assumptions of second order stationary random errors (zero mean and the covariance between any two depends only to the distance and direction) following a Gaussian distribution.

Variogram modelling is a key step between spatial description and spatial prediction. The modelling of the variogram begins with the construction of the empirical variogram, for all pairs of locations separated by distance h. However, they do not provide information for all possible directions and distances. For this reason it is necessary to fit a model (i.e., a continuous function or curve) to the empirical variogram/covariogram. There are several functions used to fit the variogram. We chose the spherical function as it fitted better to our experiments both by visual analysis and by means of minimizing the mean square error.

$$\gamma\left(h, \Phi\right) = \begin{cases} c_0 + c_s \left(\frac{3}{2}\frac{h}{a} - \frac{1}{2}\frac{h}{a}^3 \right) \text{ for } 0 < \text{h} \leq \text{a} \\ \\ c_0 + c_s \text{ for h} \geq \text{a} \end{cases} \tag{3.9}$$

where, c_0 = nugget effect, $c_0 + c_s$ = sill, a = range

Kriging overcomes other interpolation methods as it allows selecting the number and dis-

tribution of sample data to be used for interpolation, calibrating the amount of deviation from the sample data by means of the nugget model and also evaluating the error of each estimate through the kriging variance. This allows to reduce the amount of necessary field data, to make interpolation unaffected by the known measurement errors and to obtain an assessment of the quality of the output surface.

We implement the interpolation in Fortran-90 using a code that calculates the variogram function (including the main direction of anisotropy), integrates the search and optimization of variogram model parameters to distribute the weights among the neighbouring points through the least squares method (LSM), performs the interpolation to the grid points and calculates the glacier volume and estimates the different error sources intervening explained in Section 3.7. The interpolation algorithm that we used is based on a spherical variogram model (Equation 3.9) and its parameters, sill, nugget and range that are tuned to the best fit. Every estimation obtains information from up to 64 neighbours, 8 data-points per octant. Anisotropy is applied in the cases where glaciers show one main direction.

3.7 Error estimates

Knowing the accuracy of our glacier volumes estimates is important in order to estimate the error of the volume of Svalbard using V-A relationships, as is considered in Farinotti and Huss (2013). However they are not often well described or even quantified in the literature. For instance, any of the estimated glacier volumes from the Soviet flights in the seventies are accompanied with an accuracy estimation (Macheret and Zhuravlev, 1982). Neither the glacier volume estimations from the joint Norwegian-British venture in the eighties (Dowdeswell et al., 1984a). More recent studies such as Saintenoy et al. (2013), where they derive the ice thickness and volume of Austre Lovénbreen report an error estimate from the different sources (instrumental and interpolation errors), but they do not detail how they combine these errors to derive the final error in volume. Similarly, in their work Bælum and Benn (2010) describe the thermal structure of Tellbreen and calculate its volume reporting an error estimate, but they only focus on the accuracy of the ice thickness point measurements, meanwhile other error sources such us positioning errors, interpolation errors or the accuracy on the boundary determination are absent.

The fact of considering dependency or correlation among the errors will strongly influence the value of the final error in volume, as we show in a test performed with synthetic glaciers in Section 3.7.4. We compute the error in glacier volume from the errors of its main components.

In Section 3.7.2 we introduce how to calculate the error of an ice thickness digital elevation model (ice thickness-DEM) derived from GPR measurements. In addition to the analysis and estimation of the individual error sources, we describe how to combine them to obtain the total error in ice thickness (ϵ_H). We also propose a novel method to estimate the interpolation error of an sparse, non-homogeneous distributed data set (characteristics of GPR data). This method also corrects for the possible bias introduced by the interpolation method. The second Section 3.7.3 analyses the error produced when deriving a glacier volume from an ice thickness-DEM, which has been delimited by a given boundary. This boundary could be determined by different methodologies (i.e. aerial photography, satellite images, GPS measurements) and it is used to impose the zero ice thickness boundary to the interpolation (except along ice divides and calving fronts). And finally we propose a novel method based on the degree of statistical dependency among the errors at the grid points, to combine the error sources intervening in the estimation of a glacier volume.

3.7.1 Preliminars

We define the error as the random variable characterizing the difference between the measured/interpolated/estimated value and the real value. According to this, a positive error is produced when the measured/interpolated/estimated value is above the real value and negative when below. We also distinguish between the variable random error, the punctual value of the error of a specific measurement (ε_i) and the mean (also known as bias) and standard deviation of the random error (which is defined in absolute value and usually represented with $\pm$). It should be remarked that the difference between two error-containing measurements cannot be referred to error but discrepancy between them (Bevington and Robinson, 2003).

3.7.2 Ice-thickness error

Given an ice thickness-DEM of a glacier, its volume can be computed as sum of cell area times the average ice thickness for the cell.

$$V = \sum_{k=1}^{N} A_k H k \tag{3.10}$$

Under such a scenario, where the grid cells have a pre-defined error-free area, the error in volume would depend only on the errors in thickness of each individual grid point. However, an ice thickness-DEM is constructed from a given boundary and a set of non-uniformly

distributed ice thickness data points obtained from GPR measurements along certain lines called radar profiles. They are normally positioned by a GPS connected to the radar or by an odometer assuming equidistant traces.

The errors in ice thickness arise from different sources. First, we have error in the dataset (ε_{Hdata}), which embrace the ice thickness errors related to the GPR (ε_{HGPR}) assuming a correct position of the profiles, and the ice thickness error due to an incorrect positioning of the profiles (ϵ_{HGPS}). Both error sources are considered independent allowing to estimate the ice thickness error at each data point as a root means squared summation:

$$\varepsilon_{Hdata_i} = \sqrt{\varepsilon^2_{HGPR_i} + \varepsilon^2_{HGPS_i}} \tag{3.11}$$

Next, we consider the error introduced by the interpolation at the grid points. Finally we will combine them to obtain the ice thickness error.

GPR-related ice-thickness error

GPR measurements are taken at particular points, and their output are two-way traveltime (TWTT) (time lapse since the pulse is emitted until is registered back) which are converted to ice thickness multiplying them by half the radiowave velocity (RWV) in the medium. Consequently, there is a point-dependent GPR error which depends on both the error in the assumed RWV and the errors in timing. The latter, in turn, include the errors associated to the time discretization of the radar signal (though these are actually superseded by the range or vertical resolution of the radar) and the picking errors incurred when improperly picking the bed reflections from the radargram. The latter are interpretation errors that are minimized when working with properly migrated radargrams, as has been done with our GPR data set. Following Navarro and Eisen (2010), we estimated the GPR error assuming that the error in TWTT is given by the inverse of the central frequency of the radar system and that the error in RWV is typically of the order of 2%.

$$e_{HGPR} = \frac{1}{2}(\tau^2\varepsilon_c^2 + c^2\varepsilon_\tau^2)^{1/2} \tag{3.12}$$

where ε denotes the error on the sub-indexed variable and c is the RWV in the medium. The error assessment as described here assumes: 1)Radar data processing includes the migration step to restore the real shapes and slope. 2)Picking in the radargram is only done in areas where bottom return is clear; errors produced otherwise are not considered and can be large

(e.g. in temperate ice areas) 3) Our measurements come from a *common offset* profile where processing must include a conversion to *zero offset* profile so the ice thickness H is computed as

$$H = c\tau/2 \tag{3.13}$$

Positioning-related ice-thickness error

Additionally, the location of the measurement points is affected by a horizontal positioning error(ε_{GPS}) which induces, for sloping surface/bed, an error in thickness (ε_{HGPS}) as we erroneously attribute a measured ice thickness to nearby location. This error is disregarded if we use a differential GPS (DGPS) for positioning as it get an accuracy of cm. But for a stand-alone GPS system we assume a typical horizontal accuracy of 5 m (Sharma and Banerjee, 2009). To estimate the thickness change that could be expected from such error in horizontal positioning (ε_{HGPS}) we need to know how much ice thickness variability exists in 5 meters around the measurement points. This variability would be theoretically measured as the standard deviation of ice thickness differences in measured points 5 meters apart. As it is not common to have such kind of measurements, we estimate them from the interpolated ice thickness map. We evaluate the standard deviation of the ice thickness difference between the measurement point and other (at least 8) surrounding points situated 5 meters apart.

$$e_{HGPS} = \left[\frac{1}{n-1}\sum_{k=1}^{N}\left(d_k - \bar{d}_i\right)\right]^{1/2} \tag{3.14}$$

This error increases with the difference in slope between glacier surface and bedrock or equivalently, with the increasing gradients in ice thickness. Sometimes the traces in the GPR profiles have not been positioned with GPS, but they have been set as equidistant using an odometer where the initial and ending points are known. In this case we can use the same procedure but the horizontal accuracy should be estimated. Depending on the length of the profile, this deviation could be much larger than 5 meters.

Interpolation errors

The ice thickness maps are calculated by means of interpolating the ice thickness data at the GPR measurement points to unknown locations within a regular grid. This step involves an interpolation error. A proper estimate of the interpolation error should relate well to the quantity and the distribution of field data available.

Different approaches have been followed in the literature for estimating these errors. Some authors (e.g. Pettersson et al. (2011)) have estimated the interpolation error through cross-validation techniques. The idea behind these techniques resides in that the most robust interpolation methods will continue to produce good estimates despite the reduction of the data point sample. However, when dealing with uneven distributions of data, as happens with GPR profiles, cross-validation does not infer correctly the interpolation error in areas where measurements are scarce, leading to a systematic underestimation of the interpolation error. Another commonly used parameter for estimating the interpolation error, in the case of kriging, is the kriging variance (Cressie, 1990). It is widely used by the geostatistics community, but it has been criticized for considering only the geometrical arrangement of the sample data and not being value-based, because it simply assumes that the accuracy decreases with growing distance to the input data (Rotschky et al., 2007). Our study implements a novel method to account for interpolation error which has been designed to work with data distributions with a high density of data along particular directions (profiles), often intersecting, but lacking data in the areas between profiles. Such data distributions are typical of GPR or seismic profiling, bathymetric studies, etc. Our method aims to calculate an average interpolation error following the rationale of cross-validation techniques, but taking into account the variance of the error with the distance to the nearest neighbour. We first construct a function relating the interpolation error at any given point with the distance to the nearest GPR-measured data point, named "*Distance-Error Function*"(DEF) (see algorithm steps below). Then, we calculate a glacier-wide interpolation error by averaging the interpolation errors computed by the *DEF* at each grid point. This method has the added benefit that it also provides a way to detect and correct any possible bias involved in the interpolation process. The algorithm of the *DEF* method, which also integrates an step for bias correction, is summarized in the following steps:

- Center a blanking circumference with a fixed radio R_1 on a data point (as shown in Figure 3.9, left). Interpolate with remaining data falling outside the circumference and compare the predicted value at the central point of the circumference with the real value to obtain the discrepancies in that interpolation (shown in Figure 3.9, right). This is repeated for each data point. The mean of all the discrepancies constitutes the bias for R_1. This bias is corrected by summing it (with sign) to the interpolated values. After this correction, the standard deviation of all the discrepancies constitutes the error for R_1.

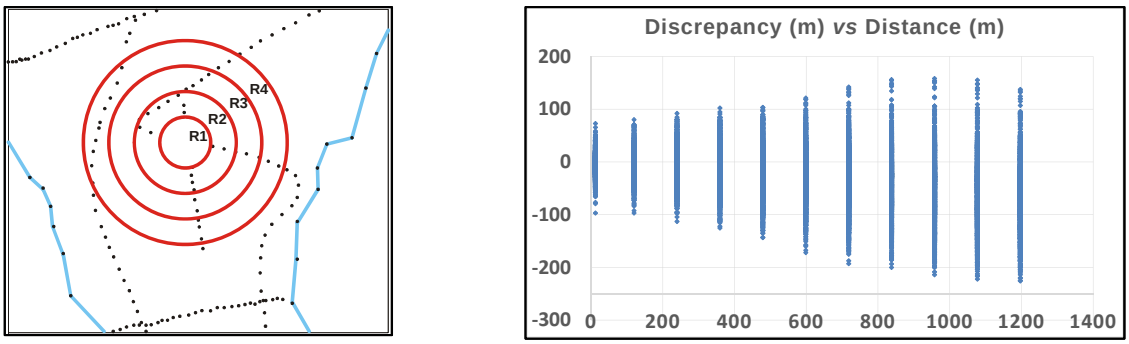


Figure 3.9: Figure to the left shows the blanking circumferences of growing radios centred on a data point. Figure to the right displays the discrepancies caused by interpolating after blanking data points for growing distances.

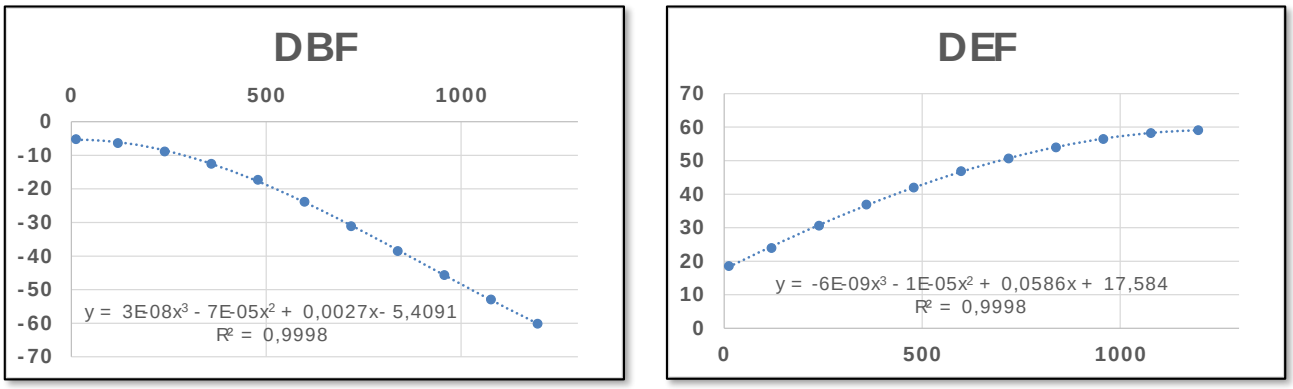


Figure 3.10: DBF shows how the bias has negative values that grows with increasing the distance to the nearest measurement. DEF shows how the error grows with increasing the distance to the nearest measurement.

- The same process is repeated using different values of R=R_1,R_2,R_3..., obtaining mean discrepancies (bias) and their standard deviations (errors) for each R_i.
- Distance-Bias Function (DBF): It is generated by fitting a curve to the R_i-bias pairs. An example is displayed in Figure 3.10 left.
- Distance-Error Function (DEF): It is generated by fitting a curve to the R_i-error pairs. An example is displayed in Figure 3.10 right.
- We apply DBF and DEF to every value in the interpolated grid: for each value in the grid, we measure the distance to the nearest data point, we add the bias, positive or

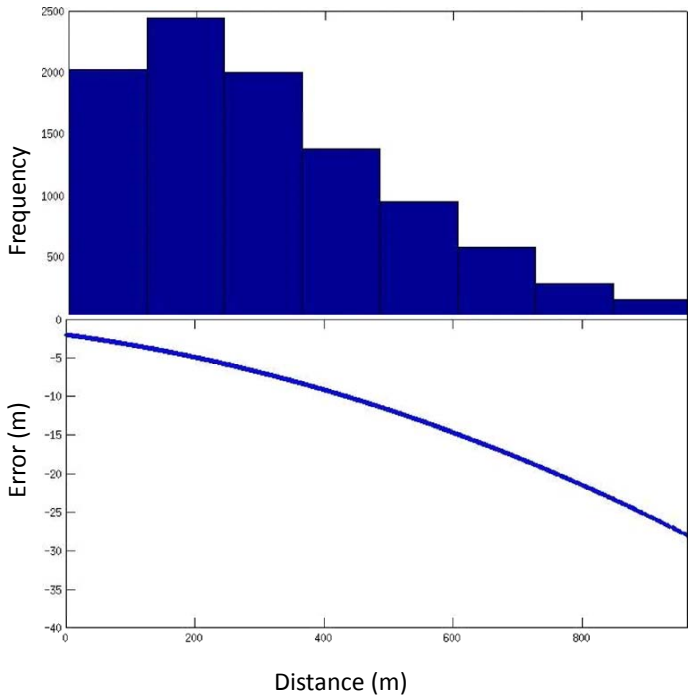


Figure 3.11: Example of a frequency distribution of the corrections for bias at an interpolated grid (above) and their corresponding RBF (below) in Werenskiöldbreen.

negative, obtained by DBF according to this distance and attribute to the grid value the interpolation error given by DEF.

Kriging is by definition an unbiased predictor. It holds as long as the data fulfil the kriging assumptions of normality and stationary of the mean and second-order stationary. Stationary of the mean assumes that the mean of the interpolated variable is constant between samples and is independent of location; second-order stationary is the assumption that the covariance is the same between any two points that are at the same distance and direction apart no matter which two points you choose. Kriging also relies on the assumption that all the random errors are second-order stationary, which is an assumption that the random errors have zero mean and the covariance between any two random errors depends only on the distance and direction that separates them, not their exact locations. The most straightforward reason for the bias we find in the interpolation relates with the unfulfillment of hypothesis that kriging is based on. Another possible explanation for this bias is the overall curvature of the ice thickness surface, which tends to be convex-shaped (zero thickness are fixed at the boundary and positive thickness towards the inside) and therefore the interpolation tends to underestimate the ice thickness as we can see in our negative bias functions.

After an exploratory analysis of the data we identified a global trend in our data. A

trend is the non-random (deterministic)component of a surface that can be represented by some mathematical formula. We used a wide range of polynomials in order find the best trend description and finally chose applying the MSE criterion. After removing the trend, we continue the variogram analysis by modelling the residuals (the short-range variation in the surface) and then, the interpolation process. However, after the detrending process we still detected a remaining bias proving that the global trend has not being removed totally. Therefore we correct the gridded ice thickness by adding to each node, the bias found for the distance to each node to the nearest field measurement. For instance, by looking at the Figure 3.11 we set the bias for a node separated to the nearest measurement by 200 meters, to be 4.5 meters that will be added to the predicted value.

Ice-thickness error in the grid

To assess the quality of the digital ice thickness model we need to combine the ice thickness error of the data points with the interpolation error in the grid points. This requires to evaluate how the ice thickness errors measured at the data points affect the quality of the interpolated values: in short, we need to move the error from the data to the nodes in the grid. Measurement errors will affect the value of the ice thickness at every grid cell as they are weighted combinations from the neighbouring measurement points h_k, $h_i = \varphi(\sum_{k=1}^{m} w_k h_k)$. We can approximate the error propagation from the dataset (ε_k) to the grid nodes (ε_i)using the same interpolation function (Φ),the same neighbour distribution (h_k) and weights (w_k) but applied to the errors instead of to the ice thickness.

$$\varepsilon_i = \varphi\left(\sum_{k=1}^{m} w_k \varepsilon_k\right) \tag{3.15}$$

Once we have estimated for each grid value an interpolation error and a data-derived error, we can combine them assuming independence between them (although it exist a certain degree of dependency, it can be disregarded as it of a higher order). Consequently, the ice thickness error for each grid point (an example is shown in Figure 3.12) is obtained as the root square of the squared summation between the interpolation error and the data-derived error.

3.7.3 Error in volume

This section deals with the assessment of the error in ice volume calculated from a digital ice thickness model delimited by a given boundary. As we saw in Section 3.7.2, determining the

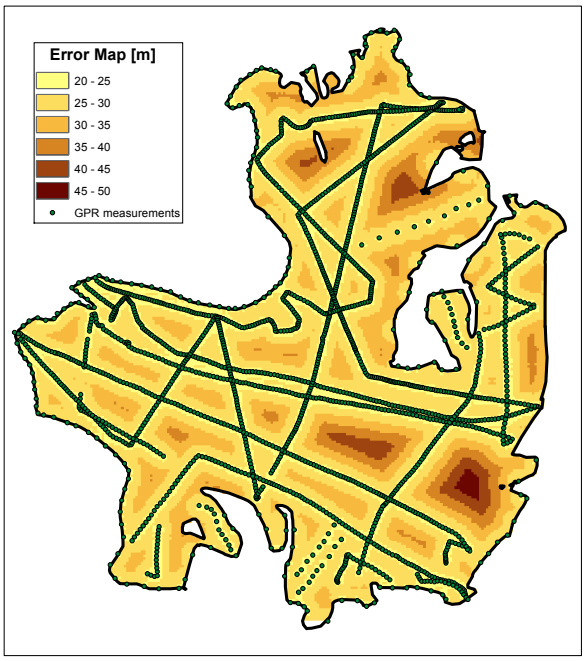


Figure 3.12: Ice thickness error map

ice thickness at the grid points from the GPR measurement points (which are in turn affected by measurement errors) involves an interpolation error. Estimating all of these errors, and their combined effect, is not straightforward. To help in doing it, we will conceptually separate the errors in volume as that stemming from the uncertainty in boundary delineation, ε_{VD}, which we will estimate separately, and, once assumed a given boundary, those incurred by all other ice thickness error sources at the DEM,ε_{VH}. Once assumed a given boundary delineation, it is possible to correct for possible biases introduced by the mapping software employed to construct the grid, and the magnitude of the random pixellation error, ε_{VPix}, that remains after the removal of the systematic error. Both of them become smaller with the reduction of the grid size. Of course the pixel size of the satellite image, or the horizontal positioning error, in the case of ground-based boundary delineations, play the role of a lower bound in the computation of the pixellation error, so the grid size should be chosen accordingly to avoid unnecessary computational load (the grid size should not be lower than the pixel size or the error in horizontal positioning). After correction for biases, the magnitude of the pixellation error is usually negligible as compared with the uncertainty in boundary delineation that is discussed below. As concerns to how to combine all of these errors, we first note that the boundary delineation error and the ice thickness error are nearly independent, so they can be combined as root of the sum of squares:

$$\varepsilon_V = \sqrt{\varepsilon_{VB}^2 + \varepsilon_{VH}^2} \tag{3.16}$$

Error in volume due to boundary uncertainty

Regarding the uncertainty in boundary delineation, glacier outlines are often defined from aerial photos or satellite images taken at the end of the summer, when the snow cover on the terrain surrounding the glacier is expected to be minimal. But, even so, on the valley walls surrounding the accumulation area often remain snow patches that make difficult the proper definition of the glacier boundary. Similarly, on the ablation area, near the contact with the glacier valley walls and also near the snout of land-terminating glaciers, the presence of debris makes difficult a proper interpretation of the glacier limits. These errors are strongly glacier-dependent (e.g. they depend on glacier orientation and altitude of surrounding mountains, and associated shadowing, and on the slope and petrology of glacier valley walls, among other factors) and their estimation is subject to strong uncertainties, even in the case of boundaries delineated from ground-based measurements such as GPS positioning of the glacier outlines. Bernard et al,.(2013) analyse the bias occurred for this reason in Austre Lovénbreen, a small mountain glacier in north west Spitsbergen. This error can result in positive or negative net errors for individual cases, but we assume a zero mean error. This error in boundary delineation not only influences the glacier area but the glacier volume. We refer to this error as boundary uncertainty-related volume error. This error in area implies a corresponding error in volume, which could at a first glance be thought to be not large, because the uncertainty in boundary delineation occurs where the ice thickness is expected to be smallest, namely near the zero-thickness points at the contact with the glacier valley walls and at the glacier front of land-terminating glaciers. However, the relatively scarce coverage of the glacier surface by the radar profiles, especially near the glacier walls, implies that an improper definition of the glacier limits has an impact on the ice thickness interpolation that extends well into the glacier.

To estimate this error, we define the boundary uncertainty as a fraction (p) of the total glacier area, A. Following a conservative criterion, we evaluate ε_{VB} as the increment in the volume of the ice thickness-DEM when we change the glacier area by an amount pA. In the DEM, this corresponds to a shift in the glacier boundary in / outwards (note we don't consider random shifts at each point in the boundary but simultaneous increases or reductions of the area).

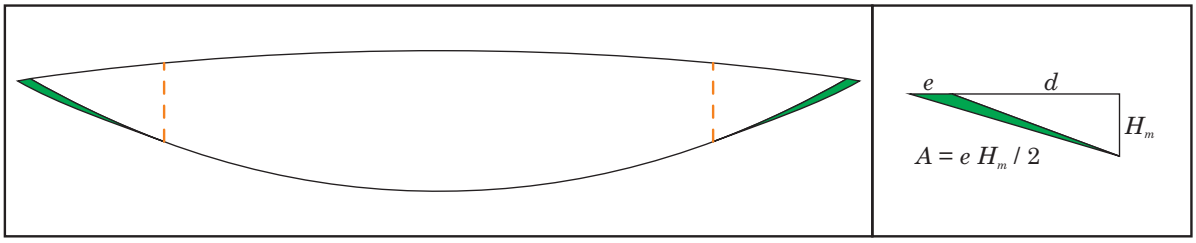


Figure 3.13: Volume error induced by boundary uncertainty

We first evaluate the volume involved in this error considering a land-based glacier, with a zero ice thickness boundary. Figure 3.13 shows in a a cross-section of a glacier how a shift in the boundary impacts the ice thickness in the inner parts until reaching the nearest GPR measurement. The error section (in green) is $eH_m/2$. This triangle is characterized by the glacier mean values: e is the horizontal distance of the boundary shift, H_m is the mean ice thickness for a distance d between the boundary and the closest GPR measurement. Based on our experience, we estimate H_m as half of the mean ice thickness of the glacier. If we make a three-dimensional extension of this error section, we get an error ring around the glacier with a triangular section. An approximation to the volume involved is a triangular-based prism with length equal to the perimeter of the glacier boundary. Given that $pA = e * d$, we do not actually need to know e neither d. So the volume of the prism:

$$\varepsilon_{VB} = \frac{1}{2} pV \tag{3.17}$$

is a reasonable approximation to the volume error induced by uncertainty in the glacier boundary definition. We have choose as uncertainty in boundary delineation the 8 % error in area estimated for the most recent Svalbard glacier inventory (Köning et al., 2013) for land based glaciers.

In cases where the glacier boundary is not completely zero-ice thickness defined (i.e. if existing calving fronts or ice divides) we can still use Equation 3.17 but including a weight for the land based area fraction f_l. The remaining area (where the boundary has non zero thickness), the volume involved is obtained by multiplying the non-zero boundary area fraction by the mean thickness in found in the non-zero boundary.

Error in volume error due to ice-thickness errors

Considering a given error free glacier boundary, we are now estimating the ε_{VH}, that is the error in volume induced by the ice thickness errors at the grid cells. We already expressed the glacier volume as as sum of the individual cell volumes (Equation 3.10). To estimate this error we want to know to what extent exits correlation between the grid values. This is estimated from the semivariogram (explained in Section 3.6.2) relating the correlation of ice thickness measurements (from GPR) with the distance. The *range*, R, of the semivariogram (Figure 3.8) indicates the maximum separation distance where we can expect correlation between pairs of points. We use this distance to estimate a number of independent data points we have in the grid. Let's break the glacier in a number N_R independent subgrids in a way that their centres are separated among each other by a distance R. We can also consider anisotropy (Cressie, 1988) to obtain the range in the two orthogonal directions R_a, R_b, so we consider N_R independent subgrids keeping distances R_a, R_b among their centres. We then estimate N_R as the number of rectangular subgrids with lengths R_a, R_b could be fit within the glacier area.

$$N_R = \frac{A}{R_a R_b} \tag{3.18}$$

Taking into account that N is the total number of grid cells within the glacier DEM, each independent subgrid will contain an average value of N/N_R cells, with area $A_R = (N/N_R)A_c$ We can write Equation 3.10 as the summation of the products of the area A_{R_j} and mean ice thickness H_{R_j} of each independent subgrid. As the glacier ice thickness-DEM has been divided in N_R independent subgrids we can now estimate the total ice thickness-derived volume errors the root square of the squared summation of the volume errors, ε_{VR_j} , in each of the N_R independent subgrids.

$$\varepsilon_{VH} = \sqrt{\sum_{j=1}^{N_R} \varepsilon_{VR_j}^2} \tag{3.19}$$

This is a conservative approach as within each subgrid we consider a lineal positive dependency between the all cell values (summing their standard deviations). That is how we get the cumulative error within each independent subgrid, ε_{VR_j}, summing the ice thickness-derived volume errors in each of the N/N_R cells within each subgrid. The error in each cell in the grid is expressed as the product of the cell area (A_c) and the ice thickness error in that cell.

So the error in each independent subgrid is:

$$\varepsilon_{VR_j} = \left(\sum_{k=1}^{N/N_R} A_c \varepsilon_{H_k} \right)_j \tag{3.20}$$

can be also expressed as:

$$\varepsilon_{VH} = \sqrt{A_c^2 \sum_{j=1}^{N_R} \left(\sum_{k=1}^{N/N_R} \varepsilon_{H_k} \right)_j^2} \tag{3.21}$$

To evaluate Equation 3.21 we would need to know which exact cells lie within each independent subgrid; we would linearly sum their errors and then make a squared summation between the independent subgrids. However this can be simplified by characterizing glacier DEM with a unique value of the ice thickness error, ε_H that is the standard deviation of the random variable ice thickness error, calculated as the mean square of the ice thickness errors (ε_{H_k}) of the N grid cells of the glacier ice thickness-DEM.

3.7.4 Tests performed on synthetic glaciers

To test the performance of our method, we have compared the estimated and real ice thickness-derived volume error on a sample of synthetic glaciers. Synthetic glaciers were generated interpolating real ice thickness profiles into regular grids using different interpolation methods except with kriging. Then, we calculated the exact volumes for each synthetic glacier ice thickness-DEM. A sample of ten synthetic glaciers were generated.

Then, we asked experienced people to draw different simulated GPR profiles over the synthetic models and extracted ice thickness from the model. We used those synthetic profiles to perform a kriging interpolation and calculated a set of synthetic volumes and errors following our methodology for error estimation. We also calculate the error assuming each node as an independent variable. Results are shown in Table 3.4, and clearly confirm the dependency among the errors as the total volume error becomes negligible when composed as independent variables. Kriging variance systematically yields to greater errors representing a conservative error estimation. Finally, the error calculated according to our methodology performs better in all the cases studied here, giving a more accurate description of the volume differences.

Table 3.4: Volume error computation on synthetic glaciers

Glacier	Vol. interp.	Error	Error as independ.	Kriging Variance	Real Vol.
	(km^3)	(km^3)	(km^3)	(km^3)	(km^3)
Syn. 1	2.80	0.10	0.001	0.21	2.88
Syn. 2	1.02	0.05	0.0001	0.08	1.04
Syn. 3	0.44	0.02	0.0001	0.05	0.45
Syn. 4	0.43	0.03	0.0001	0.08	0.45
Syn. 5	1.24	0.09	0.0001	0.12	1.28
Syn. 6	1.30	0.04	0.001	0.13	1.27
Syn. 7	0.991	0.05	0.001	0.10	1.04
Syn. 8	0.993	0.05	0.001	0.16	1.04
Syn. 9	2.76	0.13	0.001	0.27	2.88
Syn. 10	0.46	0.02	0.0001	0.06	0.45

Chapter 4

An inventory of Svalbard radio-echo sounded glaciers and their associated volume estimates

4.1 Outline

The potential contribution of glaciers and ice caps (GICs) to sea-level rise (SLR) depends on their total volume, and therefore its estimation has recently received much attention. In 2012, the number of glaciers with catalogued volume estimates was only 271 (Cogley, 2012). Due to the scarcity of ice thickness measurements, the global estimates of the volume of GICs are based either on volume-area scaling relationships (e.g. Radić and Hock (2011), Grinsted (2013)) or on physically-based models (Huss and Farinotti, 2012), as presented in Chapter 2. We aim to derive a regional V-A scaling relationship to obtain a reliable estimate of the total ice volume stored in Svalbard glaciers, and therefore to assess its total potential contribution to sea-level rise. The volume data will be based on GPR-retrieved ice- thickness measurements on Svalbard glaciers. We have gathered all the available information related to radio-echo soundings carried out in Svalbard in an updated inventory of radio-echo sounded glaciers. Glacier areas and other glaciological parameters such as length or maximum and minimum altitude are available from the updated version of the Digital Glacier Database for Svalbard (Köning et al., 2013). In this chapter we review the radio-echo soundings carried out in Svalbard and present the ice-thickness distribution for 40 glaciers in Spitsbergen, in addition to that for the ice caps of Austfonna and Vestfonna, and give their computed volumes and associated error estimates. Whenever our volume estimates differ from some previously

published values, we discuss the reason for the discrepancies. Finally, we briefly discuss on the polythermal structure of the studied glaciers on the light of the scattering pattern visible in the available radargrams.

4.2 History of echo soundings in Svalbard aimed to ice-thickness measurements

The earliest radio-echo soundings made in Svalbard was carried out on a small glacier, Foxfonna, in 1972, related to the assessment of a coal mine in the Adventfjorden region (Liestøl, 1974). Some later, during the summer seasons in 1974-1975 and in 1978-1979, researchers from the former Soviet Union conducted extensive helicopter-borne GPR campaigns, obtaining ice thickness data from 87 Svalbard glaciers (including glacier tributaries), from which around 85% were mountain glaciers. The total length of radar profiles reached about 2000 km (Macheret, 1981; Macheret and Zhuravlev, 1982). Airbone-based measurements were taken approximately along the centre line of the glaciers (positioning was visually determined) using high frequency radar equipments, of 440 and 620 MHz. During the first two field seasons (1974-1975) they used a 440 MHz standard altimeter, whereas for the last two seasons (1978-1979) a special-purpose 620 MHz radar equipment was used. They also performed detailed ground-based echo soundings on some glaciers (Austre Brøggerbreen, Voringbreen and Bogerbreen) to determine the ice thickness distribution, subglacial relief and internal layers, and other radio-physical properties (Macheret and Zhuravlev, 1982). In spring 1980, a joint team from the Norsk Polarinstitutt (NPI) and the Scott Polar Research Institute (SPRI) performed 740 km of airborne echo soundings in Svalbard using a SPRI MkIV 60 MHz equipment designed originally for deep cold ice in Antarctica and Greenland (Dowdeswell et al., 1984a), and bed reflections were detected for about 50% of the total profile length. They studied 45 Spitsbergen glaciers, some of them coincident with those formerly studied by the Soviet researchers. In April 1983 and in May 1986, the NPI and SPRI performed airborne echo soundings over Nordaustlandet (Dowdeswell et al., 1986), the island of Kvitøya (Bamber and Dowdeswell, 1990) and the ice masses of Barentsøya and Edgeøya (Dowdeswell and Bamber, 1995) using the same SPRI MkIV 60 MHz equipment that successfully worked in the previous campaign. For positioning they used a ranging system (accurate to ±30 m) from aircraft to ground-based transponders, located by satellite georeceivers, supplemented by the aircraft's navigational instruments and timed crossings of known features. They extensively flew over

Austfonna (the eastern ice cap of Nordaustlandet and the largest in Svalbard), recording profiles every 5 km apart, whereas a 15 km-spaced grid was flown over Vestfonna. In the islands of Barentsøya and Edgeøya they recorded ice thickness and elevation data along 340 km of flight tracks. Ice thickness maps and subglacial bedrock maps were produced for the first time in these areas. Dowdeswell et al. (1984a) explain the discrepancies between the results obtained from the Soviet and the SPRI-NPI campaigns. The maximum ice thickness recorded by the Soviets with the GPR operating at 440 MHz was 250 m, whereas the maximum penetration of the 620 MHz equipment was 540 m due to the antenna gain. The SPRI MkIV sounder recorded a maximum ice thickness of 530 m in 1980. Soviet echo soundings made at 440 MHz did not reach the glacier bedrock in most cases and it led to the misinterpretation of any continuous internal reflection as basal. Reasons for discrepancies with the 620 MHz sounder are not that obvious (since both penetrated approximately similar depths), but echo sounding results from Soviet soundings in Negribreen, Hansbreen and Penckbreen show an inner layer reflection rather than a bed reflection. On the other hand, radio-echo sounding during 1980 with the SPRI MkIV 60 MHz system had two principal advantages over the Soviet 620 MHz equipment: sounding was conducted at a lower radio frequency and flying took place before the start of the melting season. Both reduce the effects of absorption and scattering by inhomogeneities within and on the surface of the glaciers (Dowdeswell et al., 1984b). In a later compilation, (Macheret et al., 1984) acknowledged these errors. They omitted 26 of the 57 glaciers, modified others and left the estimates for others unchanged.

Airborne echo soundings from the seventies and eighties are a valuable source of information. They provided the largest number of glaciers ever sounded in Svalbard up-to-date, giving an insight on the overall ice volume of Svalbard glaciers through Svalbard-specific scaling relationships (e.g. Macheret and Zhuravlev (1982), Hagen et al. (1993)), and confirmed their overall polythermal structure. However, due to the available technology at the time, their quality standards are quite poor as compared with present ones, for example as concerns to positioning systems. We have already mentioned the problems of the high-frequency systems to receive echoes from the glacier bed, often leading to underestimate the ice thickness. The 60 MHz SPRI system recorded the bed reflection 2-3 times deeper on many glaciers (Dowdeswell et al., 1984b), seeming to be correct within $\pm 10\%$ (Hagen and SæTrang, 1991). But neither the Soviet nor the SPRI equipments received any bed echoes from most of the accumulation areas due to the subpolar hydrothermal regime of most Svalbard glaciers, with ice under the accumulation areas usually at the melting point throughout due to firn soaking

during the summer (Hagen and SæTrang, 1991). This causes an increase of the absorption and scattering of radio signals, specially at high frequencies.

4.3 Inventory of radio-echo sounded glaciers in Svalbard

Glacier volume computations are based on GPR-retrieved ice-thickness data. Therefore a GIS-based inventory of all echo-sounded glaciers in Svalbard has been developed in the context of this thesis, being also one of the objectives of the ESF PolarCLIMATE-Svalglac project. The location of the radio-echo sounded glaciers on Svalbard are shown in Figure 4.1, for Spitsbergen, the largest island of the Svalbard archipelago, and in Figure 4.2, for its surrounding islands Nordaustlandet, Barentsøya and Edgeøya.

The inventory is organized on a fieldwork-base, so each different GPR fieldwork campaign, although not specifically focused in the determination of glacier volumes, yield to an entry in the database. There are a total of 313 entries in the inventory that corresponds to 155 different glaciers. However we have determined the glacier volume of just 103 glaciers. The reason for this discrepancy is due to the interest of some GPR campaigns was sometimes restricted to a specific area in the glacier (e.g. to study a englacial channel or to survey the glacier front) where the bunch of measurements were concentrated, meanwhile the remaining glacier area was not surveyed. The oldest compiled echo-soundings are from 1974 and the newest corresponds to the fieldworks carried out in 2013. The old airborne-based echo soundings (Macheret and Zhuravlev, 1982; Dowdeswell et al., 1984a) embody about a 40% of the entries in the inventory, although as it has been pointed out, some of them lacked in accuracy and some did not reach the bottom of the glacier. 15 entries are not due to radio-echo sounding but to CMP measurements. They are included in this inventory as they are of interest when using GPR data.

Table 4.1 summarizes the meta-data that has been compiled for each item in the inventory database. Every glacier included in the inventory has an ID code following the nomenclature introduced by Hagen et al. (1993) or its updated version included in the Digital Glacier Database for Svalbard (Köning et al., 2013). Surge dates are assumed to be complete for tidewater glaciers. However, some land-based glacier surges could be missing. GPR data were requested to the different research groups to carry out an homogeneous processing of the glacier volume estimates and error assessments, as described in Chapter 3. We collected actual GPR ice-thickness data for 36 glaciers, while for 6 others, including the ice caps of Austfonna and Vestfonna, we obtained ice-thickness maps. In cases in which neither GPR ice-

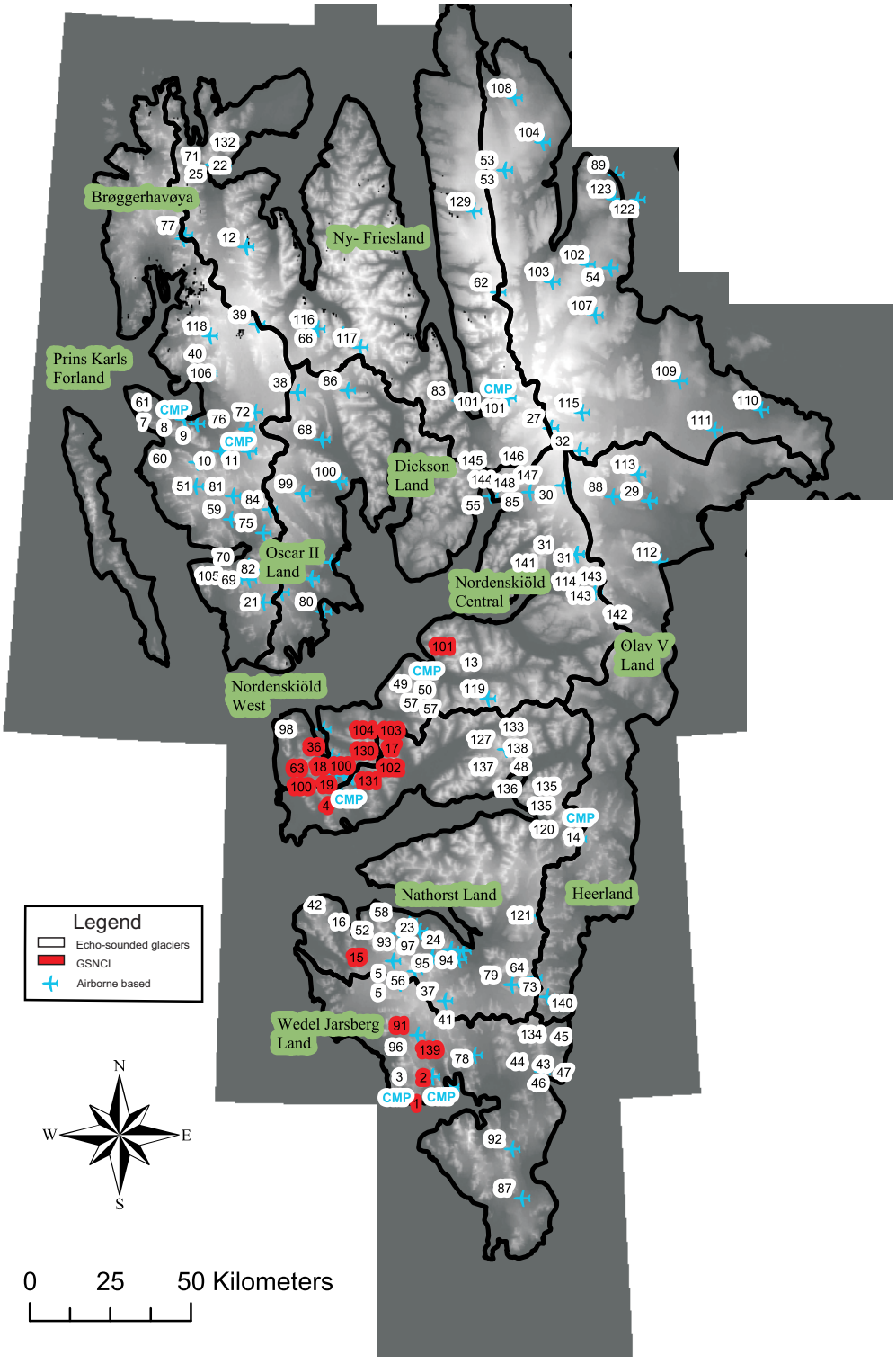


Figure 4.1: Radio-echo sounded glaciers on Spitsbergen. Each glacier is numbered according with the inventory of echo-sounded glaciers available in the Appendix. Airborne echo soundings, mostly done during the seventies and eighties, are denoted by an aeroplane icon. The echo soundings carried out by our research team and colleagues appear as red-coloured. The figure also shows the locations where common mid-point measurements (CMP) have been done for calculating the radio-wave velocity.

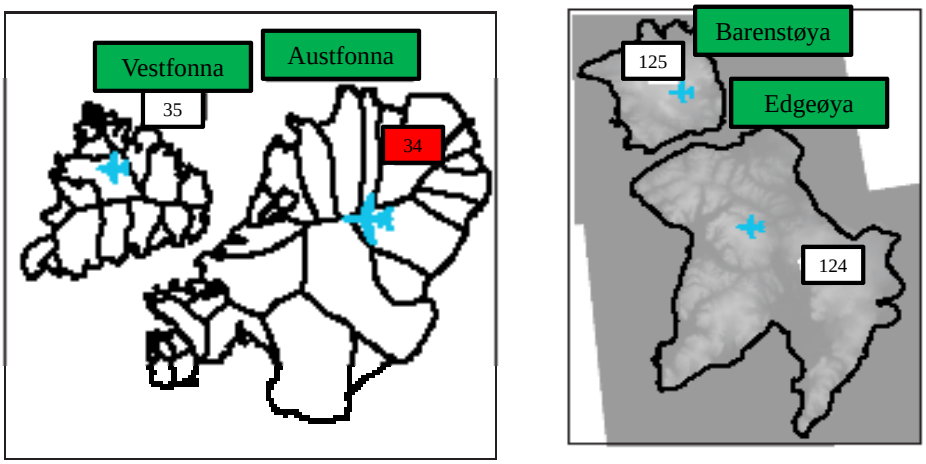


Figure 4.2: Radio-echo sounded glaciers on Nordaustlandet (left) and the islands of Barentsøya and Edgeøya (right). The numbering is according with the inventory of echo-sounded glaciers in the Appendix.

thickness data nor ice-thickness maps were available, but published volumes estimates made with sufficient and reliable data could be found, these were also included in our database of glacier volumes.

4.3.1 Available GPR data

Ground-penetrating radar in glaciology is one of the research focus of the Group of Numerical Simulation in Science and Engineering (GSNCI) of the Technical University of Madrid (UPM), to which the author of this thesis belongs. Figures 4.1 and 4.2 show the glaciers where extensive radio-echo soundings have made by GSNCI, often together with Russian colleagues, and occasionally with Polish and Norwegian colleagues, during fieldwork campaigns starting in 1999. They are mostly distributed over two regions, western Nordenskiöld Land (central Spitsbergen) and Wedel Jarlsberg Land (southern Spitsbergen). In western Nordenskiöld Land, data from thirteen glaciers were collected during several field campaigns between 1999 and 2013 in a joint venture with Russian colleagues (Martín-Español et al., 2013), whereas in Wedel Jarlsberg Land we collected GPR data from eight glaciers during fieldworks between 2004 and 2011 in cooperation with our Polish colleagues (Navarro et al., 2013).

As commented in the background Chapter 1, this thesis has been developed in the context of the ESF-PolarCLIMATE SvalGlac project. This has promoted the interaction and collaboration with many other research institutions that have worked on Svalbard, and has facilitated the collection a large amount of available GPR data sets. Table 4.2 summarizes the radar data sets that we have gathered from different research teams, with detail of the

Table 4.1: Meta data compiled in the Inventory of radio-echo sounded glaciers in Svalbard.

Meta-data	Explanation
Glacier	
ID	According to the Randolph Glacier Inventory
Glacier name	According to the Randolph Glacier Inventory
X-cent	Approx. position of the glacier centre (UTM coordinate)
Y-cent	Approx. position of the glacier centre (UTM coordinate)
Glacier type	Tidewater, land-based, ice cap
Thermal structure	Temperate, cold, polythermal
Bathymetries	If any available, source and year
Boreholes	If any available, source and year
Surge	If any recorded, source and year
Contact Person	
Reference	If published
Fieldwork	
Year	
Radar model	Manufacturer and model
Frequency	Central frequency of the radar system (MHz)
RWV	RWV used for time to thickness conversion ($m\mu s^{-1}$)
Platform	Type of convoy to mount the GPR
Comments	e.g. CMP measurement
Data availability	Yes / No

radar equipments used, their central frequency and the total length of radio-echo sounding profiles.

Table 4.2: GPR surveys, with listing of radar equipment used and total number of km of radar profiles done on each glacier. An asterisk next to the year of the campaign indicates that the radio-echo sounding was done by our research team, often together with Russian/Polish/Norwegian colleagues. Further details, such as the research teams responsible for the fieldwork, are listed in the Inventory in the Appendix.

Glacier	Profile length (km)	Year	Radar equipment	Region
Austre Brøggerbreen	38	1988	Mark II - 8 MHz	Brøggerhalvøya
Austre Lovénbreen	48	2006	PulseEKKO - 50 and 100 MHz	
Midre Lovénbreen	50	1990	Synthetic pulse radar 5-20 MHz	
		1998	HAESCAN IIIv2 - 50 MHz	
		2006	PulseEKKO - 50 and 100 MHz	
Pedersenbreen	46	2009	PulseEKKO - 100 MHz	
Bertilbreen	4	2012	RAMAC - 100 MHz	Dickson Land
Bertrambreen	8.5	2012	RAMAC - 100 MHz	
Svenbreen	34	2012	RAMAC - 100 MHz	
Hornbreen	61	2000	RAMAC - 50 MHz	Heerland
Stauppbreen	7	2000	RAMAC - 50 MHz	
Höganasbreen	30	2001	PulseEKKO - 50 and 100 MHz	Reindalen
		2002		
Marthabreen	49	2005	RAMAC - 50 and 6.5 MHz	
		2007	RAMAC - 50 MHz	
		2009	RAMAC - 50 MHz	
Slakbreen	52	2000	PulseEKKO - 50 and 100 MHz	

Table 4.2: GPR surveys, with listing of radar equipment used and total number of km of radar profiles done on each glacier. An asterisk next to the year of the campaign indicates that the radio-echo sounding was done by our research team, often together with Russian/Polish/Norwegian colleagues. Further details, such as the research teams responsible for the fieldwork, are listed in the Inventory in the Appendix.

Glacier	Profile length (km)	Year	Radar equipment	Region
		2001		
		2002		
Varpbreen	8	2002	PulseEKKO 50 and 100 MHz	
Tellbreen	30	2004	PulseEKKO, RAMAC - 50, 100 MHz	CentralNordenskiöld Land
		2005		
		2009		
		2010		
Larsbreen	6	1994	Synthetic pulse radar - 30-80 MHz	
			320-370 MHz	
Lonyearbreen	Km	1994	Synthetic pulse radar - 30-80 MHz	
			320-370 MHz	
Blekumbreen	14	2013*	VIRL6 - 20 MHz	
Aldegondabreen	40	1999*	VIRL2 - 15 MHz	West Nordenskiöld Land
Baalsrudbreen	8	2013*	VIRL6 - 20 MHz	
Dalhfonna Austre	8	2010*	VIRL6 - 20 MHz	
Dalhfonna Vestre	26	2012*	VIRL6 - 20 MHz	
Erdmanbreen	31	2012*	VIRL6 - 20 MHz	

Table 4.2: GPR surveys, with listing of radar equipment used and total number of km of radar profiles done on each glacier. An asterisk next to the year of the campaign indicates that the radio-echo sounding was done by our research team, often together with Russian/Polish/Norwegian colleagues. Further details, such as the research teams responsible for the fieldwork, are listed in the Inventory in the Appendix.

Glacier	Profile length (km)	Year	Radar equipment	Region
Fridtjovbreen	180	2006*	RAMAC - 200 MHz	West Nordenskiöld Land
		2012*	VIRL6 and VIRL7 - 20 MHz	
Gleditchfonna	19	2011*	VIRL6 - 20 MHz	
Grønfjorbreen Austre	53	2010*	VIRL6 - 20 MHz	
Grønfjorbreen Vestre	102	2010*	VIRL6 - 20 MHz, RAMAC - 100 MHz	
Marstranderbreen	22	2013	VIRL6 - 20 MHz	
Passtjelbreen Austre	18	2013*	VIRL6 - 20 MHz	
Passtjelbreen Vestre	9	2013*	VIRL6 - 20 MHz	
Tavlebreen	18	2010*	RAMAC, VIRL6-7 - 200, 100, 20 MHz	
Tungebreen	13	2011*	VIRL6 - 20 MHz	
Ariebreen	7	2006*	RAMAC - 200 MHz	Wedel Jarlsberg Land
		2007	RAMAC - 25 MHz	
		2009	RAMAC - 25 MHz	
Finsterwalderdbreen	N/A	1994	Synthetic pulse radar - 30-80 320-370,600-650,950-1000 MHz	
Hansbreen	90	2008*	RAMAC - 25 MHz	
		2009*	VIRL6,7 - 20 MHz	

Table 4.2: GPR surveys, with listing of radar equipment used and total number of km of radar profiles done on each glacier. An asterisk next to the year of the campaign indicates that the radio-echo sounding was done by our research team, often together with Russian/Polish/Norwegian colleagues. Further details, such as the research teams responsible for the fieldwork, are listed in the Inventory in the Appendix.

Glacier	Profile length (km)	Year	Radar equipment	Region
Paierlbreen	73	2011*	VIRL7- 20 MHz)	Wedel Jarlsberg Land
		2004*	VIRL6 - 20 MHz	
		2006*	VIRL6,7 - 20 MHz	
		2008*	RAMAC- 25 MHz	
		2011*	VIRL7 - 20 MHz	
Recherchebreen	51	2009	RAMAC - 25 MHz	
		2011*	VIRL7 - 20 MHz	
Renardbreen	42	2008	RAMAC - 25 MHz	
Scottbreen	10	2010	RAMAC - 25 MHz	
Torellbreen Austre	73	2004*	VIRL6 - 20 MHz	
		2006*	VIRL6,7 - 20 MHz	
		2011*	VIRL7 - 20 MHz	
		2013	RAMAC- 30 MHz)	
Werenskioldbreen	37	2008	RAMAC - 25 MHz	
Austfonna ice cap	4800	1983	SPRI MkIV - 60 MHz	Nordaustlandet
		1986	SPRI MkIV - 60 MHz	
		2007	DTU- 60 MHz	

Table 4.2: GPR surveys, with listing of radar equipment used and total number of km of radar profiles done on each glacier. An asterisk next to the year of the campaign indicates that the radio-echo sounding was done by our research team, often together with Russian/Polish/Norwegian colleagues. Further details, such as the research teams responsible for the fieldwork, are listed in the Inventory in the Appendix.

Glacier	Profile length (km)	Year	Radar equipment	Region
Vestfonna ice cap	880	2008*	VIRL6- 20 MHz	Nordaustlandet
		1983	SPRI MkIV - 60 MHz	
		1986	SPRI MkIV - 60 MHz	
		2008	Pulsed radar system- 10 MHz	
		2009	Pulsed radar system- 10 MHz	

4.4 Ice-thickness maps and glacier volumes

Following the data assimilation, interpolation and error estimation techniques described in Chapter 3, we have compiled the ice-thickness maps for the glaciers whose ice-thickness data were available from radio-echo sounding surveys, and calculated their volumes and associated error estimates.

There were some exceptions in which the original GPR (X,Y,H) data were not available: from certain sources we got interpolated ice-thickness maps in digital version, or maps showing the ice thickness contour lines in paper version, or internal reports displaying the GPR profiles over the glacier together with their volume calculations. This was valuable information that we took advantage of, though in each case it was required a particular data-treatment procedure. Glacier volume can be directly inferred from ice-thickness maps, and thus the glacier volumes given in Table 4.3 do not differ from the original volume estimates. In these cases the interpolation method is normally unknown, as is the measurement and interpolation error, unless given in any available publication. Within our dataset, we faced this situation for Finsterwalderbreen and Tellbreen and the two largest ice caps, Austfonna and Vestfonna. In the case of Tellbreen, it existed a volume error estimate in the original reference (Bælum and Benn, 2010), and that is the one used in Table 4.3. The volume of

Finsterwalderbreen was published in Nuttall et al. (1997) and in Nuttall (2001) but it lacked an estimate of its accuracy. The volume of Vestfonna ice cap was published in Pettersson et al. (2011), accompanied by its error estimate. However, the latter seemed unreasonably low and, consequently, we recalculated it from the individual error sources following the technique described in Section 3.7. The ice volume of Austfonna ice cap has been published in (Dowdeswell and Benham, 2008), and some later in Dunse (2011). Neither of them gave a volume error estimate, although they gave error estimates for the individual error sources contributing to the error in volume. Consequently, we calculated the error value appearing in Tables 4.3 and 4.3 from the mentioned error sources, following the methodology explained in Section 3.7. The volume of Austre Brøggerbreen was calculated from the digitization of the ice-thickness contour lines previously published by Björnsson et al. (1996). This volume lacks an error estimate. The last exceptions are those of Longyearbreen and Larsbreen, where the only available information was a report displaying a layout of the GPR profiles. Fortunately it contained the ice volume estimates for both glaciers, which we have included in Table 4.3. For these last two cases, we give the illustrations from the original sources in figures 4.5d and 4.5e.

The computed glacier areas and volumes are shown in Table 4.3, together with their error estimations, computed as explained in Section 3.7. We also show descriptive values of the glaciers such as the mean (H_{mean}) and the maximum values (H_{max}), with their attached uncertainties $\varepsilon_{H_{mean}}$ and $\varepsilon_{H_{max}}$. The errors ε_{GPR} and ε_{GPS} correspond to the root mean squared summation of the variables ε_{HGPR} and ε_{HGPS} defined in Section 3.7 and calculated for each measured data. The error ε_{Int} is the root mean squared summation of the interpolation error ε_{HInt} defined in Section 3.7 and calculated on each node of the grid.

The individual areas, volumes and average ice thickness of the glacier units analysed cover a wide range of values, lying within 0.373-8105 km^2, 0.01-2559 km^3 and 27-319 m, respectively. The maximum recorded ice thickness, 619±13 m, corresponds to Austre Torellbreen, in the Amundsenisen Icefield, Wedel Jarlsberg Land, although deeper ice thickness have been found in this icefield, reaching 646±13 m in the glacier basin of Vestre Torellbreen (personal communication from Evgeny Vasilenko). The largest average thickness (319±30 m) corresponds to the Austfonna ice cap. The total area and volume of the ensemble of Svalbard glaciers for which we have available ice volumes computed from GPR data are 11,473.34±338.35 km^2 and 3,135.731±123.341 km^3, respectively. The relative errors in volume are in general below 10%, except for Midre Lovénbreen and Tellbreen. In Tellbreen, as commented above, we used

the error estimate given in the original source (Bælum and Benn, 2010). In Midre Lovénbreen we computed the individual error sources, any of them leading to values larger than average,as shown in Table 4.3. We find the reason to this large volume error in the high degree of correlation among the data, deriving a high dependency among the errors calculated at each grid cell an a consequent large final volume error(see Section 3.7.3). In general, we have obtained errors larger than those usually found in the literature, which we believe that are unrealistically small because they are often based on the assumption that all error sources are independent.

Figures 4.8 to 4.11 show the location of the different studied regions in Svalbard, the layout of the GPR profiles made on each glacier, and the corresponding ice-thickness maps.

Table 4.3: Estimated area based on the boundaries of the RGI, calculated ice volume from GPR ice-thickness data, average and maximum ice thickness for each glacier, all with their estimated accuracy, and main components of the error in ice thickness. An asterisk next to the glacier name indicates a new volume estimate, i.e. that it does not appear in Cogley (2012) catalogue of glacier volumes, whereas a cross indicates that the volume is an improved estimate with respect to that included in Cogley (2012) catalogue.

Glacier	A	εA	V	εV	εV	H_{mean}	εH_{mean}	H_{max}	εH_{max}	εGPR	εGPS	εInt
	(Km^2)		(Km^3)		(%)	(m)				(m)		
Aldegondabreen$^+$	7.18	0.29	0.468	0.031	6.6	65	7	191	25	5.74	14.21	6.96
Ariebreen*	0.37	0.01	0.010	0.001	7.3	27	3	78	3	2.83	2.15	2.95
Baalsrudbreen*	2.7	0.11	0.077	0.004	5.6	28	3	98	5	4.34	1.51	4.18
Bertilbreen$^+$	3.82	0.15	0.285	--	--	75	--	142	--	--	--	--
Bertrambreen*	3.04	0.12	0.199	0.011	5.5	66	6	147	3	1.95	0.55	4.86
Blekumbreen*	2.16	0.09	0.083	0.006	6.8	38	4	106	5	4.35	1.53	5.59
Brøggerbreen Austre$^+$	10.25	0.41	0.756	--	--	74	--	154	--	--	--	--
Dalhfonna Austre$^+$	2.55	0.10	0.184	0.012	6.5	72	7	189	5	4.936	0.85	8.55
Dalhfonna Vestre$^+$	6.92	0.28	0.259	0.025	9.7	37	5	151	6	4.38	3.93	9.95
Erdmanbreen$^+$	8.96	0.36	0.823	0.041	5	92	9	190	5	4.74	2.5	10.63
Finsterwalderbreen*	29.00	1.16	3.500	--	--	121	--	260	--	--	--	--
Fridtjovbreen$^+$	50.37	2.01	5.433	0.246	4.5	108	10	265	16	5.17	8.81	18.55
Gleditchfonna*	2.76	0.11	0.076	0.005	6.9	27	3	79	4	4.33	1.94	5.17
Grønfjordbreen Austre$^+$	8.41	0.34	0.671	0.046	6.8	80	8	162	5	4.63	1.70	7.78
Grønfjordbreen Vestre*	18.09	0.72	1.775	0.094	5.3	98	9	215	5	4.75	1.41	20.41
Hansbreen*	64.16	2.57	10.752	0.729	6.8	169	18	384	9	5.81	5.13	18.74
Höganasbreen*	11.49	0.46	0.733	0.066	9	64	8	265	6	3.26	10.84	14.21
Hornbreen*	173.28	6.93	18.240	1.228	6.7	105	9	329	6	2.92	2.61	20.92
Larsbreen*	2.96	0.12	0.152	--	--	49	--	--	--	--	--	--
Longyearbreen*	2.52	0.10	0.132	--	--	53	--	115	--	--	--	--

Table 4.3: Estimated area based on the boundaries of the RGI, volume, average and maximum ice thickness for each glacier, with their estimated accuracy, and main components of the error in ice thickness.

Glacier	A	εA	V	εV	εV	H_{mean}	εH_{mean}	H_{max}	εH_{max}	εGPR	εGPS	εInt
	(Km^2)		(Km^3)		(%)	(m)				(m)		
Lovénbreen Austre*	5.01	0.20	0.376	0.026	7.0	75	8	160	4	2.59	1.08	12.26
Lovénbreen Midre+	5.20	0.21	0.257	0.034	13.5	50	8	184	4	3.33	0.75	13.68
Marstanderbreen*	6.92	0.55	0.233	0.017	7.1	34	4	125	4	4.36	2.37	9.68
Marthabreen*	15.11	0.60	0.961	0.075	7.9	64	7	209	3	2.85	2.32	13.04
Paierlbreen*	99.19	3.97	13.265	0.639	4.8	135	13	526	11	6.03	2.41	27.26
Passfjellbreen Austre*	5.13	0.41	0.198	0.015	7.5	39	4	87	5	4.33	4.34	7.21
Passfjellbreen Vestre*	2.32	0.19	0.103	0.007	6.8	44	5	108	5	4.30	4.34	8.16
Pedersenbreen*	6.30	0.25	0.398	--	--	63	--	183	9	--	--	--
Recherchebreen+	136.31	5.45	27.284	2.205	8.1	161	20	533	11	7.99	0.81	26.91
Renardbreen*	30.58	1.22	5.141	0.224	4.4	168	15	348	8	5.67	1.69	17.24
Scottbreen*	4.71	0.19	0.301	0.019	6.4	64	7	167	5	4.01	0.82	11.17
Slakbreen*	36.69	1.47	4.303	0.219	5.1	117	11	282	6	3.55	5.82	14.34
Stauppbreen*	15.33	0.61	1.197	0.125	10.5	78	10	161	4	3.02	0.77	8.37
Svenbreen*	3.72	0.15	0.217	0.010	4.5	58	5	137	3	1.72	1.36	3.11
Tavlebreen*	8.02	0.32	0.426	0.019	4.5	53	5	128	3	3.12	1.07	15.72
Tellbreen*	3.00	0.12	0.150	0.030	20.0	50	--	99	--	5.80	--	--
Torellbreen Austre*	140.99	5.64	31.981	1.288	4.1	226	20	619	13	7.21	1.57	62.08
Tungebreen*	2.88	0.12	0.093	0.006	6.3	32	3	88	5	4.28	1.39	6.49
Varpbreen*	1.33	0.05	0.068	0.006	9.5	51	6	210	4	2.03	2.63	7
Werenskioldbreen+	26.60	1.06	3.173	0.237	7.5	119	13	284	7	4.58	1.78	27.91
Austfonna+	8105	324.2	2559	74.888	3.0	319	30	587	--	--	--	--
Vestfonna+	2402	96.08	442	31.221	7.1	184	20	413	--	22.8	--	9.5
TOTAL	11473.34	338.35	3135.731	66.447								

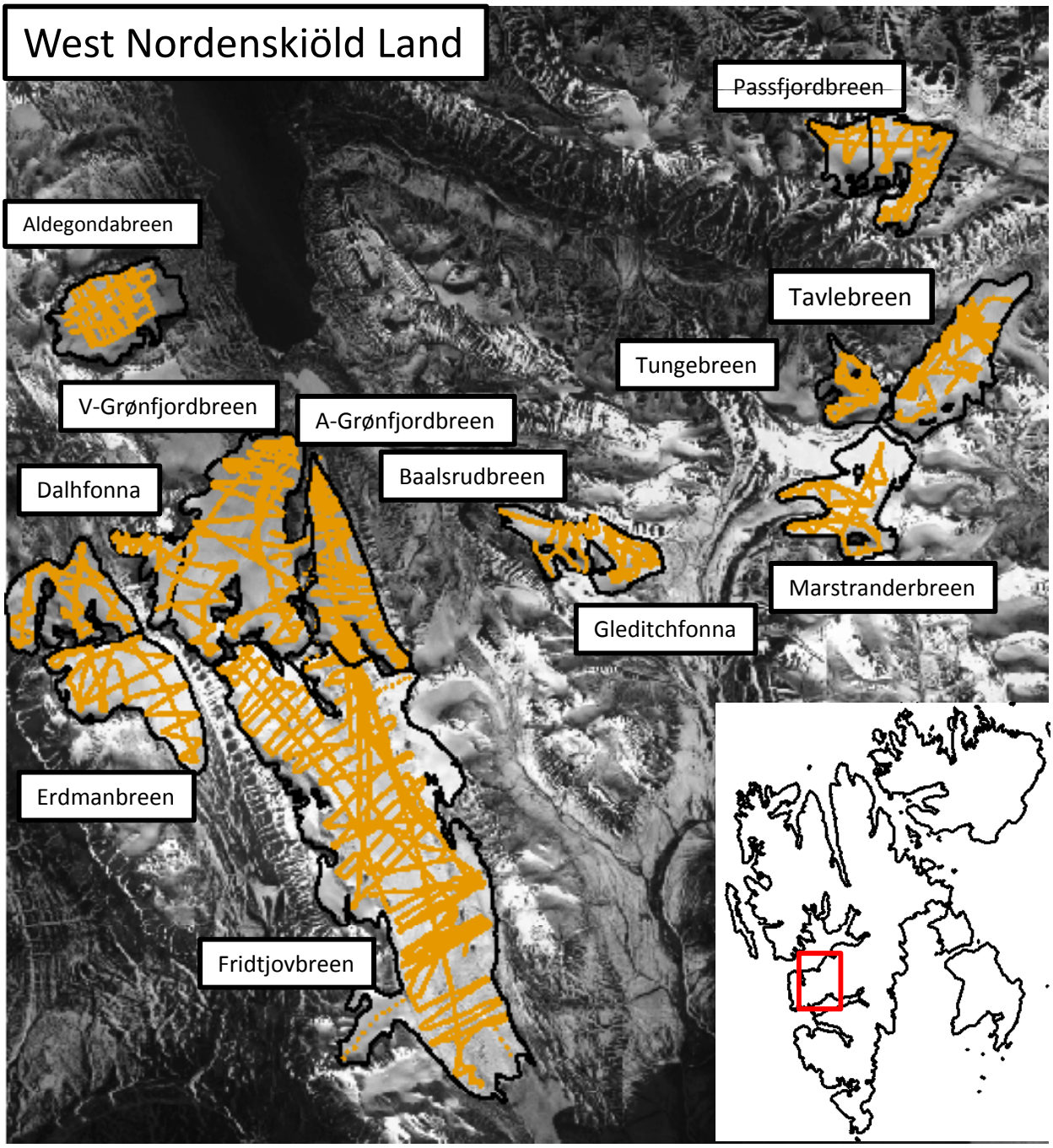


Figure 4.3: GPR profiles carried out on western Nordenkiöld Land glaciers, undertaken by GSNCI and collegues from the Russian Academy of Sciences between 1999 and 2013. Published results can be found in Navarro et al. (2005); Lavrentiev et al. (2011) and Martín-Español et al. (2013).

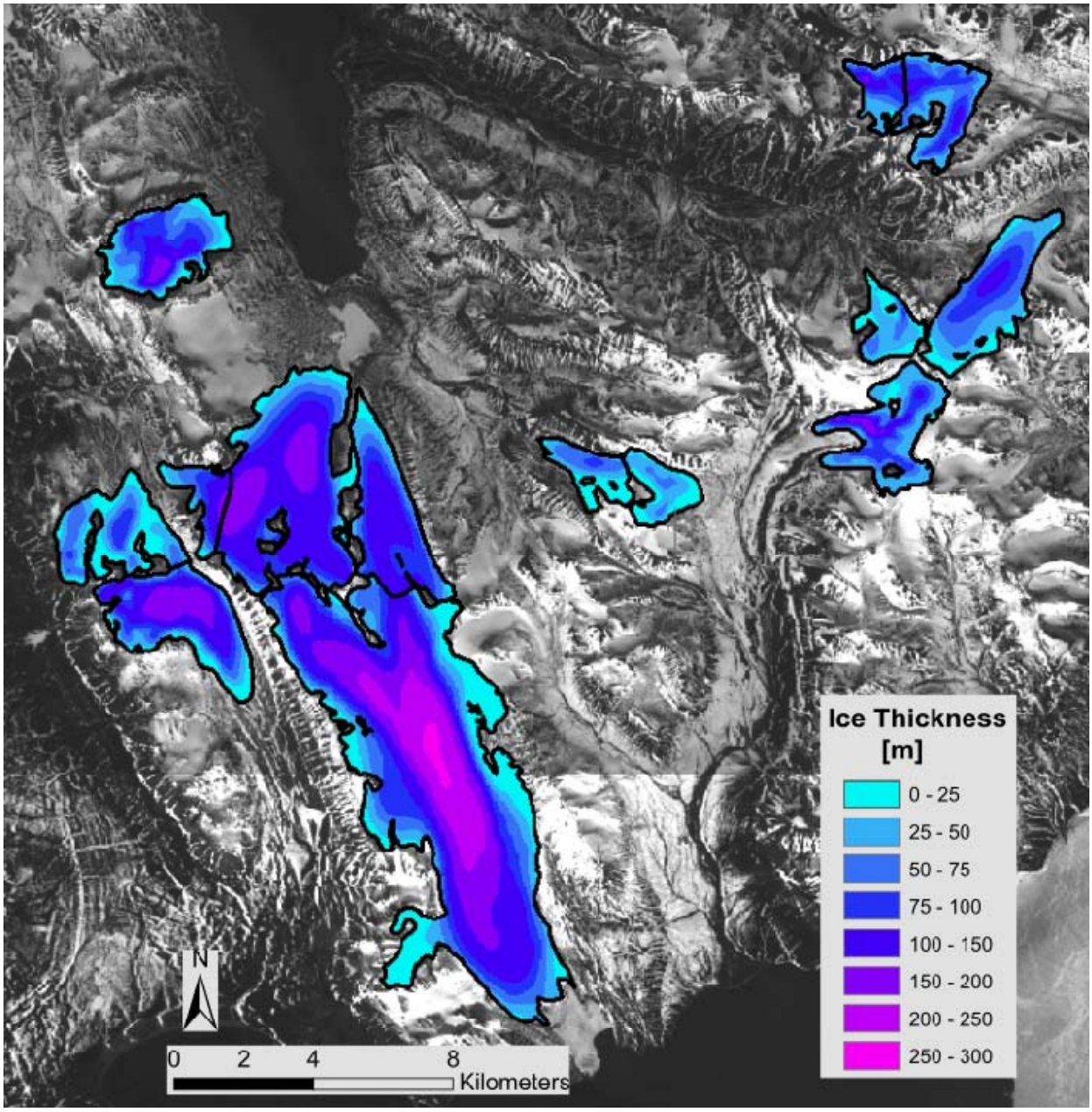


Figure 4.4: Ice thickness map of West Nordenkiöld Land glaciers (Martín-Español et al, 2013). The individual areas, volumes and average ice thickness lie within 2.6-50.4 km^2, 0.08-5.48 km^3 and 27-108 m, respectively. The maximum recorded ice thickness, 265±15 m, corresponds to Fridtjovbreen, which has also the largest average thickness (108±1m). The total area and volume of the ensemble are 133.21±4.53 km^2 and 10.817±0.275 km^3, respectively.

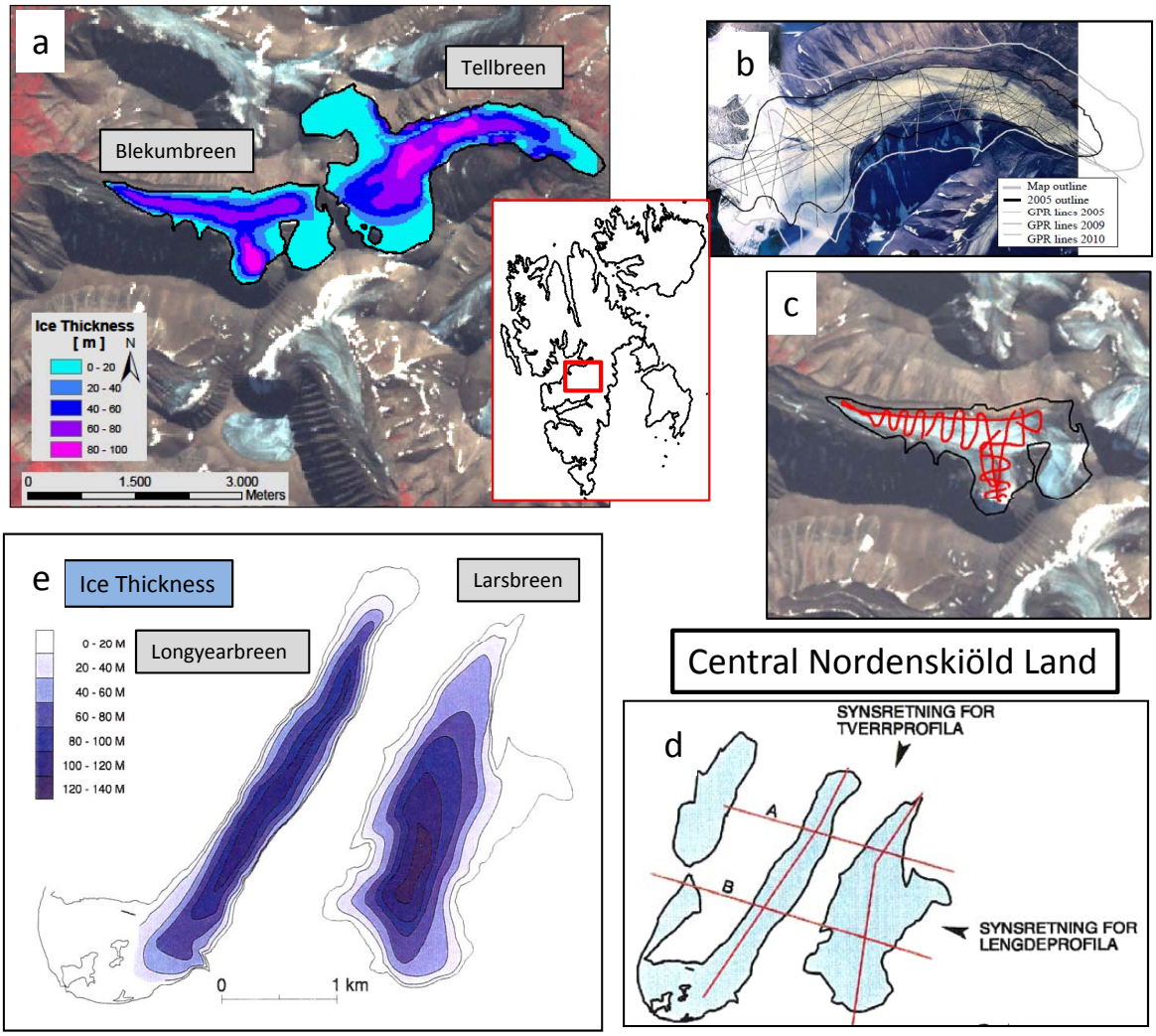


Figure 4.5: Ice thickness map and GPR profiles on Central Nordenskiöld Land glaciers. GPR data from Larsbreen and Longyearbreen were provided by J.O. Hagen from Oslo University and were published in Etzelmüller et al. (2000). Data from Tellbreen was provided by D.Benn (UNIS) and their published study on this glaciers is found on Bælum and Benn (2010). Radar data on Blekumbreen were obtained by GSNCI and colleagues from the Russian Academy of Sciences in spring 2013.

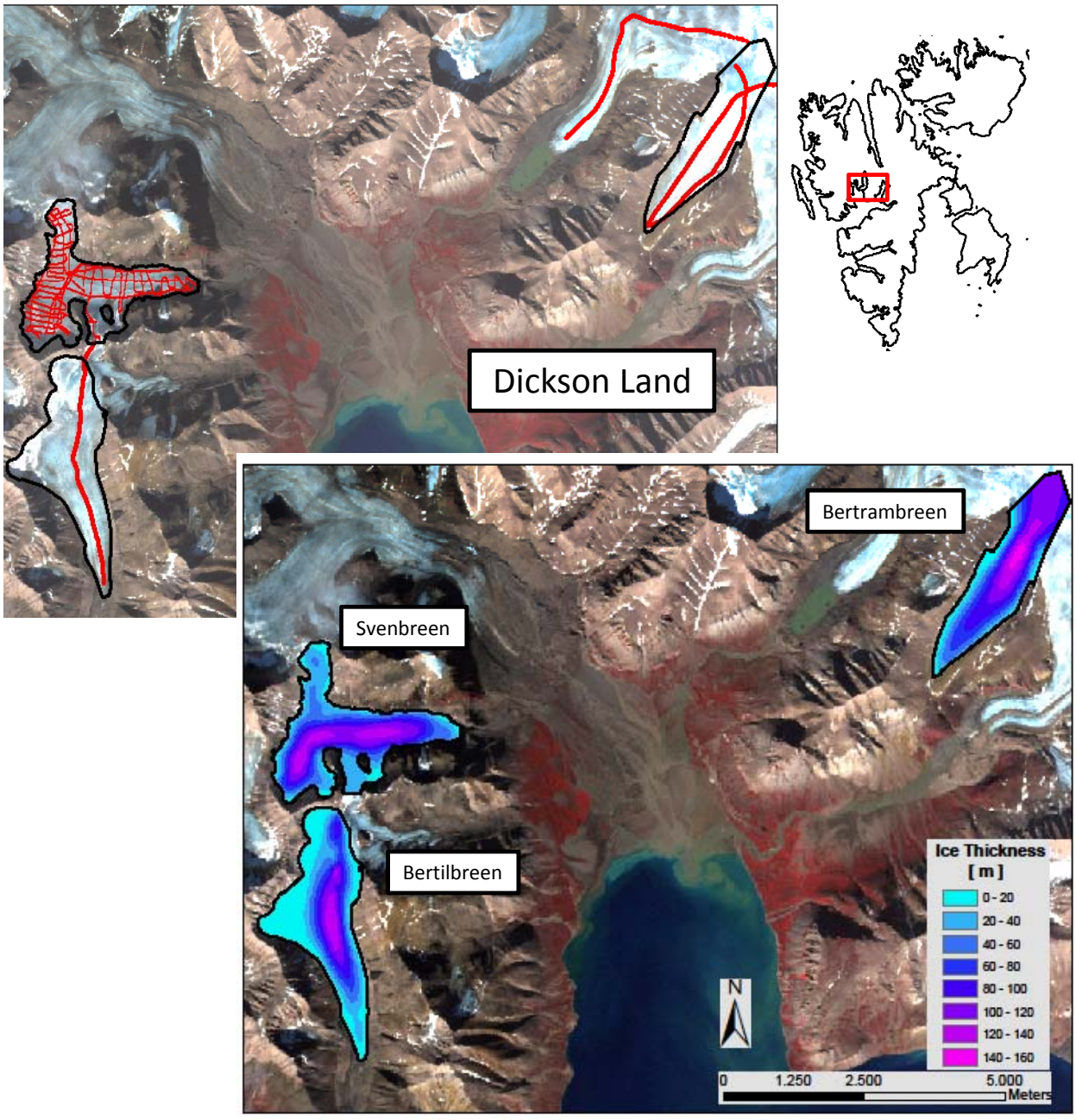


Figure 4.6: Ice thickness map and GPR profiles on three glaciers located on Dickson Land. These GPR surveys were undertaken and provided by K.Malecki, from Adam Mickiewicz University (Malecki, 2013). They have an average ice thickness of 66±8 m, and the maximum depth is reach in Betrambreen at 147±3 m.

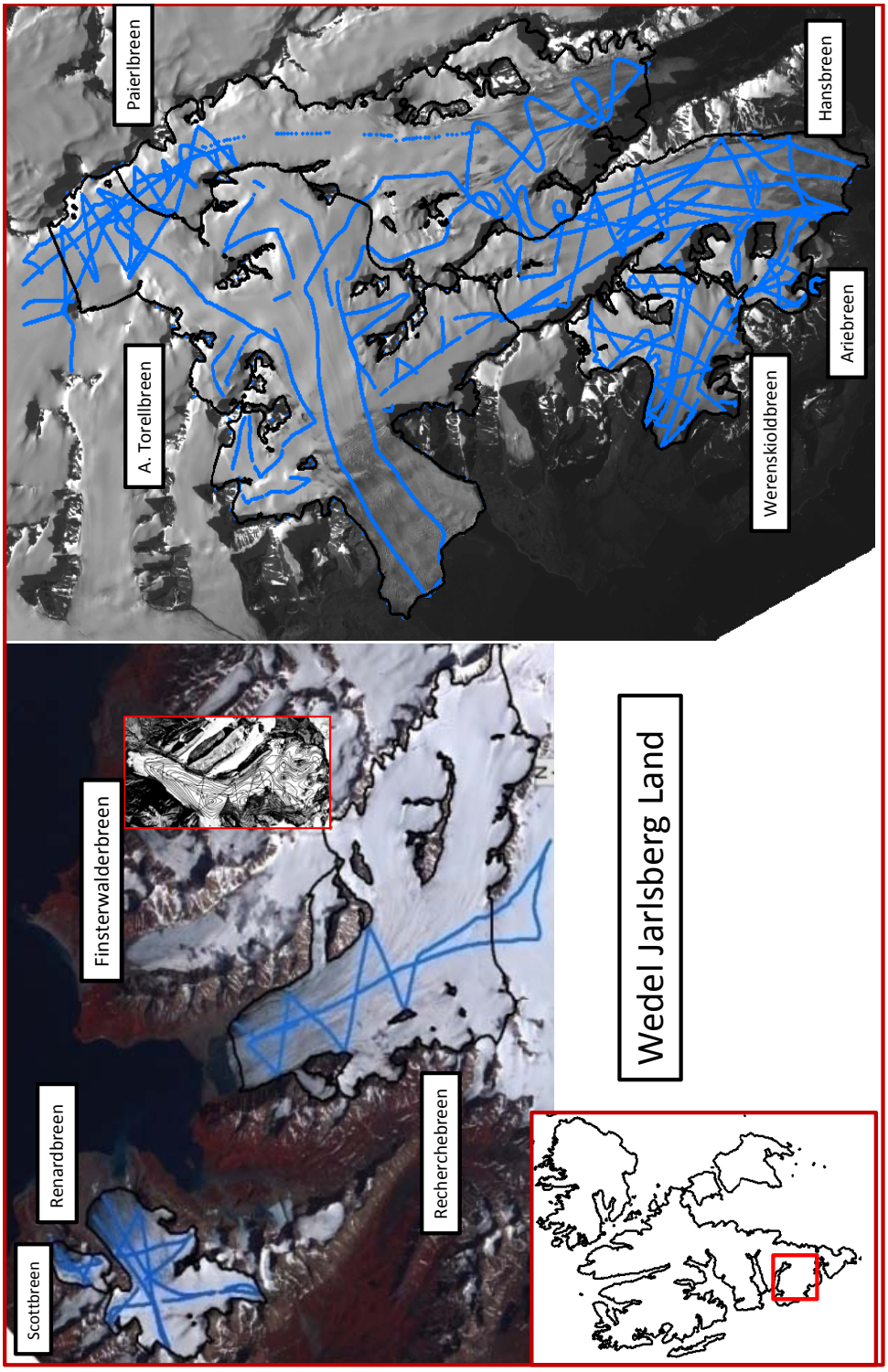


Figure 4.7: GPR profiles on Wedel Jarlsberg Land glaciers. The gross of the GPR surveys were undertaken by GSNCI and collegues from the Department of Geomorphology, University of Silesia (Poland) and the Institute of Geography, Polish Academy of Science, between 2007 and 2013. GPR data from Amundsenisen plateau, within Paierlbreen and A. Torellbreen basins, recorded in 2004 and 2006, was kindly offered by A. Glazovsky, from the Russian Academy of Sciences. The ice thickness map of Finsterwalderbreen is available at A.M. Nuttal Ph.D thesis (1997). Published results can be found on Grabiec et al. (2012); Nuttall et al. (1997)

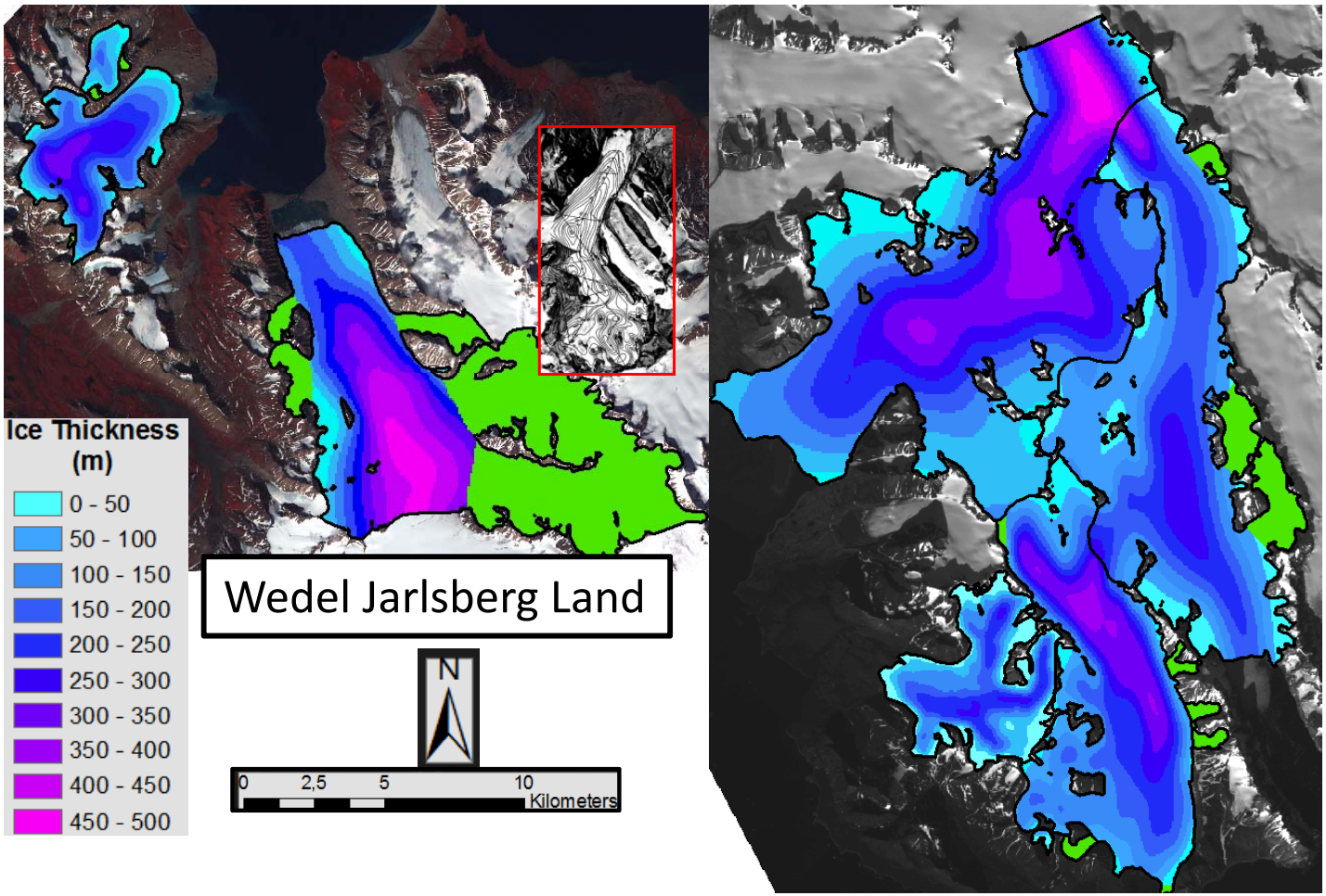


Figure 4.8: Ice thickness map of Wedel Jarlsberg Land glaciers (Navarro et al., 2013). The green areas are unsurveyed tributary glaciers whose volumes were estimated using the procedure described in section **??** The total area and volume of the ensemble are 502.91±18.60 km^2 and 91.91± 2.75 km^3, respectively. The individual areas, volumes and average thickness show large spans, of 0.37-140.99 km^2, 0.01-31.98 km^3 and 28-227 m, respectively. The maximum ice thickness, reaching 619±13 m, is found in the northernmost part of Austre Torellbreen, near its ice divide with Vestre Torellbreen, within the Amundsenisen ice field.

4.4.1 Comparison with other volume estimates in the literature

For some of the studied glaciers there are previous volume estimates in the literature. Some of them, even if being based on the same GPR data sets, report glacier volumes slightly different from those given here. We explain below the reason for the differences.

The majority of the glacier volumes previously reported for Svalbard glaciers were based either on volume-average thickness relationships (Hagen et al., 1993) or on estimates using airborne radio-echo sounding data along glacier centre lines and assuming a parabolic cross-section (Macheret and Zhuravlev, 1980; Macheret, 1981; Macheret and Zhuravlev, 1982). These volumes are part of Cogley's compilation of worldwide glacier volumes (Cogley, 2012). Compared against our volume estimates, the previous estimates of areas and volumes are larger, as is expected considering the overall thinning of Svalbard glaciers during the recent decades (Nuth et al., 2007, 2010). The only exception is that of Recherchebreen, simply because the glacier boundary has been modified incorporating some tributary glaciers to the main basin. Excluding this case, the volume estimates available at Cogley's compilation are about 28% larger than our volume estimates and 16% larger their respective areas. However, these changes do not imply significant changes in the volume-area relationship.

The volume of Aldegondabreen reported in Navarro et al. (2005) was 0.558 (km^3), without an accompanying error estimate. Our present volume estimate, based upon the same GPR field data, is about 16% smaller. This discrepancy is mostly introduced by the removal, in our volume estimates, of the radar profiles parallel and close to the very steep side walls of Aldegondabreen. This was recommended by the results of our crossover analysis described in Section 3.3. Removing such profiles resulted in smaller glacier thickness near both the northern and southern side walls. In these areas, a large amount of seasonal snow remains accumulated in early spring and, given the high RWV of dry snow (typically 215-255 $m\mu s^{-1}$, e.g. Harper and Bradford (2003)), the glacier thickness calculated for these zones by Navarro et al. (2005) are expected to be overestimated, leading to a larger total volume.

Our volume estimate for Hansbreen, a tidewater glacier in Wedel Jarlsberg Land, is about 1 km^3 (9%) smaller than that recently published in Grabiec et al. (2012). The main reason is that the outlines of this glacier in the Digital Glacier Database for Svalbard (used here) and in Grabiec et al. (2012) differ substantially at the ice divide between Paierlbreen and Hansbreen, implying a difference in the surface area of Hansbreen, which is some 8 km^2 larger in the Digital Glacier Database for Svalbard. Additionally, Grabiec et al. (2012) used a lower RWV (164 m μs^{-1}) for the time-to-depth conversion, thus further contributing to a smaller

volume.

Saintenoy et al. (2013) calculated the ice volume of Austre Lovénbreen as 0.3487±0.041 km^3, a 7% smaller than our estimate. The most likely reason for this discrepancy is that they considered a different glacier boundary, implying a surface area of 4.6 ±0.28 km^2, which is 9% smaller than the one that we used.

Malecki (2013) calculated the volumes of the glaciers in the region of Reindalen using a slightly different glacier boundary. The most noticeable change occurred in Bertranbreen, a glacier partially bounded with an ice divide. The impact in the volume computation is larger if the shift of the glacier boundary happens with an ice divide, where the ice thickness are larger, than with a land-terminating glacier. In this case, both the glacier area and volume computed in Malecki (2013) was smaller than those reported in Table 4.3.

4.4.2 Review of the thermal structure of the analysed glaciers

The presence or absence of scattering in the radargrams has often been used to interpret the hydrothermal structure of the glacier (e.g. Navarro and Eisen (2010)). On this basis, the majority of the radio-echo sounded glaciers in Svalbard have been interpreted as polythermal, with an upper layer of cold ice (at temperature below the pressure melting point) on top of a temperate ice layer (temperature at the pressure melting point) in their ablation zones, and temperate ice below the firn layer in the accumulation zones (Pälli, 2003). We summarize below the main interpretations of the hydrothermal structure of Svalbard glaciers found in the literature, with emphasis on the two main regions which have been the focus of the GPR fieldwork by our research team (GSNCI), together with Russian and Polish colleagues.

- Wedel Jarlsberg Land: To our knowledge, the hydrothermal structure of the glaciers studied in this region has been discussed in the literature for Hansbreen (e.g. Dowdeswell et al. (1984b,a); Macheret and Zhuravlev (1982); Jania (1996); Moore et al. (1999); Pälli et al. (2003a); Grabiec et al. (2012)), Recherchebreen (e.g. Dowdeswell et al. (1984b); Macheret and Zhuravlev (1982)), Werenskioldbreen (e.g. Dowdeswell et al. (1984b,a); Macheret and Zhuravlev (1982); Pälli et al. (2003a)), Finsterwalderbreen (Ødegård et al., 1997) and Ariebreen (Lapazaran et al., 2013), all of them polythermal except the latter, which is entirely made of cold ice. We have recently interpreted that Austre Torellbreen, Paierlbreen, Renardbreen and Scottbreen have also a polythermal structure (Navarro et al., 2013).

- Western Nordenskiöld Land: The hydrothermal structure of Fridtjovbreen, prior to its

surge in the nineties (Murray et al., 2003), was interpreted from airborne (Macheret and Zhuravlev, 1980; Dowdeswell et al., 1984b) and ground-based (Glazovsky et al., 1991) radio-echo sounding data. However, neither the Russian (Macheret and Zhuravlev, 1980; Macheret, 1981; Macheret and Zhuravlev, 1982) nor the British (Dowdeswell et al., 1984b,a) echo soundings revealed the polythermal structure of Austre Grønfjordbreen shown in our GPR data. Neither was the Russian airborne echo sounding able to detect the polythermal structure of Aldegondabreen, though it was later inferred from ground-based GPR (Navarro et al., 2005). GPR data from our campaigns 2010 onwards have revealed the polythermal structure of Tavlebreen (Lavrentiev et al., 2010), Austre and Vestre Grønfjordbreen and Tungebreen (Lavrentiev et al., 2011), as well as the cold structure of Gleditchfonna (Lavrentiev et al., 2011). We have recently reported the polythermal structure of of Erdmanbreen, Austre Dahlfonna and Vestre Dahlfonna (Martín-Español et al., 2013). However, smaller glaciers such as Baalsrudbreen, Marstranderbreen and Passtjellbreen do not present scattered signals and we have not find evidence of water inclusions so we believe they are entirely cold.

- Central Nordenskiöld Land: The glaciers Longyearbreen and Larsbreen, very close to Longyearbyen, have been characterized as non-typical polythermal glaciers (Etzelmüller et al., 2000). The only area that shows clear indications of temperate ice is the western upper area of Longyearbreen. At Larsbreen there are no clear indications of temperate ice from the radio-echo sounding. Except for the mentioned areas of Longyearbreen, the radio-echo sounding shows that these glaciers are either cold-based or cold with a thin layer of temperate ice at the bed. In Blekumbreen there is not a clear presence of water intrusion in the radargrams so we suggest it has an entirely cold hydrothermal structure. The hydrothermal structure of Tellbreen is detailed discussed in Bælum and Benn (2010), reaching the conclusion that Tellbreen is currently entirely cold-based, with the possible exception of a small, isolated region near the thickest part of the glacier.

- Heerland, south Spitsbergen: Pälli et al. (2003a) studied the glaciers Hornbreen and Hambergbreen and confirmed their polythermal regime. In addition, they found temperate ice patches in the frontal parts of Hornbreen which were thought to be an evidence of transport from a previously temperate accumulation area by a surge.

- Kongsfonna-Brøggerlalvøya: Björnsson et al. (1996) studied the predominantly cold

structure of Austre Brøggerbreen and inferred the polythermal regime of Midre Lovénbreen (also Kongsvegen and Uversbreen) from radio-echo sounding and boreholes. Songtao et al. revealed the polythermal structure of Pedersenbreen. inferred from the radargrams in Austre Lovénbreen two areas with an important scattering that is attributed to the presence of temperate ice.

- Reindalen: The studied glaciers in this area (Slakbreen, Marthabreen, Høganesbreen and Varpbreen) are fed by Gruvefonna ice cap. Their polythermal character was first suggested by Liestøl, (1977) and then it was further explored during the studies at the Svea Coal Mine, situated below Gruvefona, due to water intrussions originated from the glacier above the mine (Melvold et al., 2004; Hauck and Christof).

- Dickson Land: Malecki (2013) interpreted the hydrothermal regime of this region from ground-based echo-soundings. He found polythermal evidences in Bertilbreen and Svenbreen meanwhile the results found in Bertrambreen point out that this glacier is entirely cold.

- Nordaustlandet: Austfonna is characterized as being mostly cold, although there is evidence of a temperate layer near the bedrock (Dowdeswell, 1986). Recent studies in Vestfonna have shown their polythermal character (Pettersson et al., 2011). They found a widespread scattering of the upper 100 meters of the ice column which are associated to water pockets.

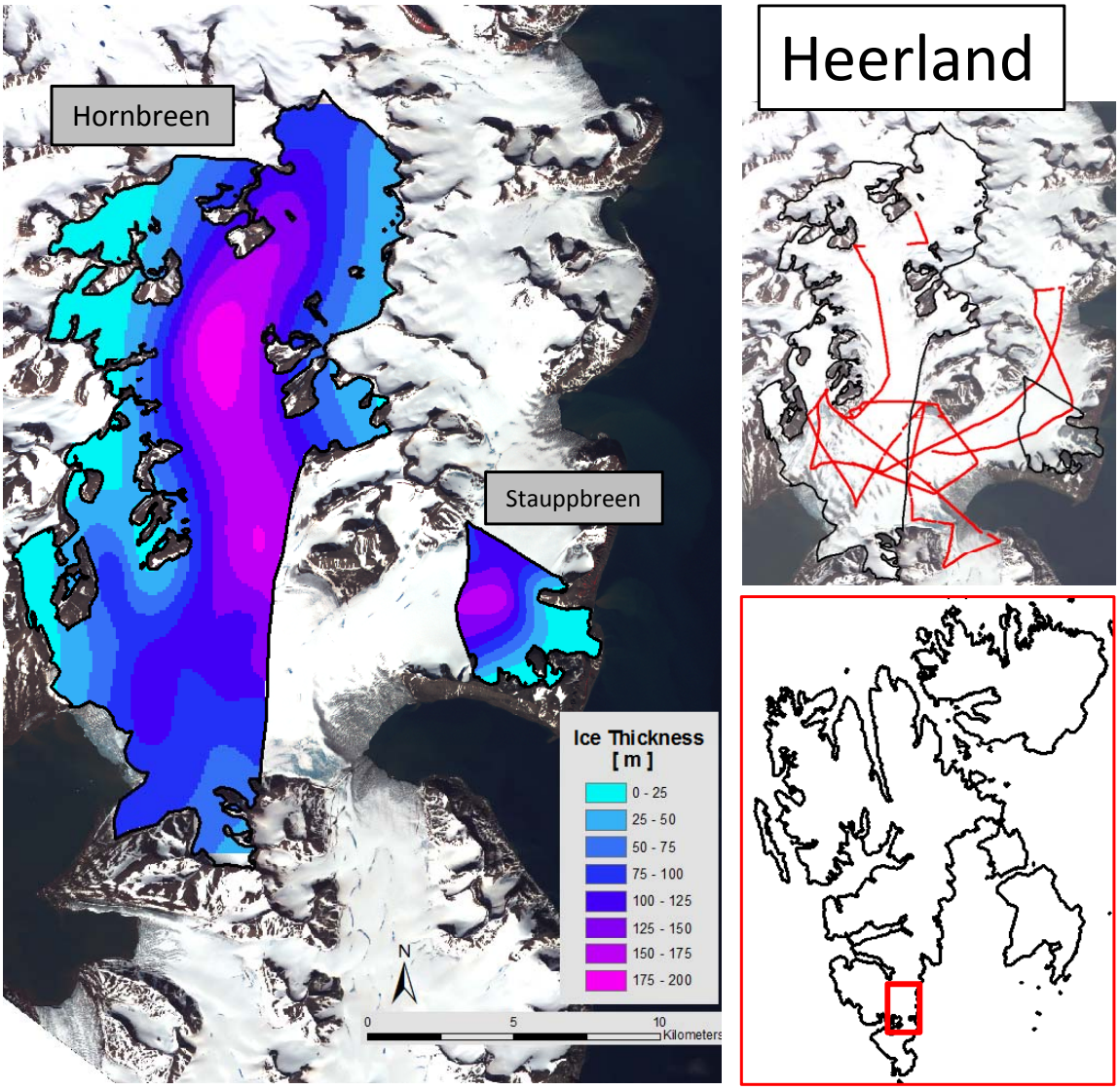


Figure 4.9: Ice thickness maps and GPR profiles of Hornbreen and Stauppbreen, in Heerland, southern Spitsbergen. GPR surveys were carried out by A.Pälli and results were published in Pälli et al. (2003a); Pälli (2003). Although the GPR profiles covered several other glaciers nearby, complete basins were not surveyed and therefore they are not included in this study. The maximum measured ice thickness is reached in Hornbreen at 329 m.

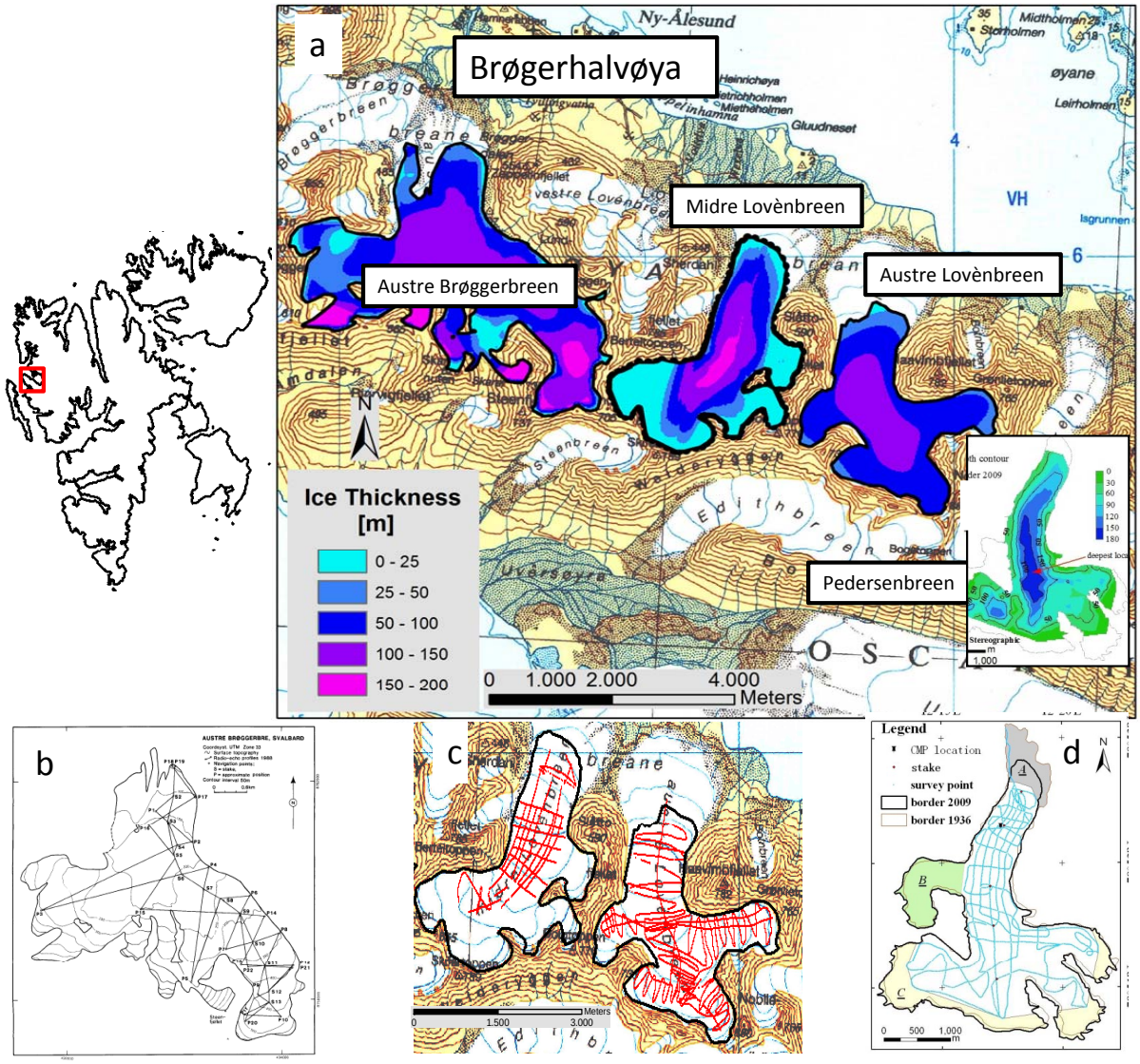


Figure 4.10: Ice thickness map (A) and GPR profiles of four small valley glaciers on Brøggerhalvøya. GPR data for this subregion were provided from different research groups: B: Austre Brøggerbreen (Hagen and SæTrang, 1991), C: Midre Lovénbreen (provided by D.Rippin from the SPRI (unpublished), H.Bjornsson (Björnsson et al., 1996) and J. Moore (Zwinger and Moore, 2009)) and Austre Lovénbreen (provided by I.Willis (unpublished), D: Pedersenbreen, available at (Songtao et al., 2013). The average thickness of these four small glaciers is 65 m with a standard deviation of 11 m. The largest glacier in volume is Austre Brøggerbreen although the maximum depth is reached in Midre Lovénbreen at 184 m

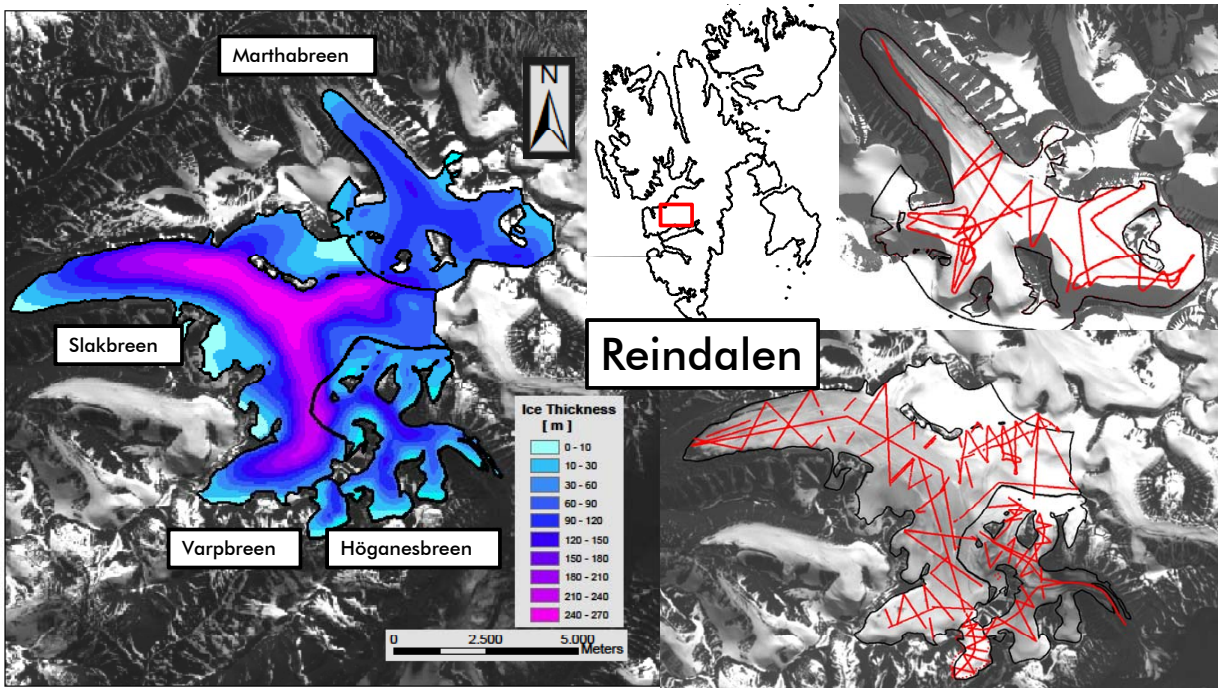


Figure 4.11: Ice thickness map and GPR profiles of four glaciers situated in Reindalen area, central Spitsbergen. Marthabreen data has been provided by T.V. Schuler. GPR data sets from Slakbreen, Varpbreen and Höganesbreen were provided by K. Melvold and published in (Hauck and Christof; Melvold et al., 2004). About 70 m ice thickness is an average value for this area. Maximum ice thickness of about 290 m was found beneath Slakbreen just downstream of the confluence of the Slakbreen Valley and Gruvefonna Valley (towards Marthabreen). An over-deepened trough at this location indicates enhanced erosion in the confluence area (Hauck and Christof).

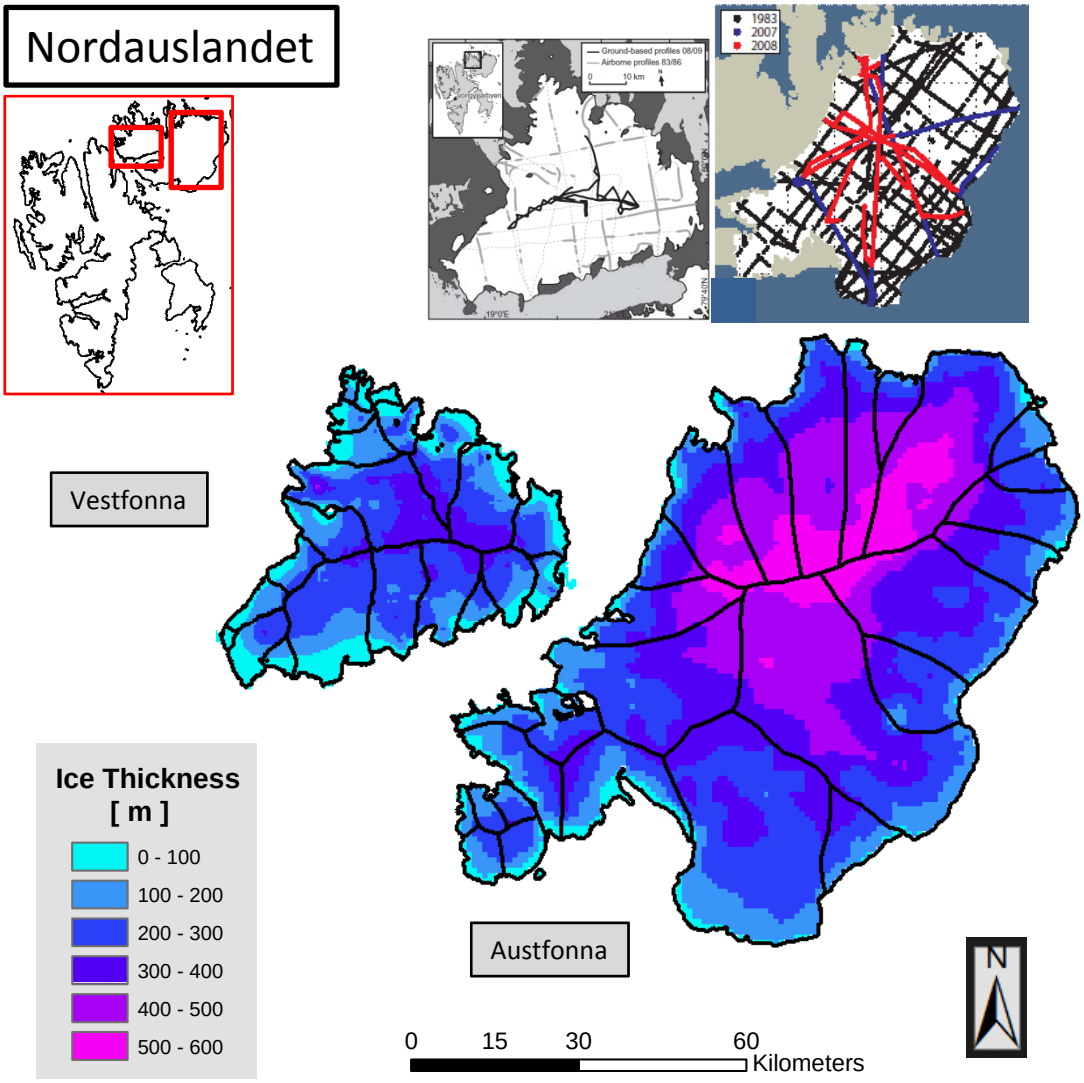


Figure 4.12: GPR profiles and ice thickness of the two largest ice masses in Svalbard, Austfonna and Vestfonna ice caps, on Nordaustlandet island. Both have been the focus of extensive radio-echo sounding campaigns. The first radio-echo soundings flights were done in 1983 and 1986 (Dowdeswell et al., 1986). Years later, in 2007-2009, new airborne and ground-based echo soundings have been carried out over both icecaps (Pettersson et al., 2011; Dunse, 2011). The maximum ice depth measured in Vestfonna was about 410 meters whereas in Austfonna they reached 587 m.

Chapter 5

A new volume-area relationship for Svalbard glaciers and its associated total volume estimate

5.1 Outline

This chapter aims to estimate the potential contribution of Svalbard glaciers to sea-level rise by calculating the total volume of glacier ice stored in Svalbard using a volume-area scaling relationship specific for Svalbard glaciers. First we summarize our compiled data set of calculated volumes, discussed in the previous chapter and extended in the present one using additional previously published volume data (Cogley, 2012; Grinsted, 2013), and perform a sensitivity analysis to elucidate if this addition leads to substantially different results. We then compare the histograms of size distribution of our sample and the complete population of Svalbard glaciers, to detect the existence of any possible bias. This is followed by the comparison of different methods to estimate the predictive skills of distinct V-A scaling relationships, with the aim of establishing a model selection criterion. We also compare different regression techniques, to find the most suitable fitting strategy. Afterwards, we study the sensitivity of the scaling parameters to different glacier settings, in terms of glacier size, aspect ratio and average slope. This is followed by a multivariate analysis, aimed to assess if the addition of further variables (such as glacier length or elevation range) to the scaling law yields improved results, as suggested by Cogley (2012) and implemented by Grinsted (2013). The particular case of the volumes of Vestfonna and Austfonna ice caps is analysed afterwards. We then present our total volume estimate for Svalbard glaciers and compare it

with those derived from other existing V-A scaling laws, and from physically-based methods. Finally, we present some error estimates, and conclude the chapter giving our best estimate of the potential contribution of Svalbard glaciers to sea-level rise.

5.2 Establishing a basis data set for a volume-area relationship

To accomplish our aim of deriving a volume-area relationship specific for Svalbard glaciers, we fist need to count on a large enough data set of measured volume and area pairs, (V, A)-pairs, each one calculated with sufficient accuracy. Moreover, the sample of measured glaciers should be representative of the size distribution of the total population of Svalbard glaciers. As a starting point for the sample data set, we count on the inventory of radio-echo sounded Svalbard glaciers discussed in Chapter 4 and detailed in Appendix A. But not all of the glaciers in the inventory have coverage of GPR profiles sufficient to warrant an accurate volume estimate. For instance, the nets of GPR profiles of certain glaciers are limited to the accumulation, or to the ablation, zones, or to a particular area of the glacier, and these glaciers should clearly be discarded. In some cases, the net of profiles could be not dense enough. However, in certain cases a volume estimate based upon a centre-line profile all along a valley glacier, combined with parabolic (or other polynomial) cross-sections, could be good enough for our purposes.

It is well known that the volume estimates based on V-A scaling relationships can involve very large errors when applied to individual glaciers, though the errors are much smaller, because of statistical compensation, when applied to large sets of glaciers, as happens for regional volume estimates, which is our case. For instance, according to Meier et al. (2007), estimated errors in volume for individual glaciers could exceed 50% but these uncertainties are reduced to 25% for an ensemble of glaciers. Consistent with these results, a recent study by Adhikari and Marshall (2012), using a V-A relationship based in a sample of 280 synthetic random mountain glaciers, has shown that, when estimating the volumes for all of the individual glaciers in their ensemble, the average error in glacier volume is small (2.8%), with a mean absolute error of 18.3%. Their interquartile spread of results is also reasonable, with 50% of errors in the range [-14.7, 15.9] %, but errors for individual glaciers can be high, in the range [-47.6, +99.7] %. Their mean and mean absolute errors for individual glacier volume estimates are reduced to 1.5% and 14.4%, respectively, when shape-based parameters

are applied to their random ensemble of glaciers.

Our main interest, however, lies in knowing the accuracy that could be expected when computing the volume of the complete population of Svalbard glaciers using a V-A relationship constructed from a given sample of measured (V, A)-pairs, estimated with a certain accuracy. This subject is addressed by a very recent study (Farinotti and Huss, 2013), which derives an upper bound estimate for the accuracy with which the total volume can be recovered in relation to the size of the glacier population, the size of the sample of glaciers used to estimate the scaling parameters and the uncertainty of the measured volumes. They show that a low level of accuracy is expected if scaling is applied with coefficients estimated from a small set of samples. On the other hand, accuracy increases with increasing size of the considered glacier population. For example, they state that using 280 (V, A)-pairs for estimating the scaling coefficients, assuming an uncertainty in the measured volumes of 20%, implies recovering the total volume of a population of 1,000, 10,000 and 100,000 glaciers with 32%, 23% and 20% accuracies, respectively. They also pointed out that volume measurement uncertainty plays a secondary role if a sufficient number of measured glacier volumes are available. According to these ideas, in our case it seems to be worth to increase the size of our sample of (V, A)-pairs, even if this increase is done at the expense of adding (V, A)-pairs not having a high accuracy. Upon our request, Farinotti and Huss have kindly generated a figure (Fig. 5.1) similar to Figure 1a in their paper but adapted to the particular settings of Svalbard, with a glacier population of ca. 1,500 glaciers (1,668 in the most recent Svalbard inventory, the Digital Database of Svalbard Glaciers (DDSG) by Köning et al. (2013), which was the basis of the Randolph Glacier Inventory (RGI) (Arendt et al., 2012)). As shown in the figure, their results suggest that, with a sample size of about 100 glaciers, with volume accuracy of 5-25% (parameters close to our case study of Svalbard glaciers), the total volume of the population of glaciers could be retrieved with ca. 40% accuracy. We note, however, that Farinotti and Huss (2013) results, as concern to target accuracy, are very pessimistic as compared to those by Meier et al. (2007) and by Adhikari and Marshall (2012). Nevertheless, Farinotti and Huss (2013) still provides suitable guidelines regarding a proper selection of our sample of (V, A)-pairs.

We have calculated, from the original GPR ice-thickness data, 36 glacier volumes with accuracy better than 10%. We have also gathered from the literature the ice-thickness maps and volumes of 4 other glaciers with a dense coverage of GPR profiles and an accuracy better than 20%, according to the original sources. This sample size of 40 glaciers (those

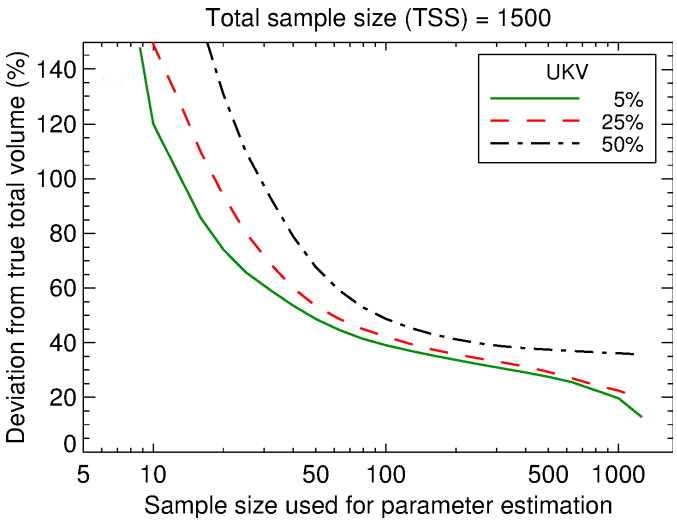


Figure 5.1: Expected accuracy with which the total true volume of a population of 1500 glaciers will be recovered (at 95% confident) using volume-area scaling relationships. The different curves correspond to different measurement uncertainties of individual glacier volumes. The figure has been kindly generated by D. Farinotti.

in Table 4.3, excluding Austfonna and Vestfonna ice caps) is clearly insufficient to reach an acceptable accuracy in the total volume estimate: according to Figure 5.1, such a sample size from a population of 1,500 glaciers gives an estimated accuracy for the total volume of the population close to 55%. There is a straightforward way to increase the sample size. The different basins of the ice caps of Austfonna and Vestfonna are defined (by their outlines) in the DDSG and in the RGI. Thereby, we have estimated their volumes at the basin unit level, thus generating additional (V, A)-pairs. In particular, we have calculated the volumes for 19 out of 24 basins in Vestfonna, and 26 out of 29 basins in Austfonna. We had to exclude a minor part of the basins due to lack of ice-thickness measurements on them, which would have lead to an underestimation of their interpolated ice thicknesses. There is an added reason for using Austfonna and Vestfonna individual basins rather than the entire ice-caps. Due to the distinct and characteristic geometries of glaciers and ice caps, it is customary, in global volume estimates from V-A relationships, to generate different V-A relationships for glaciers and for ice caps (Radić and Hock, 2011; Grinsted, 2013). However, in our regional Svalbard study the number of echo-sounded ice caps is clearly insufficient to allow constructing a separate V-A relationship for ice caps. On the other hand, adding the total volumes of the ice caps of Austfonna and Vestfonna to our set of (V, A)-pairs would worsen the V-A relationship. Moreover, different regions in Spitsbergen (and other Svalbard islands) have glacier basin units morphologically similar to the separate basins of Austfonna and Vestfonna (i.e. they have geometries not characteristic of valley glaciers, but rather glacier basins delimited to a

large extent by ice divides, and showing large, often unconfined, terminal areas instead of confined tongues, either on sea or on land). Consequently, it seems reasonable to increase the size of our set of (V, A)-pairs by adding the mentioned individual basins of Austfonna and Vestfona. With this addition, the number of (V, A)-pairs increases to 85. We will come back to the volumes of Austfonna and Vestfona later in the chapter (cf. Section 5.8).

There is a last addition of (V, A)-pairs that we could consider to increase our sample size. There is available a collection of 264 measured glacier volumes for the whole world (Grinsted, 2013), mostly collected by Graham Cogley and Regine Hock and used in Cogley (2012) (for brevity, henceforth we will refer to these glaciers as Cogley's catalogue), from which 31 glaciers belong to Svalbard and 19 of them are different from those included in our former dataset of 85 glaciers. These 19 glaciers correspond to SPRI-NPI and Soviet airborne radio-echo soundings (Macheret and Zhuravlev, 1982; Dowdeswell et al., 1984a) which only covered the glacier centre lines, but they exclude the glaciers with doubtful bed reflection interpretation from Soviet flights discussed in Section 4.2. Moreover, these glaciers have been used by other authors (e.g. Grinsted (2013)) to build V-A relationships. From these 19 glaciers we exclude one, Åsgårdfonna, because it is in fact an ensemble of different glacier basins and we do not have the possibility of calculating the volumes of the individual basins. We still do a last test before incorporating the remaining 18 glaciers into our data base of (V, A)-pairs. We build two different V-A relationships, one using only our data set of 85 glaciers (denoted D_{own}) and another using our data set plus the 18 glaciers from Cogley's catalogue (denoted $D_{own+Cogley}$), thus making a total of 103 (V, A)-pairs, and apply them to calculate the volume of the entire population of Svalbard glaciers (as compiled in the DDSG). For building the V-A relationship, we follow the usual procedure of plotting in the log-log space volume vs. area, and fitting the data by regression analysis to establish a power-law relation between area and volume of the type

$$V = cA^{\gamma} \tag{5.1}$$

Table 5.1 shows the estimates of total volume of Svalbard glaciers using the scaling laws derived from both data-sets. The difference in total volume difference is only about 2%, which is far below the typical accuracy provided by the volume estimates of large ensembles of glaciers by scaling laws. Given this small difference, and following the ideas of Farinotti and Huss (2013), we prefer to use the larger sample data set ($D_{own+Cogley}$) as a means to warrant a theoretically larger accuracy of the total volume estimate. The final sample of 103 (V, A)-pairs is shown in Table 5.2. This will be the basis data set for building all of the V-A

Table 5.1: Selecting the data set of (V, A)-pairs.

Data set	Scaling law	Svalbard Vol. Estimate (km^3)
D_{own}	$0.0317\ A^{1.373}$	7704
$D_{own+Cogley}$	$0.0332\ A^{1.361}$	7546

relationships developed in the present chapter.

A last test for consistency remains. We want that our sample data set be representative of the total population of Svalbard glaciers, in particular as concerns to size distribution. In Figure 5.2 we represent the area distribution of the calibration data set and compare it against the area distribution of the entire Svalbard inventory. The most recent inventory (Köning et al., 2013) contains 1,668 individually labelled glacier units, with a total area of 33,775 km^2. There are about 350 glaciers (22% of the inventory) larger than 10 km^2 that make up 93% of the glacier area. The remaining ca. 1,320 glaciers (78% of the inventory) are smaller than 10 km^2 and make up only 7% of the glacier area. Among the latter, there are 630 glaciers, glacierets and snow patches smaller than 1 km^2 that represent 38% of the inventory and 1% of the glacier area. As compared to that, our sample of 103 glaciers has 74 glaciers (72% of the sample) larger than 10 km^2, representing 99% of the total area of the sample, and only 29 glaciers (28% of the sample) equal or smaller than 10 km^2, representing 1% of the total glacierized area of the sample. We thus observe in our sample dataset a bias towards large glaciers. The area distribution histograms shown in Figure 5.2 clearly show this fact: whereas in the sample data set the highest percentages of area are occupied by the largest size bins, in the Svalbard data set the largest percentages of area correspond to the smallest size bins. This was expected, as we included the volumes of the Austfonna and Vestfonna glacier basins, which are among the largest in Svalbard, whereas small valley glaciers, which are often difficult to access, are customarily ignored when planning fieldwork because they do not appear as appealing as larger glaciers. To counterbalance this bias towards large glaciers in our sample data set, we will later introduce an area-related weighting function (cf. Section 5.4).

Table 5.2: Sampled glaciers for obtaining the scaling coefficients of the V-A relationship. A ◊ next to the glacier name indicates that the volume accuracy has been computed and is better than 10%; • indicates a computed accuracy better than 20 % and □ indicates an estimated accuracy better than 30%. Glacier names in italics indicate that the volume has been taken from Cogley's catalogue.

Glaciar	A	V	Length	R	Shape	Slope
	(km^2)	(km^3)	(km)	Z_{max} - Z_{min} (Km)		
Aldegondabreen◊	7.18	0.468	3.29	0.28	0.67	0.09
Antoniabreen □	32.00	5.640	11.7	0.70	0.23	0.06
Ariebreen◊	0.37	0.010	1.17	0.32	0.27	0.27
Austfonna. - unnamed-1◊	153.58	38.377	16.97	0.48	0.53	0.03
Austfonna. - unnamed-2◊	1226.52	462.335	59.66	0.83	0.34	0.01
Austfonna. - unnamed-3◊	249.19	69.539	22.24	0.60	0.50	0.03
Austfonna. - unnamed-4◊	663.07	227.287	39.89	0.82	0.42	0.02
Austfonna. - unnamed-5◊	176.08	49.124	21.68	0.65	0.37	0.03
Austfonna. - unnamed-6◊	218.69	65.658	24.38	0.60	0.37	0.02
Austfonna. - unnamed-7◊	79.94	20.385	14.45	0.39	0.38	0.03
Austfonna. - unnamed-8◊	328.22	115.794	31,00	0.66	0.34	0.02
Austfonna. - unnamed-9◊	111.67	28.359	13.25	0.40	0.64	0.03
Austfonna. Brösvellbreen◊	1095.79	278.235	45.91	0.77	0.52	0.02
Austfonna. Duvebreen◊	356.42	136.127	40.5	0.70	0.22	0.02
Austfonna. Etonbreen◊	640.90	194.868	35.66	0.71	0.50	0.02
Austfonna. Leighbreen◊	692.88	287.814	48.03	0.61	0.30	0.01
Austfonna. Nilsenbreen◊	241.41	93.465	42.67	0.62	0.13	0.01
Austfonna. Schweigaardbreen◊	472.52	189.390	45.89	0.69	0.22	0.02
Austfonna. Sexebreen◊	101.33	34.208	19.65	0.35	0.26	0.02
Austfonna. Winsnesbreen◊	242.63	78.213	27.01	0.71	0.33	0.03
Austfonna. Worsleybreen◊	84.69	16.993	13.46	0.40	0.47	0.03
Austfonna.Palanderisen -1◊	129.10	28.029	14.46	0.49	0.62	0.03
Austfonna.Palanderisen -2◊	57.55	6.982	4.35	0.38	3.04	0.09
Austfonna.Palanderisen -3◊	190.74	33.476	11.42	0.54	1.46	0.05
Austfonna.Palanderisen -3◊	291.36	59.192	14.59	0.50	1.37	0.03
Austfonna.Vegafonna -1◊	46.76	9.531	9.18	0.33	0.55	0.04
Austfonna.Vegafonna -2◊	69.06	10.672	9.66	0.46	0.74	0.05
Austfonna.Vegafonna -3◊	41.61	7.212	10.91	0.30	0.35	0.03
Austfonna.Vegafonna -4◊	80.18	15.872	8.85	0.46	1.02	0.05
Austre Brøggerbreen•	10.25	0.756	5.23	0.55	0.37	0.11
Baalsrudbreen◊	2.70	0.077	2.56	0.39	0.41	0.15
Balderfonna □	418.00	66.040	21.00	1.10	0.95	0.05
Bertilbreen•	3.82	0.285	4.07	0.42	0.23	0.10
Bertrambreen◊	3.04	0.199	3.29	0.40	0.28	0.12

Table 5.2: Sample of glaciers used for obtaining the scaling coefficients of the V-A relationships.

Glaciar	A	V	Length	R	Shape	Slope
	(km^2)	(km^3)	(km)	Z_{max} - Z_{min} (Km)		
Blekumbreen◊	2.16	0.083	3.63	0.49	0.16	0.14
Bogerbreen □	4.50	0.300	4,00	0.60	0.28	0.15
Vestre Brøggerbreen □	5.60	0.240	4.30	0.52	0.30	0.12
Comfortlessbreen □	56.4	9.890	14.9	1,00	0.25	0.07
Cookbreen □	18.00	3.520	14,00	1.02	0.09	0.07
Dalhfonna Austre◊	2.55	0.184	3.54	0.32	0.20	0.09
Dalhfonna Vestre◊	6.92	0.259	2.36	0.34	1.24	0.14
Eidembreen □	103.00	17.060	20.20	0.74	0.25	0.04
Erdmanbreen◊	8.96	0.823	4.80	0.34	0.39	0.07
Finsterwalderbreen•	29.00	3.500	9.92	0.95	0.29	0.10
Foxfonna □	14.80	0.960	3.40	0.60	1.28	0.18
Fridtjovbreen◊	50.37	5433	11.45	0.51	0.38	0.04
Gleditchfonna◊	2.76	0.076	1.87	0.15	0.79	0.08
Grønfjordbreen Austre◊	8.41	0.671	4.78	0.37	0.37	0.08
Grønfjordbreen Vestre◊	18.09	1.775	5.62	0.37	0.57	0.07
Hansbreen◊	64.16	10.752	15.16	0.48	0.28	0.03
Hessbreen □	7.20	0.460	5.50	0.87	0.24	0.16
Höganasbreen◊	11.49	0.733	4.94	0.42	0.47	0.09
Hornbreen◊	173.28	18.240	23.52	0.78	0.31	0.03
Kantbreen □	24.90	3.740	21,00	1.10	0.06	0.05
Larsbreen•	2.96	0.152	2.92	0.45	0.35	0.15
Longyearbreen•	2.52	0.132	4.51	0.70	0.12	0.16
Lovénbreen Austre◊	5.01	0.376	3.44	0.45	0.42	0.13
Lovénbreen Midre•	5.20	0.257	3.57	0.55	0.41	0.15
Marstanderbreen◊	6.92	0.233	4.43	0.32	0.35	0.07
Marthabreen◊	15.11	0.961	8.41	0.80	0.21	0.10
Odinjøkulen □	58.00	6.440	9,00	0.65	0.72	0.07
Osbornebreen □	118.00	18.410	20.1	0.95	0.29	0.05
Paierlbreen◊	99.19	13.265	21.11	0.67	0.22	0.03
Passfjellbreen Austre◊	5.13	0.198	2.90	0.28	0.61	0.10
Passfjellbreen Vestre◊	2.32	0.103	2.54	0.17	0.36	0.07
Pedersenbreen•	6.30	0.398	4.86	0.60	0.27	0.12
Recherchebreen◊	136.31	27.284	22.79	0.68	0.26	0.03
Renardbreen◊	30.58	5.141	9.75	0.50	0.32	0.05
Scottbreen◊	4.71	0.301	3.49	0.57	0.39	0.16

Table 5.2: Sample of glaciers used for obtaining the scaling coefficients of the V-A relationships.

Glaciar	A	V	Length	R	Shape	Slope
	(km^2)	(km^3)	(km)	$Z_{max} - Z_{min}$ (Km)		
Slakbreen◊	36.69	4.303	13.11	0.73	0.21	0.06
Stauppbreen◊	15.33	1.197	3.65	0.22	1.15	0.06
Svenbreen◊	3.72	0.217	3.34	0.45	0.33	0.13
Tavlebreen◊	8.02	0.426	5.64	0.45	0.25	0.08
Tellbreen•	3.00	0.150	3.91	0.53	0.20	0.14
Torellbreen Austre ◊	140.99	31.981	20.32	0.75	0.34	0.04
Vestre Torellbreen □	217.00	59.16	33.50	0.80	0.19	0.02
Torsfonna □	83.00	10.96	8,00	0.62	1.30	0.08
Tungebreen◊	2.88	0.093	2.19	0.52	0.60	0.24
Uversbreen □	74.00	13.180	20.5	0.75	0.18	0.04
Valhallfonna □	410.00	88.560	17.5	0.85	1.34	0.05
Varpbreen◊	1.33	0.068	1.83	0.27	0.40	0.15
Vestfonna. Franklinbreen◊	117.36	21717	19.96	0.63	0.29	0.03
Vestfonna.Aldousbreen◊	179.38	41.894	20.45	0.61	0.43	0.03
Vestfonna.Amenfonna◊	56.27	5.852	9.78	0.52	0.59	0.05
Vestfonna.Bodleybreen◊	109.8	22.249	15.47	0.63	0.46	0.04
Vestfonna.Bragebreen◊	28.74	2.947	7.07	0.46	0.58	0.06
Vestfonna.Croftbreen◊	112.02	17.538	11.73	0.57	0.81	0.05
Vestfonna.Eltonbreen◊	44.94	7.349	8.42	0.53	0.63	0.06
Vestfonna.Frazerbreen◊	200.73	44.821	22.16	0.61	0.41	0.03
Vestfonna.Gimlebreen◊	98.96	14.027	16.48	0.54	0.36	0.03
Vestfonna.Idunbreen◊	333.16	58.79	25.79	0.61	0.50	0.02
Vestfonna.Maudbreen◊	158.92	30.563	21.79	0.59	0.33	0.03
Vestfonna.Nordre Franklinbreen◊	331.27	85.701	32.65	0.63	0.31	0.02
Vestfonna.Rijpbreen◊	224.64	48.607	20.08	0.62	0.56	0.03
Vestfonna.Sabinebreen◊	67.35	9.826	10.83	0.62	0.57	0.06
Vestfonna.unnamed -1◊	38.74	3.738	10.48	0.60	0.35	0.06
Vestfonna.unnamed -2◊	82.13	10.633	11.70	0.44	0.60	0.04
Vestfonna.unnamed -3◊	61.63	8.990	6.77	0.49	1.34	0.07
Vestfonna.unnamed -4◊	54.75	6.634	5.26	0.45	1.98	0.09
Vestfonna.unnamed -5◊	13.57	1.290	3.05	0.38	1.46	0.13
Veteranenbreen □	165.00	35.970	44.00	1.41	0.09	0.03
Voringbreen □	2.10	0.130	1.60	0.37	0.82	0.23
Werenskioldbreen◊	26.60	3173	8.72	0.52	0.35	0.06
Total ensemble	13134	3476				

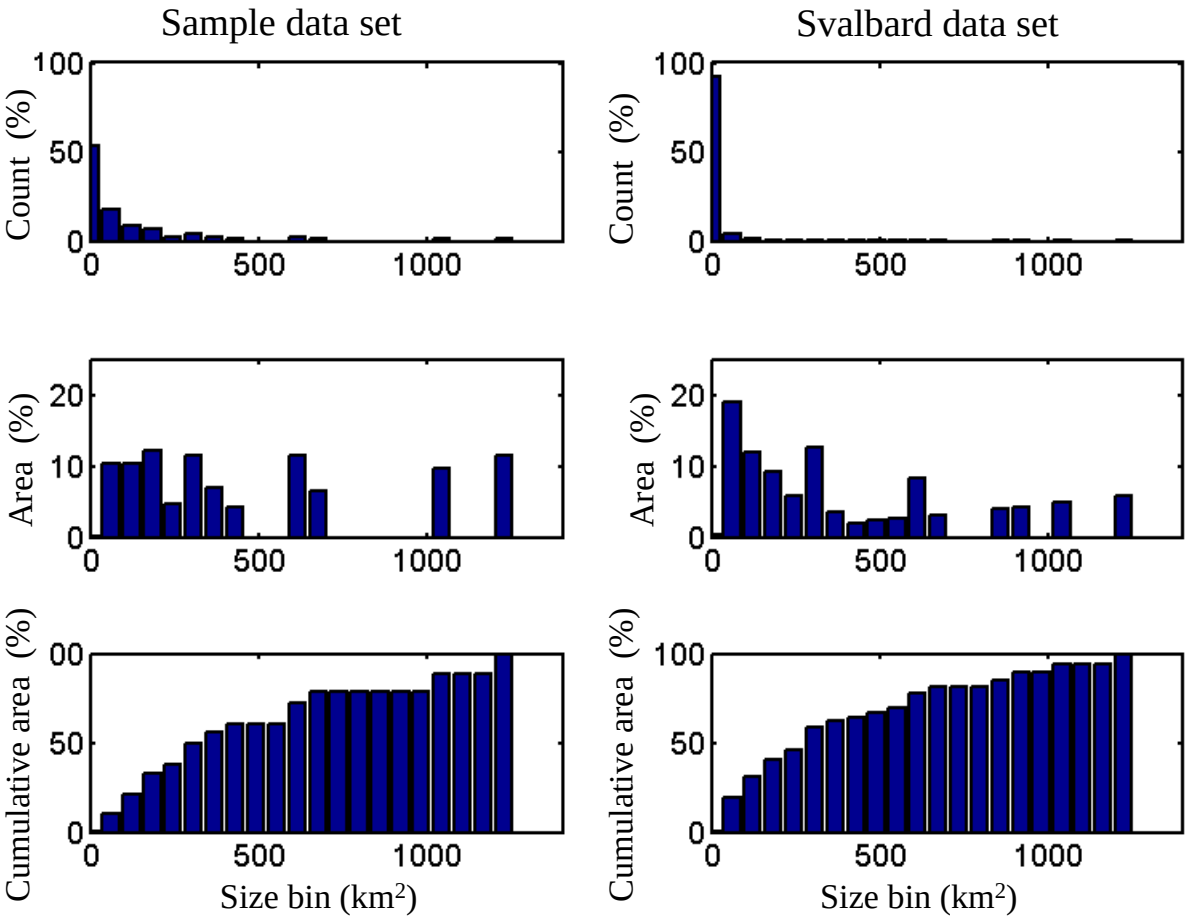


Figure 5.2: Area distribution of the sample data set versus the area distribution of the complete population of Svalbard glaciers.

5.3 Estimating accuracy from cross-validation

It is possible to build different scaling regressions for predicting glacier volumes. In order to compare their predictive skills we need to stablish a criterion for model selection. As we do not have any additional data against which we could validate our model, we will compare it against the same data used to build the model, through cross-validation methods (Geisser, 1993). Here we compare three widely used cross-validation types: 4-fold, 10-fold and leave one out cross-validation, with the aim of selecting the most suitable one. In k-fold cross-validation, the original sample is randomly partitioned into k equal size subsamples. Of the k subsamples, a single subsample is retained as the validation data for testing the model, and the remaining k-1 subsamples are used as training data. The cross-validation process is then repeated k times (the folds), with each of the k subsamples used exactly once as validation data. Leave-one-out cross-validation is the same as a k-fold cross-validation with k being equal to the number of observations in the original sample. In each case all observations are used for both training and validation, and each observation is used for validation exactly once.

Table 5.3: Error expressed as the percentage difference between the predicted and the real total volume of the sample, using different cross-validation methods.

4-fold	10-fold	Leave-one-out
5.5 %	4.3%	4.2 %

As expected, the cross-validation error gets reduced as the training data increases in each fold, although the results from the three approaches do not show a significant difference. Many authors have pointed out the negative impact on the results of predicting glacier volumes using a power-law model derived from a reduced set of observations (Grinsted, 2013; Farinotti and Huss, 2013). If using 4-fold cross-validation, we would be estimating the prediction error from samples of about 25 *(V,A)*-pairs that would significantly reduce the expected accuracy. There is not a significant difference between 10-fold and leave-one-out cross-validation (whose training sets are formed by about 90 and 102 *(V,A)*-pairs, respectively), so we will use leave-one-out cross-validation to estimate the accuracy of different scaling tests. Though useful to compare different scaling relationships, we note that cross-validation is not an indication of the expected error in the estimation of the volume of the entire population of Svalbard glaciers; such an error is expected to be significantly larger than that.

5.4 Selecting a fitting strategy: *logmse* versus *absdev* misfit functions

The traditional technique for estimating the parameters of the scaling relationship (c and γ) is least squares regression (LSR) in a log-log space (Bahr, 1997), which minimizes the *logmse* misfit function

$$logmse(p) = \sum_i \left(log\left(V_{model}\left(p,i\right)\right) - log\left(V_{obs,i}\right)\right)^2 \tag{5.2}$$

where i is an index representing the entry in the glacier volume database, V_{model} are the volumes predicted by the scaling law with a set of parameters p, and V_{obs} are the observed volumes. This model has been pointed out to be biased towards small and medium sized glaciers, for which most observations are available, and to be very sensitive to outliers (Grinsted, 2013). Alternatively, Grinsted (2013) has suggested that least absolute deviation regression (LAR), that minimizes the misfit function

$$absdev(p) = \sum_i \frac{\left|V_{model}\left(p,i\right) - V_{obs,i}\right|}{\sqrt{A_{obs,i}}} \tag{5.3}$$

is an strategy better suited for sea-level rise studies as it minimizes the absolute volume misfit, and is robust to outliers and asymmetric distributions. Additionally, it is weighted by the inverse root of the area, which reduces the sampling bias described in Section 5.2.

The results of applying the two above strategies to calculate the volume of the entire population of Svalbard glaciers are shown in Table 5.4. Though the values of c and γ are quite different, the result of varying both simultaneously has little effect in the final result for the total volume of Svalbard glaciers computed by the two methods, which differ by less than 2%. For this reason, we will use both strategies for our next test.

Table 5.4: Selecting a fitting strategy

Strategy	Scaling law	Svalbard vol. estimate (km^3)	ϵ_{Sample} (%)	$\epsilon_{crossval}$ (%)
logmse	$0.0332\ A^{1.361}$	7546	4.3	4.8
absdev	$0.0452\ A^{1.303}$	7424	0	1.1

5.5 Comparison between inventories

As we pointed out in Chapter 1, there are some differences between the latest version (V3) of the Randolph Glacier Inventory (Arendt et al., 2012) and the Digital Database of Svalbard Glaciers (Köning et al., 2013), in which we have based all of our calculations. Even though both databases have been developed by the same team (mostly from the Norwegian Polar Institute), each inventory was based on different definitions of individual glaciers and drainage basins. Also the identification codes are slightly different. The total glacierized area of Svalbard is 33,775 (km^2) according to Köning et al. (2013), who established 1,668 entries for individual basins, versus 33,673 (km^2) and 1,615 individual glaciers according to the RGI V3 (Arendt et al., 2012)). In table 5.5 we compare the results of computing the total volume of Svalbard glaciers using the Digital Database of Svalbard against the results versus those obtained using the Randolph Glacier Inventory V3.0.

Table 5.5: Comparing the estimates of the total volume of Svalbard glaciers using the different available glacier inventories: the Digital Database of Svalbard glaciers (DDSG) and the Randolph Glacier Inventory V3.0 (RGI.3).

Inventory	Strategy	Scaling law	Svalbard vol. estimate (km^3)	SLE (mm)
DDSG	*logmse*	$0.0332\ A^{1.361}$	7546 ± 611	19 ± 2
RGI.3	*logmse*	$0.0332\ A^{1.361}$	7639 ± 624	19 ± 2
DDSG	*absdev*	$0.0452\ A^{1.303}$	7424 ± 478	18 ± 1
RGI.3	*absdev*	$0.0452\ A^{1.303}$	7527 ± 488	19 ± 1

As shown in Table 5.5, for a given fitting strategy the differences due to the use of either inventory are very small, of 1.2% for the *logmse* fitting strategy, and 1.4% for the *absdev* strategy. Given such small differences, henceforth we will adhere to the the Digital Database of Svalbard glaciers (DDSG), since our intention is to incorporate our volume calculations into such database.

5.6 Scaling-law parameters for different glacier settings

It could be thought a priori that scaling relationships derived for specific types of glaciers would perform better, for predicting glacier volumes, than a general-purpose V-A scaling relationship. However, as discussed earlier, the expected accuracy of the scaling relationships improves both with the size of the total population of glaciers under study and with the size of the sample used to derive the scaling-law parameters. Since partitioning a given sample

into subgroups by glacier characteristics such as size, shape or slope would imply reducing the size of the sample from which the scaling parameters are derived, an hence a reduction of the expected accuracy in the total volume estimate, there is a trade-off between the improvement expected by the use of glacier-type specific scaling relationships and the worsening implied by the reduction of the sample size.

In this section we present a set of experiments aimed to verify whether scaling relationships obtained through characterization of individual glacier size or morphology imply significant differences in the estimated volume of the total population of Svalbard glaciers, and whether this partitioning implies any noticeable pattern in the scaling relationship parameters indicative of the influence of particular glacier settings. In particular, we considered partitions of our available sample of Svalbard glaciers by size, shape and slope, as done by Adhikari and Marshall (2012). Shape refers to the horizontal aspect ratio of a glacier, given by W/L, where L is the glacier length measured along the central flowline and W is the mean glacier width, defined as $W{=}A/L$. Slope is the mean bedrock slope in the principal flow direction. As it is not available from the surface, we take the mean surface slope, given by *(R/Max Length)*, where R is the altitude range, as a proxy of the mean bedrock slope, as done by Adhikari and Marshall (2012).

We calculate the best-fit scaling parameters c γ and for each subgroup of glaciers, using both the *logmse* and *absdev* fitting strategies. The size, shape and slope intervals defining each subgroup of glaciers can be seen in Table 5.6. We also calculate γ for a constrained value of $c = 0.0332$, taken from the *logmse* regression. We use the *logmse* misfit function rather than *absdev* because *logmse* is most often used in the literature and it provides a c value closer to those obtained by other authors, which facilitates the comparison of the γ values. Overall, we note that the poorer fits (lower coefficients of determination R^2) correspond to the partitioning by size. Concerning calculated volumes for the entire population of Svalbard glaciers, we note that the largest volumes ($V \subset [7719, 7820] km^3$) are produced by the partitioning by shape, whereas the smallest correspond to the partitions by size ($V \subset [7222, 7573] km^3$) and slope (($V \subset [7219, 7641] km^3$).

Table 5.6: Scaling-law parameters for different glaciological settings. The coefficients of determination r^2 of the different regressions are given, as well as the total volume of Svalbard glaciers V_{Sv} calculated using the given partitions into subgroups of glaciers. Figures enclosed by brackets indicate the number of glaciers in each subgroup.

	Class A			Class B			Class C			Global Results
	c	γ	r^2	c	γ	r^2	c	γ	r^2	V_{Sv}
Size, A, (km^2)		≤ 10 [29]			10-100 [37]			≥ 100 [37]		
logmse	0.0378	1.288	0.88	0.0362	1.3449	0.92	0.0652	1.240	0.89	7222
constrained	-	1.307	0.97	-	1.367	0.99	-	1.361	0.99	7573
absdev	0.0379	1.251	0.79	0.0426	1.308	0.82	0.057	1.265	0.99	7375
Shape, ϕ		≤ 0.3 [32]			0.3-0.5 [36]			≥ 0.5 [36]		
logmse	0.0365	1.372	0.99	0.0313	1.379	0.99	0.0297	1.358	0.98	7768
constrained	-	1.394	0.99	-	1.366	0.99	-	1.334	0.99	7719
absdev	0.025	1.456	0.99	0.0489	1.303	0.99	0.0523	1.243	0.99	7820
Slope, α		≤ 0.05 [47]			0.05-0.1 [33]			≥ 0.1 [23]		
logmse	0.0516	1.283	0.94	0.0326	1.354	0.96	0.0378	1.254	0.93	7219
constrained	-	1.366	0.99	-	1.348	0.99	-	1.327	0.98	7641
absdev	0.0624	1.253	0.99	0.0619	1.179	0.99	0.0436	1.194	0.96	7237

The results of the constrained experiment show that γ values decrease as slope and shape increases, whereas size-based classifications do not reveal any clear trend, in agreement with the results obtained by Adhikari and Marshall (2012) for a collection of synthetic glaciers. This implies that steep slopes and cirque-type glaciers are less sensitive to changes in glacier area.

Concerning the unconstrained experiments, let us first remind that, as shown in Table 5.4, the total volumen of Svalbard glaciers computed using, for a given fitting strategy, a single scaling-law for all glaciers, were 7,546 and 7,424 km^3, for the *logmse* and *absdev* misfit functions, respectively. Comparing these values with those in Table 5.6 for the unconstrained experiments, we see that the volumes of the total population of Svalbard glaciers calculated according to partitioning in subgroups by size and slope are smaller (by amounts between 1% and 4%, depending on the fitting strategy) than that obtained considering all glaciers without partitioning into subgroups, whereas the volumes calculated according to partitioning in subgroups by shape are 3-5% larger.

We conclude, in agreement with Adhikari and Marshall (2012), that using shape and slope-based scaling laws provide refined volume estimates, in our case for the total volume of Svalbard glaciers, even though in general it would be expected that using smaller sample sizes for deriving the scaling laws would degrade the expected accuracy of the volume estimates for the entire population of glaciers (Farinotti and Huss, 2013).

We have not considered, for deriving type-specific scaling laws, other possible glacier groupings. In our Svalbard study, a straightforward partitioning would be to distinguish between tidewater and land-terminating glaciers. However, for our sample of *(A,V)*-pairs this partitioning is nearly equivalent to a partitioning by size (with the tidewater glaciers being the largest), so it gives no further insight. Another clear classification criterion would be the grouping into surging and non-surging glaciers. In this case, the available set of *(A,V)*-pairs for surging glaciers is so small that it does not allow deriving a specific scaling law. Moreover, the volume-area ratios of surging glaciers are dependent upon the surge phase: while during the early post-surge period surging glaciers will generally have smaller volume-area ratios than non-surging glaciers, during the build-up period of the surge the converse will generally be true.

5.7 Multivariate analysis

Cogley (2012) pointed to the multivariate analysis as a way to overcome the limitations of

Table 5.7: ANOVA test: Model 1, Volume-Area.

Model	Square Sum	Df	Mean Square	F	Sig	Adjusted r^2
A	112.2	1	112.2	6776	$< 2 \times 10^{-16}$***	0.985
Residuals	1.7	101	0			

Significance codes: 0 '***', 0.001 '**', 0.01 '*', 0.05 '.', > 0.05 none

Table 5.8: ANOVA test: Model 2, Volume-Area-Length.

Model	Square Sum	Df	Mean Square	F	Sig	Adjusted r^2
A	112.2	1	112.2	7775.2	$< 2 \times 10^{-16}$***	0.886
L	0.2	0.2	1	15.9	0.00012***	
Residuals	1.4	100	0			

Significance codes: 0 '***', 0.001 '**', 0.01 '*', 0.05 '.', > 0.05 none

scaling relationships for estimating the glacier volume. Later on, Grinsted (2013) applied this analysis in his estimate of global glacier volume, yielding improved results. Following the ideas by Grinsted (2013), we attempt to optimally predict the total volume of Svalbard glaciers from a combination of different predictors: glacier area (A), glacier maximum length (L) and glacier elevation range (R). We exclude from this analysis variables such as glacier slope and shape to avoid the multicollinearity among the variables.

First, we apply ANOVA tests (Hinkelmann and Kempthorne) in order to select valuable variables for the model and to test different regression methods. ANOVA uses traditional standardized terminology based on the definitional equation of sample variance:

$$s^2 = \frac{1}{n-1} \sum (y_i - \bar{y})^2 \tag{5.4}$$

where the denominator is called the degrees of freedom (Df), the summation is called the sum of squares (Square Sum), the result is called the Mean Square and the squared terms are deviations from the sample mean. These values are shown in the tables for our ANOVA tests

Table 5.9: ANOVA test: Model 3, Volume-Area-Elevation Range.

Model	Square Sum	Df	Mean Square	F	Sig	Adjusted r^2
A	112.2	1	112	6716.2	$< 2 \times 10^{-16}$***	0.985
R	0.0	1	0	0.7	0.897	
Residuals	1.7	100	0			

Significance codes: 0 '***', 0.001 '**', 0.01 '*', 0.05 '.', > 0.05 none

Table 5.10: ANOVA test: Model 4, Volume-Area-Length-Elevation Range.

Model	Square Sum	Df	Mean Square	F	Sig	Adjusted r^2
A	112.2	1	112.2	8001.1	$< 2 \times 10^{-16}$ ***	0.987
L	0.2	1	0.2	16.4	0.0001**	
R	0.1	1	0.1	3.9	0.051	
Residuals	1.4	99	0			

Significance codes: 0 '***', 0.001 '**', 0.01 '*', 0.05 '.', > 0.05 none

results, together with other statistics: F represents the F-test statistic used for comparing the statistical model that have been fitted to the data set, in order to identify the model that best fits the population from which the data were sampled. The degree of significance reached by the model (Sig), also known as the p-value, is the probability of obtaining a value, at least as extreme as that obtained by the F statistic assuming that the null hypothesis is true (Goodman, 1999). We will reject the null hypothesis when the p-value is less than the predetermined significance level which is fixed at 0.05. r^2 is the coefficient of determination (r is used instead of R to avoid confusion with R = elevation range). r^2 indicates the proportion of the variability explained by the model. The main inconvenient of this indicator appears when we try to compare models with different number of predictors, as r^2 always grows with increasing number of variables even if the predictors do not influence the response. To avoid this, we use the *Adjusted* r^2, which is corrected for the number of explanatory terms in a model relative to the number of data points, which are in the end the degrees of freedom (Everitt, 1998).

From a simple V-A model in the log-log space we get a 98.6% of variance explanation. Additional variables do not improve our results significantly. The ANOVA tests show that only the predictor *glacier length* (L) (Table 5.8) provides statistical significance when used in addition to *glacier area* in to the model. However the coefficient of determination r^2 decreases as compared with the simpler V-A model. The predictor variable *elevation rate* (R), does not provide any additional information if it is used in addition to the *glacier area* (A) variable in the model.

In order to compare the different models we use leave-one-out cross-validation. Table 5.12 shows the regional ice volume estimates for Svalbard using different regression models. The best result (minimum $\epsilon_{crossval}$) is reached with the model $V = cL^{\gamma}$, especially when using the *logmse* fitting strategy. In this case, it shows a higher accuracy than the widely used volume-area scaling. A similar result was pointed out in a study of different scaling methods

Table 5.11: Selecting models. ϵ_{sample} represents the error of the given model in estimating the volume of our sample of glaciers, and $\epsilon_{crossval}$ is the cross-validation error.

Strategy	Scaling law	Svalbard vol. estimate (km^3)	ϵ_{sample} (%)	$\epsilon_{crossval}$ (%)
logmse	$0.0332\ A^{1.361}$	7546	4.3	4.8
	$0.0164\ L^{2.501}$	7947	-1.9	-0.8
	$0.0278\ A^{1.200}L^{0.331}$	7712	5.9	6.5
	$0.0335\ A^{1.36}R^{0.011}$	7345	4.3	4.8
	$0.0206\ A^{1.171}L^{0.451}R^{-0.229}$	7357	6.5	7.1
absdev	$0.0452\ A^{1.303}$	7424	0	1.1
	$0.0168\ L^{2.499}$	8106	0	-1.6
	$0.0385\ A^{1.081}L^{0.433}$	7539	0	1.3
	$0.0285\ A^{1.355}R^{-0.412}$	6890	0	1.1
	$0.0388\ A^{1.078}L^{0.436}R^{0.01}$	7558	0	0.95

for estimating the volume evolution of valley glaciers (Radić et al., 2008). Other than the mentioned case for the *logmse* strategy, in general the *absdev* strategy provides, for all multivariate scaling laws, lower cross-validation errors (of about 1%), the lowest corresponding to the $V = cA^{\gamma_1}L^{\gamma_2}R^{\gamma_3}$ scaling law, although the small exponent of R confirms the low predicting capability of this variable, as was pointed out from the associated ANOVA test. The negative exponents in Table 5.12 indicate an inverse correlation with the volume. Negative exponents in R are reasonable, as they can point out to increases in slope that cause an increase in ice-flow velocities, which allows a thinner glacier to accommodate to the same mass flux (Grinsted, 2013).

5.8 The case of Austfonna and Vestfonna ice caps

The extrapolation to ice caps of scaling relationships that have been calibrated for glaciers is thought to be the dominant source of error in global ice volume estimates (Grinsted, 2013), and this could be expected to hold in regional ice volume estimates where both types of ice masses are abundant. To overcome this problem, scaling laws specific for ice caps are provided by many authors, especially those deriving global ice volume estimates. In our case of Svalbard glaciers, we did not generate an ice-cap-specific scaling law, since only two ice caps (Austfonna and Vestfonna) had radio-echo sounding coverage sufficient to provide volume estimates accurate enough to warrant their inclusion in our data set of computed

volumes. Yet, there is the possibility to either use ice-cap-specific scaling laws derived from global inventories, or using ice-cap-specific regional scaling laws for Svalbard derived from older radio-echo sounding measurements, as done by Macheret et al. (1984) or by Hagen et al. (1993).

In the currently available glacier inventories (DDSG and RGI), both Austfonna and Vestfonna ice caps appear subdivided into individual basins, which, as discussed in Section 5.2, allowed us to increase the size of our sample data set of (V, A)-pairs. This, however, has the implication that a common scaling law has to be used for both glaciers and ice caps. Since the volumes of both Austfonna and Vestfonna are accurately known from dense nets of GPR profiles (relative errors of 3% and 7%, respectively), we can test how our scaling relationships, all of which consider their individual basins rather than the entire ice cap, compare with available scaling relationships specific for ice caps. Table 5.12 shows the results from our tests. From these, it is clear that our own estimates provide a much better approach to the measured volume, no matter the fitting strategy chosen. It could be argued that these results are partially skewed, as the volumes of Austfonna and Vestfonna individual basins are part of our sample of (V, A)-pairs. However, all of our results are even closer to the measured volumes than the ice-cap-specific scaling laws based on Svalbard ice caps. Among the latter, that by Hagen et al. (1993) is the one providing the best results. Among our own estimates, the results obtained using the *logmse* fitting strategy are the ones which most closely approach the measured volumes for both Austfonna and Vestfonna ice caps. In all of our estimates, the volume of Austfonna is better approached (in general, slightly underestimated) than that of Vestfonna (always overestimated). This could be due to the fact that there is a larger number of Austfonna basins (26) than of Vestfonna basins (19) in our set of *(A, V)*-pairs. On the other hand, we can see in Table 5.12 that the results for Vestfonna worsen when the scaling laws for basins larger than 100 (km^2) are used. The likely reason for this is that Vestfonna basins are in general much smaller than Austfonna basins, with Vestfonna having only 9 (out of 19 in our data set) basins larger than 100 (km^2), while Austfonna has 19 out of 26.

Table 5.12: Differences between measured and computed volumes, using our sliding laws (both general ones and those given in Table 5.6 for glacier basins larger than 100 km^2) or ice-cap-specific sliding laws, both global (Macheret et al. (1984), Hagen et al. (1993)) and regional (Radić and Hock (2010), Grinsted (2013)).

Scaling Law	Austfonna		Vestfonna	
	Vol (km^3)	Diff (%)	Vol (km^3)	Diff (%)
V from GPR	2559	-	442	-
This study *absdev*	2413	-5.7	499	12.9
This study $absdev_{>=100\text{km}^2}$	2403	-6.1	520	17.6
This study *logmse*	2561	0.1	495	11.9
This study $logmse_{>=100\text{km}^2}$	2338	-8.6	521	17.7
Ice cap Macheret	1285	-49.8	276	-37.6
Ice cap Hagen	2114	-17.4	536	21.3
Ice cap Radić and Hock	4116	60.8	885	100.2
Ice cap Grinsted	2761	7.8	608	37.6

5.9 Comparison with other V-A relationships

In Table 5.13 we summarize the total ice volume estimates derived for Svalbard found in the literature (V_{Sv}) using different scaling approaches. Note that some are given for glaciers of any type, while others distinguish between glaciers and ice caps. Note also that this table combines both published estimates for Svalbard (in this case they are sometimes based in different inventories of Svalbard glaciers) and, when no published estimate for Svalbard is available for a given scaling law, we have calculated it using such a law together with the DDSG inventory (see table footnotes). Some of the published volumes are based in the same (or nearly coincident) inventories as ours (the DDSG). This is the case for Radić et al. (2013) and for Grinsted (2013) estimates based on the RGI.

The estimates shown in the table range within 5,229-10,629 km^3, with an average value of 8,113 $\pm$ 1,743 km^3 if we exclude our own estimates, and 8,000 $\pm$ 1,578 km^3 if our estimates shown in Table 5.13 are included. In both cases, the quoted error indicates the standard deviations of the different estimates considered. Some of the scaling laws have been calibrated using only Svalbard glaciers. Apart from ours, this is the case of the relationships by Hagen et al. (1993) and by Macheret et al. (1984). There is a strong similarity among these regionally-based results, with an average volume estimate of 7,419$\pm$ 241 km^3. Note the small value of this standard deviation as compared with those given above. The fact that the

estimate by Macheret et al. (1984) is larger than that of Hagen et al. (1993) could be partly due to the fact that the former is based on and older inventory of Svalbard glaciers, several decades older than that used by Hagen et al. (1993), so the areas and volumes of the latter are expected to be lower due to the overall retreating trend of Svalbard glaciers during that period.

The largest total volume estimates are those by Radić and Hock (2010) and by the general scaling law of Adhikari and Marshall (2012) derived from their entire set of synthetic glaciers, without partitioning in groups by slope, aspect or size, as well as their size-based scaling law. Curiously, the estimates using the slope- and shape-based scaling laws by Adhikari and Marshall (2012) are those, among the global-scale relationships, producing the estimates closer to our own (and all Svalbard regional) ones. The volume derived from Huss and Farinotti (2012) relationship (based on volumes calculated using a physical-based model) are also among the largest. So does the estimate by Radić et al. (2013), who use the same relationship as in Radić and Hock (2010), but employ an updated glacier inventory. Also among the largest are the estimates by Grinsted (2013) based on the WGI/GLIMS inventory, while those based on the RGI are, by far, the smallest. Also among the smaller volume estimates are those produced using the global relationships by Chen and Ohmura (1990) and Bahr (1997).

With regard to their ability of the scaling relationships by other authors to compute the total volume of our sample data set of measured (V, A)-pairs, the shape- and slope-based relationships by Adhikari and Marshall (2012) perform clearly best, underestimating the volume of the sample by 10% and 4%, respectively. However, their size-based scaling relation is among those providing the largest overestimates of the sample volume (31% error), and their relation not considering sub-groupings produce the worst estimate of the sample volume (53% error). Among the scaling approaches not considering sub-groupings by shape or slope, the scaling derived by Grinsted (2013) and using the Randolph Glacier Inventory provides the best approximation, underestimating the volume of the ensemble by 11%, closely followed by the scaling approaches by Chen and Ohmura (1990) and by Bahr (1997), which underestimate the total volume by 13% and 14%, respectively. A result similar to the latter in absolute value, though of opposite sign, is provided by the scaling law for valley glaciers by Macheret et al. (1984), specific for Svalbard glaciers, which overestimates the volume of the ensemble by 14%. However, the other regionally-based relationship, that of Hagen et al. (1993), underestimates the sample volume by 20%. The scaling relation by Radić and Hock (2010) (the same as

used in Radić et al. (2013)) overestimates the sample volume by 25%. We remind that this scaling law has been pointed out to overestimate the glacier volumes (Grinsted, 2013). A similar overestimate (27%) is produced when using the scaling by Huss and Farinotti (2012), based on volumes computed using their physically-based method. A large underestimate, by 35%, is given by Grinsted (2013) scaling laws used with the WGI/GLIMS inventory.

Table 5.13: Total volume estimates for Svalbard glaciers (V_{Sv}) calculated using various scaling relationships found in the literature, together with our own ones, and relative errors produced when applied to our calibration data set ($\epsilon_{V_{Sample}}$).

Source	Glacier data set	Scaling law	V_{Sv}	$\epsilon_{V_{Sample}}$ (%) [a]
This study, *logmse*	Svalbard glaciers	$V = 0.0332A^{1.361}$	7546	4.3
This study, *absdev*	Svalbard glaciers	$V = 0.0452A^{1.303}$	7424	1.1[b]
This study, *absdev*	Svalbard glaciers	$V = 0.0388A^{1.078}L^{0.436}R^{0.01}$	7558	0.95[b]
Macheret et al.(1984)	Valley glaciers	$V = 0.0371A^{1.357}$	7567	13.6
Hagen(1993)[c]	Glaciers $A > 1km^2$	$H = 33ln(A) + 25$	7000	-19.7
	$A < 1km^2$	H = 25		
	Ice caps	$H = 28ln(A) + 10$		
Chen and Ohmura(1990)[d]	Valley glaciers	$V = 0.0285A^{1.357}$	6326	-12.7
Bahr et al.(1997)[d]	Glaciers	$V = 0.0276A^{1.36}$	6230	-13.9
Radić and Hock(2010)*	Valley glaciers	$V = 0.0365A^{1.375}$	10260	24.6
	Ice caps	$V = 0.0538A^{1.25}$		
Huss and Farinotti(2012)[e]	Glaciers	$H = 0.310A^{0.355}$	9690	26.6
Adhikari and Marshall[2012][d]	Glaciers	$V = 0.027A^{1.458}$	10629	52.7
	Shape - Glaciers		7061	-9.5
	Slope - Glaciers		7394	-3.8
	Size - Glacier		9423	30.9
Grinsted(2013)	Glaciers (RGI)	$V = 0.0433A^{1.29}$	5229	-11.3
	Ice caps (RGI)	$V = 0.0432A^{1.23}$		
	$A < 25\ km^2$(WGI/GLIMS)	$V = 0.0435A^{1.23}$	9573	-35.2
	$A > 25\ km^2$ (WGI/GLIMS)	$V = 0.0540A^{1.20}$		
Ràdic et al.(2013)	Valley glaciers	$V = 0.0365A^{1.375}$	9090	24.6
	Ice caps	$V = 0.0538A^{1.25}$		

[a] :$\epsilon_{V_{Sample}}$ is calculated as $(V_{model_i} - V_{sample})/V_{sample} * 100$.
[b] : As the absdev model yields an exact total volume of the sample, the cross-validation error is shown here.
[c] : H is the mean ice thickness in m, A is in km^2.
[d] : There is not a published volume for Svalbard in the original publication. The values shown here have been calculated applying the original scaling equations to the glacier areas from the Digital Database for Svalbard glaciers.
[e] : H is the mean ice thickness in m, A is the glacier area in m^2.

5.10 An error estimate of the total volume

It is of interest to know the accuracy that could be expected when computing the volume of the complete population of Svalbard glaciers using a V-A relationship. As pointed out in Section 5.2, the recent study by Farinotti and Huss (2013) derived an upper-bound estimate for the accuracy with which the total volume can be recovered in relation to the size of the glacier population, the size of the sample of glaciers used to estimate the scaling parameters and the uncertainty of measured volumes. Applied to our case study of Svalbard glaciers, their results suggest that the total volume of the population of glaciers could be retrieved with ca. 40% accuracy. We note that this value represents an upper bound of the expected accuracy.

In addition to error bounds, we are also interested in error estimates are derived following the principle of error propagation (e.q., Bevington, 1969). We here follow the approach used in Radić and Hock (2010) to calculate the error. The From the V-A scaling equation (5.1) we find the error sources in the determination of the scaling parameters (γ and c) and the total glacierized area, A, which we assume independent and random errors. We propagate these errors to obtain the total error in volume:

$$\delta V^2 = \left(\frac{\partial V}{\partial c}\right)^2 \delta c^2 + \left(\frac{\partial V}{\partial \gamma}\right)^2 \delta \gamma^2 + \left(\frac{\partial V}{\partial A}\right)^2 \delta A^2 \tag{5.5}$$

Following Radić and Hock (2010) we estimate the error in the scaling coefficient, c, as 40% of its value, which arises from the standard deviation of the probability density function for c computed by Bahr et al. (1997). The error in the scaling exponent γ is assumed to be the difference between the value for γ used in the scaling-law (which varies with the model) and γ=1.375 derived theoretically by Bahr et al. (1997). The error in the total glacierized area of Svalbard is assumed to be the 8%, according to the results presented in Köning et al. (2013). We compute the error in the volume estimation for each of the individual glaciers in the Digital Database of Svalbard Glaciers and, assuming that they are independent errors, combine them through root mean square summation.

Table 5.14 shows the results obtained from the Area-Volume model accompanied by the error estimations from error propagation techniques.

Table 5.14: Total glacier volume of Svalbard and its potential contribution to SLR

Strategy	Scaling Law	Svalbard Vol. Estimate (km^3)	SLR (mm)*
logmse	$0.0332\ A^{1.361}$	7546 ± 611	19 ± 2
absdev	$0.0452\ A^{1.303}$	7424 ± 478	18 ± 1

*Sea level is calculated assuming oceanic area of 3.62x10$^8 km^2$ and a glacier density of 900 kgm^{-3}

5.11 Potential contribution of Svalbard glaciers to SLR

In terms of sea-level equivalent (SLE), assuming an oceanic area of 3.62x10$^8 km^2$ and a glacier ice density of 900 kg m^{-3}, our volume estimates correspond to a potential contribution to sea-level rise within 17-20 mm SLE, averaging 19±1 mm SLE. The quoted error corresponds to the standard deviation of the different estimates. However, since we estimated errors of the total volume of the order of 6.6-8.1%, and these correspond to 1.2-1.6 mm SLE, we conservatively state 19±2 mm SLE as our best estimate of the potential contribution of Svalbard glaciers to sea-level rise. For comparison, the estimates using the V-A scaling relations found in the literature range within 13-26 mm SLE, averaging 20±2 mm SLE (2 mm SLE being the standard deviation of the different estimates).

Chapter 6

Conclusions and outlook

The work carried out in this PhD. Thesis can be split into three parts:

1. First, we present in chapters 1 and 2 the motivation and objectives of our research, and describe the state of art on the matter. We describe the two main methods currently available for estimating the volume of very large sets of glaciers, such as those involved in regional and global volume estimates. They are the volume-area scaling relationships and the so-called physically-based methods. We discuss their strengths and weaknesses. A physically-based method has already been applied by Huss and Farinotti (2012) to the computation of the volume of the total population of Svalbard. Although methods based on volume-area relationships have also been applied with this purpose (Radić and Hock, 2011; Grinsted, 2013), the scaling relationships used have been of global character, which motivates our development of a volume-area relationship specific for Svalbard glaciers.

2. The construction of such a regional V-A scaling relationship relies on the availability of a large set of accurate enough glacier volumes calculated from ice-thickness measurements by ground-penetrating radar (though other ice-thickness measurement methods are possible, currently only GPR can provide the necessary amount and density of measurements). In the second part of the thesis (chapters 3 and 4), we first focus (Chapter 3) on the methodology for calculating glacier volumes from ice-thickness measurements collected on nets of GPR profiles. We pay special attention to the problem of estimating the error of the computed volumes, taking into account the different error sources involved (associated to GPR, positioning, interpolation, glacier boundary uncertainty, etc.). We present a novel method to deal with the complex problem of the estimate

of the error in glacier volume. Then, we focus (Chapter 4) on the collection and construction of a large set of volume-area pairs of Svalbard glaciers. With this purpose, we first compiled an inventory of Svalbard radio-echo sounded glaciers (many of them echo-sounded by our research team -Group of Numerical Methods in Engineering of the Technical University of Madrid) and then, for a subset of them (not all of the glaciers in the inventory passed our quality requirements for an accurate volume computation), we did the volume computation an associated error estimates following a common procedure for all glaciers (the procedure described in Chapter 3).

3. Finally, in the third part of the thesis (chapter 5) we use the compiled set of volume-area pairs to build different volume-area relationships specific for Svalbard glaciers. We speak of different relationships because distinct approaches can be followed to derive a V-A relationship, which differ in the fitting methodology, whether a single relationship is applied to the entire population of glaciers or the population is subdivided into groups according to parameters such as size, shape or slope, whether only area enters int the relationship or other variables such as glacier length or elevation range can enter it, etc. We present and discuss the resulting different scaling relationships, and compare their results with those obtained applying the V-A laws derived by other authors (both of regional and global types) to the same population of Svalbard glaciers. We then present our best estimate for the range of potential contribution of Svalbard glaciers to sea-level rise. We conclude with the presentation, in Chapter 6, of the main conclusions of this thesis and the prospects for future work.

6.1 Conclusions

The following main conclusions can be drawn from the work carried out in this PhD. Thesis:

- We have developed a novel method to account for the interpolation error which has been designed to work with data distributions with a high density of data along particular directions, often intersecting, but lacking data in the areas between profiles, such as those typical of GPR profiling. This method follows the rationale of cross-validation techniques, but takes into account the variance of the error with the distance to the nearest neighbour. It has the added benefit that it also provides a way to detect any possible bias involved in the interpolation process. This method has advantages over other commonly used methods, such as cross-validation and the kriging variance, which

we believe that underestimate the error when applied to data distributions such as those typical of GPR profiling. We have applied our method to a large set of Svalbard glaciers, as discussed below.

- With the aim of estimating the total ice volume of Svalbard glaciers, we have built an inventory of Svalbard radio-echo sounded glaciers. It covers a total of 155 glaciers or ice caps (in the inventory, Austfonna and Vestfonna ice caps appear as single units), but the number of entries is much larger (313 entries), because several GPR campaigns have been done on many glaciers or ice caps. 22 of these glaciers or ice caps have been echo-sounded by our research team, often in cooperation with Russian, Polish and Norwegian colleagues. The inventory includes entries describing the glacier name, its reference number in the Digital Database of Svalbard Glaciers (Köning et al., 2013), the coordinates of a central point, the glacier type (ice cap, valley, plateau, tidewater), whether a bathymetry in the neighbourhood of tidewater glacier fronts is available, whether boreholes have been drilled, the thermal structure (cold, temperate, polythermal), the year of the radio-echo sounding, the radar type/manufacturer/model and its central frequency, whether it was airborne or ground-based RES, the radio-wave velocity used for time-to-depth conversion, a contact person, related bibliographic references, and any additional comments of interest (e.g. whether common-midpoint measurements of the RWV are available) in a comments field. In addition to being the basis for our V-A scaling developments, this inventory is intended to serve as reference for future studies by other researchers.

- Not all of the glaciers in the inventory are suitable for building a volume-area scaling relationship. The main reason for a glacier being discarded is the lack of a large enough coverage of GPR profiles, since this would lead to a large error in the volume estimate. We have selected a subset of 103 glaciers (or sub-basins, in the case of Austfonna and Vestfonna ice caps) from the inventory and computed for them the volumes and associated error estimates. In particular, out of these 103 glacier basins:

  - 78 have estimated errors in volume below 10%. For 33 of them we had a dense net of GPR profiles which allowed us to calculate the volumes and errors following the procedure described in Chapter 3. The remaining 45 correspond to the individual basins of Austfonna and Vestfonna, for which we also had a dense net of GPR profiles. In this case we did the volume and error computation (following our

standard procedure), and then computed the volumes of the individual basins using their outlines, and assumed for all of them the same error as for the ice cap (note that, in this case, the error in volume associated to boundary uncertainty is null by definition).

  - 7 have estimated errors between 10% and 20%. For 2 of these glaciers we had a rather dense net of GPR profiles but nevertheless we got errors (following our standard procedure) between 10% and 20%. For 1 glacier we had a good-quality GPR profile all along its centre line, and assumed parabolic cross-section; we assumed its error to be within 10-20%. The remaining 4 volumes were taken from published sources, mostly in form of contour maps of ice-thickness, and its error are assumed to be within 10-20%.

  - The remaining 18 volumes have been taken from entries in Cogley's catalogue of worldwide glaciers (Cogley, 2012; Grinsted, 2013) non-overlapping with our inventory. All of them correspond to Soviet and British-Norwegian airborne echo-soundings in the seventies and eighties which only covered the glacier centre lines (Macheret and Zhuravlev, 1982; Dowdeswell et al., 1984a). We have assumed for them an error in volume below 30%. Note that these glaciers exclude the Soviet echo-soundings with doubtful interpretation of the bed reflection mentioned in Section 4.2.

- The areas of our sample of 103 glacier volume-area pairs range from 0.37 to 1,226.52 km^2. 74 glaciers are larger than 10 km^2, representing 99% of the total sample area, and 29 glaciers are smaller than 10 km^2, representing 1% of the total sample area. Corresponding numbers for the total population of 1668 Svalbard glaciers are as follows: about 350 glaciers (22% of the population) are larger than 10 km^2, representing 93% of the total area of the population, whereas the remaining 1320 glaciers (78% of the population) are smaller than 10 km^2, representing 7% of the total area of the population. We have tried to compensate this bias of our sample towards larger glaciers through the fitting strategy that uses the 'absdev' misfit function, which assigns a weight to the glaciers inversely to their area. The calculated volumes of the individual glacier basins range from 0.010±0.001 to 462.335±13.870 km^3. The maximum ice thickness, reaching 619±13 m, was found in the northernmost part of Austre Torellbreen, near its ice divide with Vestre Torellbreen, within the Amundsenisen ice field.

- Since we do not have a separate data set against which to validate the different scaling relationships, for testing their accuracy we use cross-validation techniques. The results of our tests of distinct k-fold cross-validation methods (in particular, 4-fold, 10-fold and leave-one-out cross-validation) show that, as expected, the cross-validation error decreases as the fold increases, though there is not a significant difference among the three approaches. Since, on the other hand, the expected accuracy of the total population volume decreases with the reduction of the sample (Farinotti and Huss, 2013), we conclude that leave-one-out crossvalidation is the most suitable technique for estimating the accuracy of the different scaling laws.

- We tested two different regression techniques to derive the V-A scaling relationship, least squares regression in the log-log space and least absolute deviation regression. The latter has been pointed out by Grinsted (2013) as a strategy better suited for sea-level rise studies, as it minimizes the absolute volume misfit and it is robust to outliers and asymmetric distributions. It also has the additional benefit that its weighting by the inverse root of the area reduces the sampling bias in our data set described in Section 5.2. Nevertheless, our tests show that both fitting strategies produce estimates of the total volume of Svalbard glaciers very similar, with less than 2% difference, so that the choice of the fitting strategy does not seem to be a crucial matter.

- The difference in glacierized area of Svalbard between the two most recent inventories of Svalbard glaciers, the Digital Database of Svalbard Glaciers (DDSG, (Köning et al., 2013)) and the Randolph Glacier Inventory V3 (RGI.3, (Arendt et al., 2012)) is rather small, of 102 km^2, implying differences in calculated volume using our V-A relationships of the order of 1%. Consequently, we will adhere to the DDSG, as our volume data are expected to be included in this database.

- We performed experiments aimed to verify whether scaling relationships obtained through characterization of individual glacier shape, slope and size imply significant differences in the estimated volume of the total population of Svalbard glaciers, and whether this partitioning implies any noticeable pattern in the scaling relationship parameters indicative of the influence of particular glacier settings.

  - The results of the constrained experiment, in which we calculate, for a fixed value of the scaling parameter c and using the *logmse* misfit function, the best-fit scaling parameter γ for each subgroup of glaciers (subgroups according to shape, slope

or size) show that γ values decrease as slope and shape increases, whereas size-based classifications do not reveal any clear trend. This implies that steep slopes and cirque-type glaciers are less sensitive to changes in glacier area. These results are similar to those obtained by Adhikari and Marshall (2012) for a collection of synthetic glaciers.

  - The unconstrained experiments show that the volumes of the total population of Svalbard glaciers calculated according to partitioning in subgroups by size and slope are smaller (by amounts between 1% and 4%, depending on the fitting strategy - *logmse* or *absdev* misfit functions) than that obtained considering all glaciers without partitioning into subgroups, whereas the volumes calculated according to partitioning in subgroups by shape are 3-5% larger.

- We did multivariate experiments attempting to optimally predict the volume of Svalbard glaciers from a combination of different predictors: glacier area (A), glacier maximum length (L) and glacier elevation range (R). We excluded from this analysis variables such as glacier slope and shape to avoid the multicollinearity among the variables. Our results where:

  - From a simple power-type V-A model we got a 98.6% of variance explanation. Additional variables do not improved our results significantly. The ANOVA test showed that only the predictor glacier length provides statistical significance when used in addition to the predictor glacier area, though the coefficient of determination r^2 decreases as compared with the simpler V-A model. The predictor elevation range did not provide any additional information when used in addition to glacier area.

  - Leave-one-out cross-validation used to compare the performance of the different models showed that minimum cross-validation error is reached with the volume-length scaling model, especially when using the *logmse* fitting strategy, behaving even better than the widely used volume-area scaling model. Similar results were obtained in the study by Radić et al. (2008) on the use of different scaling methods for estimating the volume evolution of valley glaciers. When used the *absdev* fitting strategy, the differences in cross-validation errors among the different multivariate scaling laws are rather small (the absolute values of the cross-validation errors are of the order of 1%).

- The ice volumes of Austfonna and Vestfonna ice caps are quite accurately known from dense nets of GPR profiles (relative errors of 3% and 7%, respectively). We tested how our scaling relationships, all of which consider their individual basins rather than the entire ice cap, compare with available scaling relationships specific for ice caps, both derived from world-wide ice caps and from Svalbard-only ice caps. Our results clearly show that our own estimates provide a much better approach to the measured volume, no matter the fitting strategy chosen. It could be argued that these results are partially skewed, as the volumes of Austfonna and Vestfonna individual basins are part of our sample of (V, A)-pairs. However, all of our results are even closer to the measured volumes than those provided by the Svalbard-based ice-cap-specific scaling law producing the best results (that by Hagen et al. (1993)). Among our own estimates, the results obtained using the *logmse* fitting strategy are the ones which most closely approach the measured volumes for both Austfonna and Vestfonna ice caps.

- We tested how the different volume-area relationships available in the literature behave for estimating the volume of our sample data set of measured (V, A)-pairs of Svalbard glaciers, and calculated what volume estimate they produce when applied to the entire population of Svalbard glaciers.

  - The volume estimates for the entire population of Svalbard glaciers show a rather large spread, ranging within 5,229-10,629 km^3, with an average value of 8,157±1920 km^3 if we exclude our own estimates (the quoted error corresponds to the standard deviation of the different volume estimates).
  - With regard to their ability to compute the total volume of our sample set of measured (V, A)-pairs, the shape- and slope-based relationships by Adhikari and Marshall (2012) perform clearly best, underestimating the volume of the sample by 9.5% and 3.8%, respectively. Among the scaling approaches not considering sub-groupings by shape or slope, the scaling derived by Grinsted (2013) based on the Randolph Glacier Inventory provides the best approximation, underestimating the volume of the ensemble by 11%, closely followed by the scaling approaches by Chen and Ohmura (1990) and by Bahr (1997), which underestimate the total volume by 13% and 14%, respectively. A result similar to the latter in absolute value, though of opposite sign, is provided by the scaling law for valley glaciers by Macheret et al. (1984), specific for Svalbard glaciers, which overestimates the volume of the ensemble by 14%.

- The estimate of the error in our calculation of the total ice volume of Svalbard glaciers from V-A scaling relationships using standard error propagation techniques, following the procedure by Radić and Hock (2010), give relative errors in volume of 8.1% and 6.4%, for the *logmse* and *absdev* fitting strategies, respectively. In particular, the volume estimates and their associated error estimates are 7,546±611 km^3 (*logmse*) and 7,424±478 km^3 (*absdev*).

- Our estimates of the volume of the entire population of Svalbard glaciers using the different scaling relationships that we have derived along this thesis range within 6,890-8,106 km^3. Both extreme values correspond to estimates from multivariate scaling relations using the *absdev* misfit function. The average value of all of our estimates, which could be used as a best estimate for the volume, is 7,504±312 km^3, where the quoted error is the standard deviation of the calculated volumes.

- In terms of sea-level equivalent (SLE), assuming an oceanic area of 3.62x$10^8 km^2$ and a glacier ice density of 900 kg m^{-3}, our volume estimates correspond to a potential contribution to sea-level rise within 17-20 mm SLE, averaging 19±1 mm SLE. The quoted error, again, corresponds to the standard deviation of the different estimates. However, since we estimated errors of the total volume of the order of 6.6-8.1%, and these correspond to 1.2-1.6 mm SLE, we conservatively state 19±2 mm SLE as our best estimate of the potential contribution of Svalbard glaciers to sea-level rise. For comparison, the estimates using the V-A scaling relations found in the literature range within 13-26 mm SLE, averaging 20±2 mm SLE (2 mm SLE being the standard deviation of the different estimates).

6.2 Outlook

As a by-product of this thesis, we have produced a rather large set of high-accuracy ice-thickness maps of Svalbard glaciers. A line of future research would address the generation of volume change projections of Svalbard glaciers to the end of the twenty-first century, using the scaling laws derived from this dissertation. This modelling approach has been used e.g. by Radić et al. (2013) to model the contribution to sea-level rise of glaciers and ice caps during the 21st century.

For each glacier for which an accurate ice thickness distribution has been derived in this dissertation, we would calculate the mass balance. Mass balance could be calculated based on

a downscaled version of future climate change produced by a global climate model (GCM). The model parameters would be calibrated for each individual glacier to yield maximum agreement between the modelled and observed area-averaged winter and summer mass balances for a calibration period. The forcing mass balance implies geometrical changes of the glacier which are simulated by the glacier response model that explicitly considers the future shrinking area of glaciers and ice caps.

The methodology would be as follows: the first step would be to co-register the ice thickness datasets to the overall model domain as it is given by the Svalbard-wide ASTER GDEM2 and to calculate bedrock topographies for the test glaciers. Afterwards we would downscale the GCM dataset, for which we could use the European Arctic Reanalysis (EAR) datasets of 10-km grid as local reference data for both air temperature and precipitation. GCM air temperatures would then be downscaled by using variance inflation, while precipitation downscaling would be done using local scaling (Möller et al., 2013). Mean annual cycles of local lapse rates of both air temperature and precipitation could also be extracted from the EAR 10-km grids. They could be calculated from the set of grid cells surrounding the respective glacier by taking into account modelled climate data and the underlying terrain dataset of the WRF regional climate model. Mass balance and ice-mass evolution would be modelled for all the glaciers for the period 2006-2100 on the basis of the CMIP5 scenarios RCP 2.6, 4.5, 6.0 and 8.5 (Vuuren et al., 2007; Smith and Wigley, 2006; Riahi et al., 2007). For each of these scenarios we would run the model with downscaled climate data of 10 different global circulation models. These computations would be repeated 100 times in the course of a Monte Carlo simulation.

Chapter 7

APPENDIX

Glacier	Type	Bat.	Bor.	Therm. Struct.	Surge	Contact Person	Reference	Year	Radar	Freq. MHz	RWV	Platform
Aavatsmarkbreen	Tidewater			polythermal	1982-85	Yuri Macheret	Macheret and Zhuravlev, 1980	1974 1979	RV17	440	168	Helicopter
Abrahamsembreen	Valley			N.A.	1978	Julian Dowdeswell	Bamber, 1989	1983	MK IV	60	168	Helicopter
Akademikerbreen	Part of			N.A.		Julian Dowdeswell	Bamber, 1989	1983	MK IV	60	168	Helicopter
Aldegondabreen	Valley			polythermal		Yuri Macheret	Macheret and Zhuravlev, 1980	1974 1979	RV17	440	168	Helicopter
Aldegondabreen	Valley			polythermal		Francisco Navarro	Navarro et al., 2005, Martin-Espanol et al., 2013	1999	VIRL2	15	168	Snowmobile
Amundsenisen	Plateau		*	polythermal		Russian	Internal report	2004	VIRL6	20	168	Snowmobile
Amundsenisen	Plateau		*	polythermal		Andrey Glazovsky	Internal report	2006	VIRL6	20	168	Snowmobile
Amundsenisen	Plateau		*	polythermal		Yuri Macheret	Macheret and Zhuravlev, 1980	1974 1979	RV17	440	168	Helicopter
Amundsenisen	Plateau		*	polythermal		Mariusz Grabiec	Unpublished	2008	RAMAC	25	164	Snowmobile
Amundsenisen	Plateau		*	polythermal		Francisco Navarro	Unpublished	2009	RAMAC	100	168	Snowmobile
Amundsenisen	Plateau		*	polythermal		Francisco Navarro	Unpublished	2009	VIRL6 VIRL7	20	168	Snowmobile
Amundsenisen	Plateau		*	polythermal		Francisco Navarro	Unpublished	2011	VIRL7	20	168	Snowmobile
Antoniabreen	Valley			polythermal		Yuri Macheret	Macheret and Zhuravlev, 1980	1974 1979	RV17	440	168	Helicopter
Ariebreen	Valley			cold		Francisco Navarro	IASC 2007 abstracts pp64-66	2006	RAMAC	200	168	By foot
Ariebreen	Valley			cold		Francisco Navarro	IASC 2007 abstracts pp64-66	2006	RAMAC	200	168	By foot
Ariebreen	Valley			cold		Mariusz Grabiec	IASC 2008 abstracts pp46-49	2007	RAMAC	200	164	Snowmobile
Ariebreen	Valley			cold		Mariusz Grabiec	IASC 2008 abstracts pp79-81	2007	RAMAC	25	168	Snowmobile
Ariebreen	Valley			cold		Francisco Navarro	Lapazaran et al., 2013	2009	RAMAC	25	168	Snowmobile
Ariebreen	Valley			cold		Francisco Navarro	Lapazaran et al., 2013	2009	RAMAC	25	168	Snowmobile
Åsgårdfonna	Plateau		*	N.A.	1960	Julian Dowdeswell	Bamber, 1989	1983	MK IV	60	168	Helicopter
Åsgårdfonna	Plateau		*	N.A.	1960	Yuri Macheret	Macheret and Zhuravlev, 1980	1974 1979	RV17	440	168	Helicopter
Austfonna	Icecap		*	polythermal		Geir Moholdt	Danish National Space Center Report 2008	2007	DTU	60	168	Airplane
Austfonna	Icecap		*	polythermal		Julian Dowdeswell	Dowdeswel et al., 1986	1983	MK IV	60	168	Helicopter
Austfonna	Icecap		*	polythermal		Francisco Navarro Thorben Dunse	GEUS report 2010 pp64-67	2008	VIRL6	20	168	Snowmobile

Glacier	Type	Bat.	Bor.	Therm. Struct.	Surge	Contact Person	Reference	Year	Radar	Freq. MHz	RWV	Platform
Baalsrudbreen	Valley			N.A.		Francisco Navarro Ivan Lavrentiev	Unpublished	2013	VIRL6	20	168	Snowmobile
Bakaninbreen	Valley			polythermal	1985-95	Murray	Murray et al., 1997	1995	PulsEkko	100	167	Snowmobile
Bakaninbreen	Valley			polythermal	1985-95	Murray	Murray et al., 1997	1995	PulsEkko	100	163-173	Snowmobile
Balderfonna	Plateau			N.A.		Julian Dowdeswell	Bamber, 1989	1983	MK IV	60	168	Helicopter
Balderfonna	Plateau			N.A.		Yuri Macheret	Macheret and Zhuravlev, 1980	1974 1979	RV17	440	168	Helicopter
Barenstjøkulen	Icecap			N.A.		Julian Dowdeswell	Dowdeswell and Bamber, 1995	1986	MK IV	60	168	Airplane
Bertilbreen	Valley			polythermal		Yuri Macheret	Macheret and Zhuravlev, 1980	1974 1979	RV17	440	168	Helicopter
Bertilbreen	Valley			polythermal		Jakub Malecki	Malecki et al., 2013	2012	RAMAC	100	170	Snowmobile
Bertrambreen	Outlet			cold		Jakub Malecki	Malecki et al., 2013	2012	RAMAC	100	170	Snowmobile
Björnbreen	Part of			polythermal		Yuri Macheret	Macheret and Zhuravlev, 1980	1974 1979	RV17	440	168	Helicopter
Blekumbreen	Valley			N.A.		Francisco Navarro Ivan Lavrentiev	Unpublished	2013	VIRL6	20	168	Snowmobile
Blomstrandbreen	Tidewater			N.A.	1960	Julian Dowdeswell	Drewry et al., 1980	1980	MK IV	60		Helicopter
Boggebreen	Part of			polythermal	1980	Heidi Sevestre	Unpublished	2012	RAMAC	25		Snowmobile
Boggerbreen	Part of			polythermal	1980	Yuri Macheret	Macheret, 1976 Macheret and Zhuravlev, 1980	1974	RV17	430-685		Snowmobile
Borebreen	Tidewater			N.A.		Julian Dowdeswell	Bamber, 1989	1983	MK IV	60	168	Helicopter
Borebreen	Tidewater			N.A.		Julian Dowdeswell	Dowdeswell et al., 1984	1980	MK IV	60	168	Helicopter
Borebreen	Tidewater			N.A.		Yuri Macheret	Macheret and Zhuravlev, 1980	1974 1979	RV17	440	168	Helicopter
Brøggerbreen	Valley			polythermal		John Moore	GPR investigations of Glaciers and Sea Ice in the Scandinavian Arctic	1997	RAMAC	200	220	Snowmobile
Brøggerbreen Austre	Valley		*	polythermal	1890	Finnur Pálsson	Björnsson et al., 1996	1990	Time gated synthetic pulse radar	5-20	168	Snowmobile
Brøggerbreen Austre	Valley		*	polythermal	1890	Julian Dowdeswell	Dowdeswell et al., 1984	1980	MK IV	60	168	Helicopter
Brøggerbreen Austre	Valley		*	polythermal	1890	Jon Ove Hagen	Hagen and SæTrang, 1991	1988	MARKII	8	169	Snowmobile

Glacier	Type	Bat.	Bor.	Therm. Struct.	Surge	Contact Person	Reference	Year	Radar	Freq. MHz	RWV	Platform
Brøggerbreen Austre	Valley		*	polythermal	1890	Yuri Macheret	Macheret and Zhuravlev, 1980	1974 1979	RV17	440	168	Helicopter
Brøggerbreen Austre	Valley		*	polythermal	1890	Yuri Macheret	Macheret, 1976 Macheret and Zhuravlev, 1980	1974	RV17	430-685		Snowmobile
Brøggerbreen Austre	Valley		*	polythermal	1890	Tavi Murray	Stuart and Murray, 2003	1999	RAMAC	100	166	Snowmobile
Brøggerbreen Austre	Valley			polythermal		Tavi Murray	Stuart and Murray, 2003	1999	RAMAC	100		Snowmobile
Brøggerbreen Vestre	Valley			polythermal		Yuri Macheret	Macheret and Zhuravlev, 1980	1974 1979	RV17	440	168	Helicopter
Brucebreen	Valley			polythermal		Heidi Sevestre	Unpublished	2012	RAMAC	25		Snowmobile
Chydenuisbreen	Tidewater			N.A.		Julian Dowdeswell	Bamber, 1989	1983	MK IV	60	168	Helicopter
Comfortlessbreen	Tidewater			polythermal		Yuri Macheret	Macheret and Zhuravlev, 1980	1974 1979	RV17	440	168	Helicopter
Cookbreen	Valley			polythermal		Yuri Macheret	Macheret and Zhuravlev, 1980	1974 1979	RV17	440	168	Helicopter
Dahlbreen	Tidewater			polythermal		Yuri Macheret	Macheret and Zhuravlev, 1980	1974 1979	RV17	440	168	Helicopter
Dahlfonna	Valley			polythermal		Yuri Macheret	Macheret and Zhuravlev, 1980	1974 1979	RV17	440	168	Helicopter
Dahlfonna East	Valley			polythermal		Francisco Navarro	Martín-Español et al., 2013	2010	VIRL6	20	168	Snowmobile
Dalhfonna	Valley			polythermal		Ivan Lavrentiev	Martín-Español et al., 2013	2012	VIRL6	20	168	Snowmobile
Davisbreen	Tidewater			polythermal	1960	Anja Pälli	Pälli et al., 2003	2000	RAMAC	50		Snowmobile
Digerfonna	Plateau			N.A.		Julian Dowdeswell	Dowdeswell and Bamber, 1995	1986	MK IV	60	168	Airplane
Dobrowolskibreen	Part of			polythermal		Yuri Macheret	Macheret and Zhuravlev, 1980	1974 1979	RV17	440	168	Helicopter
Doktorbreen	Tidewater			N.A.		Julian Dowdeswell	Drewry et al., 1980	1980	MK IV	60		Helicopter
Dunerbreen	Valley			N.A.		Julian Dowdeswell	Bamber, 1989	1983	MK IV	60	168	Helicopter
Ebbabreen	Outlet			polythermal		Jakub Malecki	Malecki et al., 2013	2012	RAMAC	100	170	Snowmobile
Edgeøyjøkulen	Icecap			N.A.		Julian Dowdeswell	Dowdeswell and Bamber, 1995	1986	MK IV	60	168	Airplane
Eidembreen	Valley			N.A.		Julian Dowdeswell	Bamber, 1989	1983	MK IV	60	168	Helicopter
Eidembreen	Valley			N.A.		Julian Dowdeswell	Dowdeswell et al., 1984	1980	MK IV	60	168	Helicopter
Eidembreen	Valley			N.A.		Yuri Macheret	Macheret and Zhuravlev, 1980	1974 1979	RV17	440	168	Helicopter
Elnabren	Valley			polythermal	1930	Yuri Macheret	Macheret and Zhuravlev, 1980	1974 1979	RV17	440	168	Helicopter

Glacier	Type	Bat.	Bor.	Therm. Struct.	Surge	Contact Person	Reference	Year	Radar	Freq. MHz	RWV	Platform
Erdmannbreen	Valley			polythermal		Yuri Macheret	Macheret and Zhuravlev, 1980	1974 1979	RV17	440	168	Helicopter
Erdmannbreen	Valley			polythermal		Ivan Lavrentiev	Martín-Español et al., 2013	2012	VIRL6	20	168	Snowmobile
Erikbreen	Valley			polythermal		Rune S. Ødegård	Ødegård et al., 1992	1991	Time gated synthetic pulse	5-20	168 202	Snowmobile
Finsterwalderbreen	Valley		*	polythermal	1900	Julian Dowdeswell	Dowdeswell et al., 1984	1980	MK IV	60	168	Helicopter
Finsterwalderbreen	Valley		*	polythermal	1900	Yuri Macheret	Macheret and Zhuravlev, 1980	1974 1979	RV17	440	168	Helicopter
Finsterwalderbreen	Valley		*	polythermal	1900	Ann Marie Nuttal	Ødegård et al., 1997	1994	Time gated synthetic pulse	600-65	168	Snowmobile
Finsterwalderbreen	Valley		*	polythermal	1900	Ann Marie Nuttal	Ødegård et al., 1997	1994	Time gated synthetic pulse	950-10	168	Snowmobile
Finsterwalderbreen	Valley		*	polythermal	1900	Ann Marie Nuttal	Ødegård et al., 1997 Nuttal et al., 1997	1994	Time gated synthetic pulse	320-37	168	Snowmobile
Finsterwalderbreen	Valley		*	polythermal	1900	Ann Marie Nuttal	Ødegård et al., 1997, Hagen, 2000, Hamran and Aarhold,1993	1994	Time gated synthetic pulse	30-80	168	Snowmobile
Fjortende Julibreen	Tidewater			N.A.		Julian Dowdeswell	Bamber, 1989	1983	MK IV	60	168	Helicopter
Flatbreen	Part of			N.A.		Anja Pälli	Pälli et al., 2003	2000	RAMAC	50	168	Snowmobile
Foxfonna	Plateau			N.A.		Julian Dowdeswell	Drewry et al., 1980	1980	MK IV	60		Helicopter
Fridtjovbreen	Tidewater		*	polythermal	1861 1991-97	Julian Dowdeswell	Dowdeswell et al., 1984	1980	MK IV	60	168	Helicopter
Fridtjovbreen	Tidewater		*	polythermal	1861 1991-97	Yuri Macheret	Glazowsky et al., 1991	1988	MPI 8	8		Snowmobile
Fridtjovbreen	Tidewater		*	polythermal	1861 1991-97	Yuri Macheret	Glazowsky et al., 1991	1988	MPI 8	8		Snowmobile
Fridtjovbreen	Tidewater		*	polythermal	1861 1991-97	Yuri Macheret	Macheret and Zhuravlev, 1980	1974 1979	RV17	440	168	Helicopter

Glacier	Type	Bat.	Bor.	Therm. Struct.	Surge	Contact Person	Reference	Year	Radar	Freq. MHz	RWV	Platform
Fridtjovbreen	Tidewater		*	polythermal	1861 1991-97	Yuri Macheret	Macheret et al., 1980	1977	RSL	620	168	Helicopter
Fridtjovbreen	Tidewater		*	polythermal	1861	Yuri Macheret	Macheret, 1976	1974	RV17	430-685		Snowmobile
Fridtjovbreen	Tidewater		*	polythermal	1861 1991-97	Ivan Lavrentiev	Martín-Español et al., 2013	2012	VIRL6 VIRL7	20	168	Snowmobile
Fridtjovbreen	Tidewater		*	polythermal	1861 1991-97	Francisco Navarro	Vasilenko et al., 2006; Martín-Español et al., 2013	2005	VIRL6	20	168	Snowmobile
Gleditschfonna	Valley			polythermal		Ivan Lavrentiev	Martín-Español et al., 2013	2011	VIRL6	20	168	Snowmobile
Grøndfjorbreen Austre	Valley		*	polythermal		Julian Dowdeswell	Dowdeswell et al., 1984	1980	MK IV	60	168	Helicopter
Grøndfjorbreen Austre	Valley		*	polythermal		Yuri Macheret	Macheret and Zhuravlev, 1980	1974 1979	RV17	440	168	Helicopter
Grøndfjorbreen Austre	Valley		*	polythermal		Yuri Macheret	Macheret, 1976 Macheret and Zhuravlev, 1980	1974	RV17	430-685		Snowmobile
Grøndfjorbreen Austre	Valley		*	polythermal		Francisco Navarro	Martín-Español et al., 2013	2010	VIRL6	20	168	Snowmobile
Grøndfjorbreen Vestre	Valley			polythermal		Yuri Macheret	Macheret and Zhuravlev, 1980	1974 1979	RV17	440	168	Helicopter
Grøndfjorbreen Vestre	Valley			polythermal		Francisco Navarro	Martín-Español et al., 2013	2010	RAMAC	100		Snowmobile
Grøndfjorbreen Vestre	Valley			polythermal		Francisco Navarro	Martín-Español et al., 2013	2010	VIRL6	20	168	Snowmobile
Gruvefonna	Icefield			polythermal		Jon Ove Hagen	Hamran and Aarholt, 1993, Melvold and Schuler, 2008	1989	Time gated synthetic pulse radar	5-20	168	
Gruvefonna	Icefield			polythermal		Melvold	Melvold and Schuler, 2008	2005	RAMAC	50-6,5	168	
Hambergbreen	Tidewater			polythermal	1890 1960	Julian Dowdeswell	Drewry et al., 1980	1980	MK IV	60		Helicopter
Hambergbreen	Tidewater			polythermal	1890 1960	Yuri Macheret	Macheret and Zhuravlev, 1980	1974 1979	RV17	440	168	Helicopter
Hambergbreen	Tidewater			polythermal	1890 1960	Anja Pälli	Pälli et al., 2003	2000	RAMAC	50	168	Snowmobile
Hannabreen	Valley			N.A.		Bernd Etzelmüller	Etzelmüller, 1993 Ødegård et al., 1992	1991	Time gated synthetic pulse radar	5-20	168	Snowmobile

Glacier	Type	Bat.	Bor.	Therm. Struct.	Surge	Contact Person	Reference	Year	Radar	Freq. MHz	RWV	Platform
Hansbreen	Tidewater	*	*	polythermal		Julian Dowdeswell	Dowdeswell et al., 1984	1980	MK IV	60	168	Helicopter
Hansbreen	Tidewater	*	*	polythermal		Yuri Macheret	Glazowsky et al., 1991	1989	MPI 8	8		Snowmobile
Hansbreen	Tidewater			polythermal		Francisco Navarro	Grabiec et al., 2012	2003	RAMAC	200		Snowmobile
Hansbreen	Tidewater	*	*	polythermal		Mariusz Grabiec	Grabiec et al., 2012	2007	RAMAC	200	164	Snowmobile
Hansbreen	Tidewater	*	*	polythermal		Mariusz Grabiec	Grabiec et al., 2012	2007	RAMAC	200	164	Snowmobile
Hansbreen	Tidewater	*	*	polythermal		Mariusz Grabiec	Grabiec et al., 2012	2008	RAMAC	25	164	Snowmobile
Hansbreen	Tidewater	*	*	polythermal		Mariusz Grabiec	Grabiec et al., 2012	2008	RAMAC	25	164	Snowmobile
Hansbreen	Tidewater	*	*	polythermal		Mariusz Grabiec	Grabiec et al., 2012	2009	RAMAC	50	164	By foot
Hansbreen	Tidewater	*	*	polythermal		Francisco Navarro	Jania et al., 2005	2003	RAMAC	25		Snowmobile
Hansbreen	Tidewater	*	*	polythermal		Francisco Navarro	Jania et al., 2005	2004	RAMAC	25		Snowmobile
Hansbreen	Tidewater			polythermal		Francisco Navarro	Jania et al., 2005	2004	VIRL2 VIRL2	20		Snowmobile
Hansbreen	Tidewater			polythermal		Francisco Navarro	Jania et al., 2005	2004	VIRL2	20	168	Snowmobile
Hansbreen	Tidewater	*	*	polythermal		Francisco Navarro	Jania et al., 2005	2003	VIRL2	20	168	Snowmobile
Hansbreen	Tidewater	*	*	polythermal		Francisco Navarro	Jania et al., 2005	2004	VIRL2 VIRL6	20	168	Snowmobile
Hansbreen	Tidewater	*	*	polythermal		Francisco Navarro	Jania et al., 2005	2003	VIRL6	20	168	Snowmobile
Hansbreen	Tidewater	*	*	polythermal		Francisco Navarro	Jania et al., 2005	2004	VIRL6	20	168	Snowmobile
Hansbreen	Tidewater	*	*	polythermal		Yuri Macheret	Macheret and Zhuravlev, 1980	1974 1979	RV17	440	168	Helicopter
Hansbreen	Tidewater	*	*	polythermal		John Moore	Moore et al., 1999	1998	RAMAC	200	220	Snowmobile
Hansbreen	Tidewater	*	*	polythermal		John Moore	Moore et al., 1999 Pälli et al., 2003	1998	RAMAC	50	168	Snowmobile
Hansbreen	Tidewater	*	*	polythermal		Francisco Navarro	Navarro et al., 2013	2006	VIRL6	20	168	Snowmobile
Hansbreen	Tidewater	*	*	polythermal		Francisco Navarro	Navarro et al., 2013	2006	VIRL6	20	168	Snowmobile
Hansbreen	Tidewater	*	*	polythermal		Francisco Navarro	Navarro et al., 2013	2009	VIRL6 VIRL7	20	168	Snowmobile
Hansbreen	Tidewater	*	*	polythermal		Francisco Navarro	Navarro et al., 2013	2011	VIRL7	20	168	Helicopter
Hansbreen	Tidewater	*	*	polythermal		John Moore	Pälli et al., 2003	1998	RAMAC	25	168	Snowmobile
Hessbreen	Valley			polythermal	1974	Yuri Macheret	Macheret and Zhuravlev, 1980	1974 1979	RV17	440	168	Helicopter
Hessbreen	Valley			polythermal	1974	Jon Ove Hagen			N.A.	N.A.		
Hikmstrombreen				N.A.		Julian Dowdeswell	Bamber, 1989	1983	MK IV	60	168	Helicopter
Hinlopenbreen	Tidewater			N.A.	1969-72	Julian Dowdeswell	Bamber, 1989	1983	MK IV	60	168	Helicopter
Hochstetterbreen	Tidewater			N.A.	1895-00	Julian Dowdeswell	Bamber, 1989	1983	MK IV	60	168	Helicopter
Höganäsbreen	Valley		*	polythermal		Kjetil Melvold	Melvold et al., 2003	2001	RAMAC	25	169	Snowmobile

Glacier	Type	Bat.	Bor.	Therm. Struct.	Surge	Contact Person	Reference	Year	Radar	Freq. MHz	RWV	Platform
Höganäsbreen	Valley		*	polythermal		Kjetil Melvold	Melvold et al., 2003	2001	RAMAC	50	169	Snowmobile
Högstebreen	Part of			polythermal		Yuri Macheret	Macheret and Zhuravlev, 1980	1974 1979	RV17	440	168	Helicopter
Holmesletbreen	Valley			polythermal		Yuri Macheret	Macheret and Zhuravlev, 1980	1974 1979	RV17	440	168	Helicopter
Holmströmbreen	Valley			N.A.		Julian Dowdeswell	Bamber, 1989	1983	MK IV	60	168	Helicopter
Holmströmbreen	Valley			polythermal		Yuri Macheret	Macheret and Zhuravlev, 1980	1974 1979	RV17	440	168	Helicopter
Holtedahlfonna	Plateau			N.A.		Julian Dowdeswell	Dowdeswell et al., 1984	1980	MK IV	60	168	Helicopter
Holtedahlfonna	Plateau			N.A.		Yuri Macheret	Macheret and Zhuravlev, 1980	1974 1979	RV17	440	168	Helicopter
Hørbyebreen	Valley			polythermal	ca.1900	Jakub Malecki	Malecki et al., 2013	2012	RAMAC	100	170	Snowmobile
Hornbreen	Tidewater			polythermal		Julian Dowdeswell	Drewry et al., 1980	1980	MK IV	60		Helicopter
Hornbreen	Tidewater			polythermal		Yuri Macheret	Macheret and Zhuravlev, 1980	1974 1979	RV17	440	168	Helicopter
Hornbreen	Tidewater			polythermal		Anja Pälli	Pälli et al., 2003	2000	RAMAC	50	168	Snowmobile
Hydrografbreen	Valley			polythermal		Yuri Macheret	Macheret and Zhuravlev, 1980	1974 1979	RV17	440	168	Helicopter
Idabreen	Tidewater			polythermal		Yuri Macheret	Macheret and Zhuravlev, 1980	1974 1979	RV17	440	168	Helicopter
Isachsenfonna	Plateau			N.A.		Julian Dowdeswell	Dowdeswell et al., 1984	1980	MK IV	60	168	Helicopter
Isachsenfonna	Plateau			N.A.		Yuri Macheret	Macheret and Zhuravlev, 1980	1974 1979	RV17	440	168	Helicopter
Kantbreen	Valley			polythermal		Yuri Macheret	Macheret and Zhuravlev, 1980	1974 1979	RV17	440	168	Helicopter
Knoppbreen	Valley			polythermal	1970	Heidi Sevestre	Unpublished	2012	RAMAC	25		Snowmobile
Kongsbreen				polythermal		Yuri Macheret	Macheret and Zhuravlev, 1980	1974 1979	RV17	440	168	Helicopter
Kongsfjorden	Plateau			N.A.		Geir Moholdt	Danish National Space Center Report 2008	2007	DTU	60		Airplane
Kongsvegen	Tidewater		*	polythermal	1948	Julian Dowdeswell	Bamber, 1989	1983	MK IV	60	168	Helicopter
Kongsvegen	Tidewater		*	polythermal	1948	Finnur Pálsson	Björnsson et al., 1996	1990	Time gated synthetic pulse radar	5-20	168 202	Snowmobile
Kongsvegen	Tidewater		*	polythermal	1948	Julian Dowdeswell	Dowdeswell et al., 1984	1980	MK IV	60	168	Helicopter

Glacier	Type	Bat.	Bor.	Therm. Struct.	Surge	Contact Person	Reference	Year	Radar	Freq. MHz	RWV	Platform
Kongsvegen	Tidewater		*	polythermal	1948	Jon Ove Hagen	Hagen and SæTrang, 1991	1988	MARKII	8	169	Snowmobile
Kongsvegen	Tidewater		*	polythermal	1948	Yuri Macheret	Macheret and Zhuravlev, 1980	1974 1979	RV17	440	168	Helicopter
Kongsvegen	Tidewater		*	polythermal	1948	Heidi Sevestre	Unpublished	2012	RAMAC	25		Snowmobile
Kongsvegen	Tidewater		*	polythermal	1948	John Wooward	Wooward et al., 2003	1996	PulsEkko	200	168	Snowmobile
Kongsvegen	Tidewater		*	polythermal	1948	John Wooward	Wooward et al., 2003	1996	PulsEkko	200		Snowmobile
Konowbreen	Tidewater			polythermal		Yuri Macheret	Macheret and Zhuravlev, 1980	1974 1979	RV17	440	168	Helicopter
Kronebreen	Tidewater			polythermal	1896	Julian Dowdeswell	Bamber, 1989	1983	MK IV	60	168	Helicopter
Kronebreen	Tidewater			polythermal	1896	Julian Dowdeswell	Drewry et al., 1980	1980	MK IV	60		Helicopter
Kronebreen	Tidewater			polythermal	1896	Yuri Macheret	Macheret and Zhuravlev, 1980	1974 1979	RV17	440	168	Helicopter
Kvitøyjøkulen	Icecap			N.A.		Julian Dowdeswell	Bamber and Dowdeswell., 1990	1983	MK IV	60	168	Helicopter
Larsbreen	Valley		*	polythermal		Bernd Etzelmüller	Etzelmüller et al., 2000	1994	Time gated synthetic pulse radar	30-80		Snowmobile
Larsbreen	Valley		*	polythermal		Bernd Etzelmüller	Etzelmüller et al., 2000	1994	Time gated synthetic pulse radar	320-370		Snowmobile
Lefflerbreen Mittag	Tidewater			N.A.		Julian Dowdeswell	Dowdeswell et al., 1984	1980	MK IV	60	168	Helicopter
Lefflerbreen Mittag	Tidewater			N.A.		Yuri Macheret	Macheret and Zhuravlev, 1980	1974 1979	RV17	440	168	Helicopter
Leinbreen	Part of			polythermal		Yuri Macheret	Macheret and Zhuravlev, 1980	1974 1979	RV17	440	168	Helicopter
Lilliehöökbreen	Tidewater			N.A.		Julian Dowdeswell	Dowdeswell et al., 1984	1980	MK IV	60	168	Helicopter
Lilliehöökbreen	Tidewater			polythermal		Yuri Macheret	Macheret and Zhuravlev, 1980	1974 1979	RV17	440	168	Helicopter
Ljosfonn	Part_of			polythermal		Yuri Macheret	Macheret and Zhuravlev, 1980	1974 1979	RV17	440	168	Helicopter
Lomonosovfonna	Plateau		*	N.A.		Yuri Macheret	Macheret and Zhuravlev, 1980	1974 1979	RV17	440	168	Helicopter
Lomonosvfonna	Plateau		*	N.A.		Julian Dowdeswell	Dowdeswell et al., 1984	1980	MK IV	60	168	Helicopter
Longyearbreen	Valley			polythermal		Doug Benn	Bælum, 2006	2005	N.A.	N.A.	160	Snowmobile

Glacier	Type	Bat.	Bor.	Therm. Struct.	Surge	Contact Person	Reference	Year	Radar	Freq. MHz	RWV	Platform
Longyearbreen	Valley		*	polythermal		Bernd Etzelmüller	Etzelmüller et al., 2000	1994	Time gated synthetic pulse radar	30-80		Snowmobile
Longyearbreen	Valley		*	polythermal		Bernd Etzelmüller	Etzelmüller et al., 2000	1994	Time gated synthetic pulse radar	320-370		Snowmobile
Lovénbreen Austre	Valley			polythermal		Albane Saintenoy	Saintenoy et al., 2013	2010	RAMAC	100-50	170	Snowmobile
Lovénbreen Austre	Valley			polythermal		Ian Willis	Unpublished	2006	PulsEkko	50		Snowmobile
Lovénbreen Midre	Valley		*	polythermal	1890	Finnur Pálsson	Björnsson et al., 1996	1990	Time gated synthetic pulse radar	5-20	168	Snowmobile
Lovénbreen Midre	Valley		*	N.A.	1890	Julian Dowdeswell	Dowdeswell et al., 1984	1980	MK IV	60	168	Helicopter
Lovénbreen Midre	Valley		*	polythermal	1890	Jon Ove Hagen	Hagen and SæTrang, 1991	1988	MARKII	8	169	Snowmobile
Lovénbreen Midre	Valley		*	polythermal	1890	David Rippin	IASC 2007 abstracts pp131-133	2006	PulsEkko	50		Snowmobile
Lovénbreen Midre	Valley		*	polythermal	1890	Ed King	NERC-GEF report 2007 King et al., 2008	2000	PulsEkko	100	168	Snowmobile
Lovénbreen Midre	Valley		*	polythermal	1890	Ed King	King et al., 2008	2000	PulsEkko	100	168	Snowmobile
Lovénbreen Midre	Valley		*	polythermal	1890	Ed King	King et al., 2008	2000	SEISMIC	refl./refr.		unused
Lovénbreen Midre	Valley		*	polythermal	1890	Yuri Macheret	Macheret and Zhuravlev, 1980	1974 1979	RV17	440	168	Helicopter
Lovénbreen Midre	Valley		*	Polythermal	1890	Heidi Sevestre	Unpublished	2012	RAMAC	25		Snowmobile
Lovénbreen Midre	Valley		*	polythermal	1890	John Moore	Zwinger and Moore, 2009	1998	HAESCAN	150	168	Snowmobile
Løvenskioldfonna	Plateau			N.A.		Yuri Macheret	Macheret and Zhuravlev, 1980	1974 1979	RV17	440	168	Helicopter
Løvliebreen	Valley			polythermal		Yuri Macheret	Macheret and Zhuravlev, 1980	1974 1979	RV17	440	168	Helicopter
Mannbreen	Valley			polythermal		Yuri Macheret	Macheret and Zhuravlev, 1980	1974 1979	RV17	440	168	Helicopter
Markhambergbreen	Tidewater			N.A.	1930-36	Anja Pälli	Pälli et al., 2003	2000	RAMAC	50		Snowmobile
Marstanderbreen	Valley			N.A.		Francisco Navarro a	Unpublished	2013	VIRL6	20	168	Snowmobile
Marthabreen	Valley			polythermal	1925	Thomas Schuler	Internal Report 2010	2007	RAMAC	50	167	Snowmobile
Marthabreen	Valley			polythermal	1925	Thomas Schuler	Internal Report 2010	2009	RAMAC	50	167	Snowmobile
Monacobreen	Tidewater			polythermal	1991-97	Julian Dowdeswell	Dowdeswell et al., 1984	1980	MK IV	60	168	Helicopter
Monacobreen	Tidewater			N.A.	1991-97	Yuri Macheret	Macheret and Zhuravlev, 1980	1974 1979	RV17	440	168	Helicopter

Glacier	Type	Bat.	Bor.	Therm. Struct.	Surge	Contact Person	Reference	Year	Radar	Freq. MHz	RWV	Platform
Muhlbacherbreen	Tidewater			polythermal		Yuri Macheret	Macheret and Zhuravlev, 1980	1974 1979	RV17	440	168	Helicopter
Nansenbreen	Tidewater			N.A.	1947	Julian Dowdeswell	Bamber, 1989	1983	MK IV	60	168	Helicopter
Nansenbreen	Tidewater			N.A.	1947	Yuri Macheret	Macheret and Zhuravlev, 1980	1974 1979	RV17	440	168	Helicopter
Natashabreen	Valley			polythermal	1970	Heidi Sevestre	Unpublished	2012	RAMAC	25		Snowmobile
Nathorstbreen	Tidewater			N.A.		Julian Dowdeswell	Drewry et al., 1980	1980	MK IV	60		Helicopter
Nathorstbreen	Tidewater			N.A.		Yuri Macheret	Macheret and Zhuravlev, 1980	1974 1979	RV17	440	168	Helicopter
Negribreen	Tidewater			N.A.	1935-36	Julian Dowdeswell	Bamber, 1989	1983	MK IV	60	168	Helicopter
Negribreen	Tidewater			N.A.	1935-36	Julian Dowdeswell	Dowdeswell et al., 1984	1980	MK IV	60	168	Helicopter
Negribreen	Tidewater			N.A.	1935-36	Yuri Macheret	Macheret and Zhuravlev, 1980	1974 1979	RV17	440	168	Helicopter
Nordenskiöldbreen	Tidewater			polythermal		Yuri Macheret	Macheret and Zhuravlev, 1980	1974 1979	RV17	440	168	Helicopter
Nordenskjöldbreen	Tidewater			N.A.		Anja Pälli	Pälli et al., 2002	1999	RAMAC	50		Snowmobile
Nornebreen	Valley			polythermal		Mariusz Grabiec	Unpublished	2008	RAMAC	25	164	Snowmobile
Odinjökulen	Icecap			polythermal	1965-70	Yuri Macheret	Macheret and Zhuravlev, 1980	1974 1979	RV17	440	168	Helicopter
OlavV icecap	Plateau			N.A.		Julian Dowdeswell	Bamber, 1989	1983	MK IV	60	168	Helicopter
Olsokbreen	Tidewater			polythermal		Yuri Macheret	Macheret and Zhuravlev, 1980	1974 1979	RV17	440	168	Helicopter
Opalbreen	Part_of			polythermal		Yuri Macheret	Macheret and Zhuravlev, 1980	1974 1979	RV17	440	168	Helicopter
Orsabreen	Valley			polythermal		Yuri Macheret	Macheret and Zhuravlev, 1980	1974 1979	RV17	440	168	Helicopter
Osbornebreen	Tidewater			polythermal	987-199	Yuri Macheret	Macheret and Zhuravlev, 1980	1974 1979	RV17	440	168	Helicopter
Paierlbreen	Tidewater			N.A.		Francisco Navarro	Navarro et al., 2013	2011	VIRL7	20	168	Helicopter
Passfielbreen East	Valley			N.A.		Francisco Navarro a	Unpublished	2013	VIRL6	20	168	Snowmobile
Passfielbreen West	Valley			N.A.		Francisco Navarro a	Unpublished	2013	VIRL6	20	168	Snowmobile
Paulabreen	Tidewater			N.A.		Julian Dowdeswell	Drewry et al., 1980	1980	MK IV	60		Helicopter
Pedersenbreen	Valley			polythermal		Al Songtao	Unpublished	2009	PulsEkko	100	165	Snowmobile
Pedersenbreen	Valley			polythermal		Al Songtao	Unpublished	2009	PulsEkko	100	165	Snowmobile
Penckbreen	Valley			N.A.		Julian Dowdeswell	Dowdeswell et al., 1984	1980	MK IV	60	168	Helicopter

Glacier	Type	Bat.	Bor.	Therm. Struct.	Surge	Contact Person	Reference	Year	Radar	Freq. MHz	RWV	Platform
Penckbreen	Valley			N.A.		Yuri Macheret	Macheret and Zhuravlev, 1980	1974 1979	RV17	440	168	Helicopter
Petermannbreen	Tidewater			N.A.		Julian Dowdeswell	Bamber, 1989	1983	MK IV	60	168	Helicopter
Pollokbreen	Valley			polythermal		Yuri Macheret	Macheret and Zhuravlev, 1980	1974 1979	RV17	440	168	Helicopter
Rabotbreen	valley			polythermal		Heidi Sevestre	Unpublished	2012	RAMAC	25		Snowmobile
Ragnarbreen	Outlet			polythermal		Jakub Malecki	Malecki et al., 2013	2012	RAMAC	100	170	Snowmobile
Raudfjordbreen	Tidewater			polythermal		Julian Dowdeswell	Bamber, 1989	1983	MK IV	60	168	Helicopter
Raudfjordbreen	Tidewater			polythermal		Julian Dowdeswell	Dowdeswell et al., 1984	1980	MK IV	60	168	Helicopter
Raudfjordbreen	Tidewater			polythermal		Yuri Macheret	Macheret and Zhuravlev, 1980	1974 1979	RV17	440	168	Helicopter
Recherchebreen	Tidewater	*		polythermal	1838-45	Mariusz Grabiec	GEUS report 2010 pp27-34 Navarro et al., 2013	2009	RAMAC	25	164	Snowmobile
Recherchebreen	Tidewater			polythermal	1838-45	Yuri Macheret	Macheret and Zhuravlev, 1980	1974 1979	RV17	440	168	Helicopter
Recherchebreen	Tidewater	*		polythermal	1838-45	Francisco Navarro	Navarro et al., 2013	2011	VIRL7	20	168	Snowmobile
Renardbreen	Valley			polythermal		Mariusz Grabiec	GEUS report 2010 pp27-34 Navarro et al., 2013	2008	RAMAC	25	164	Snowmobile
Revtannbreen	Part of			polythermal		Yuri Macheret	Macheret and Zhuravlev, 1980	1974 1979	RV17	440	168	Helicopter
Russebreen	Part of			N.A.		Julian Dowdeswell	Bamber, 1989	1983	MK IV	60	168	Helicopter
Samarinbreen	Tidewater			polythermal		Yuri Macheret	Macheret and Zhuravlev, 1980	1974 1979	RV17	440	168	Helicopter
Scottbreen	Valley			N.A.	1880	Mariusz Grabiec	Navarro et al., 2013	2009	RAMAC	25	164	Snowmobile
Sefströmbreen	Tidewater			N.A.	1896	Julian Dowdeswell	Bamber, 1989	1983	MK IV	60	168	Helicopter
Sefströmbreen	Tidewater			N.A.	1896	Julian Dowdeswell	Drewry et al., 1980	1980	MK IV	60		Helicopter
Sefströmbreen	Tidewater			N.A.	1896	Yuri Macheret	Macheret and Zhuravlev, 1980	1974 1979	RV17	440	168	Helicopter
Slakbreen	Valley			polythermal		Julian Dowdeswell	Dowdeswell et al., 1984	1980	MK IV	60	168	Helicopter
Slakbreen	Valley			polythermal		Kjetil Melvold	Melvold and Schuler, 2008	2000	PulsEkko	50-100	168	
Slakbreen	Valley			polythermal		Kjetil Melvold	Melvold and Schuler, 2008	2001	PulsEkko	50-100	168	
Slakbreen	Valley			polythermal		Kjetil Melvold	Melvold and Schuler, 2008	2002	PulsEkko	50-100	168	
Sørbreen	Valley			N.A.		Yuri Macheret	Macheret and Zhuravlev, 1980	1974 1979	RV17	440	168	Helicopter
Stabbarpbreen	Valley			N.A.		Thorben Dunse	internal report	2011	RAMAC	50		
Staupbreen	Valley			N.A.	1960	Anja Pälli	Pälli et al., 2003	2000	RAMAC	50		Snowmobile

Glacier	Type	Bat.	Bor.	Therm.	Struct.	Surge	Contact Person	Reference	Year	Radar	Freq. MHz	RWV	Platform
Stubendorffbreen	Tidewater			N.A.			Yuri Macheret	Macheret and Zhuravlev, 1980	1974 1979	RV17	440	168	Helicopter
Suessbreen	Part of			N.A.			Yuri Macheret	Macheret and Zhuravlev, 1980	1974 1979	RV17	440	168	Helicopter
Sveabreen	Tidewater			N.A.			Julian Dowdeswell	Drewry et al., 1980	1980	MK IV	60		Helicopter
Sveabreen	Tidewater			N.A.			Yuri Macheret	Macheret and Zhuravlev, 1980	1974 1979	RV17	440	168	Helicopter
Sveitsarfonna	Part of			polythermal			Yuri Macheret	Macheret and Zhuravlev, 1980	1974 1979	RV17	440	168	Helicopter
Svenbreen	Valley			polythermal			Jakub Malecki	Malecki et al., 2013	2012	RAMAC	100	170	Snowmobile
Svingombreen	Part of			N.A.			Thorben Dunse	Internal report	2011	RAMAC	50		
Sykorabreen	Part of			N.A.			Anja Pälli	Pälli et al., 2003	2000	RAMAC	50	168	Snowmobile
Tavlebreen	Valley			polythermal			Ivan Lavrentiev	Lavrentiev et al., 2011	2007	Step frequency radar	850	168	Snowmobile
Tavlebreen	Valley			polythermal			Ivan Lavrentiev	Lavrentiev et al., 2011	2007	VIRL6	20	168	Snowmobile
Tavlebreen	Valley			polythermal			Francisco Navarro	Martín-Español et al., 2013	2010	RAMAC	100	168	Snowmobile
Tavlebreen	Valley			polythermal			Francisco Navarroa	Martín-Español et al., 2013	2010	RAMAC	200	168	Snowmobile
Tavlebreen	Valley			polythermal			Francisco Navarro	Martín-Español et al., 2013	2010	VIRL6 VIRL7	20	168	Snowmobile
Tellbreen	Valley			cold			Doug Benn	Bælum and Benn, 2010	2003	PulsEkko	50	170	Snowmobile
Tellbreen	Valley			cold			Doug Benn	Bælum and Benn, 2010	2003	PulsEkko	50	170	Snowmobile
Tellbreen	Valley			cold			Doug Benn	Bælum and Benn, 2010	2004	PulsEkko	100	170	Snowmobile
Tellbreen	Valley			cold			Doug Benn	Bælum and Benn, 2010	2005	PulsEkko	100	170	Snowmobile
Tellbreen	Valley			cold			Doug Benn	Bælum and Benn, 2010	2009	RAMAC	100	170	Snowmobile
Tellbreen	Valley			cold			Doug Benn	Bælum and Benn, 2010	2010	RAMAC	100	170	Snowmobile
Tirolarbreen	Part of			polythermal			Yuri Macheret	Macheret and Zhuravlev, 1980	1974 1979	RV17	440	168	Helicopter
Tommelbreen	Tidewater			N.A.			Julian Dowdeswell	Bamber, 1989	1983	MK IV	60	168	Helicopter
Torellbreen Austre	Tidewater			polythermal			Yuri Macheret	Macheret and Zhuravlev, 1980	1974 1979	RV17	440	168	Helicopter
Torellbreen Austre	Tidewater			polythermal			Francisco Navarro	Navarro et al., 2013	2011	VIRL7	20	168	Helicopter
Torellbreen Vestre	Tidewater			polythermal			Julian Dowdeswell	Dowdeswell et al., 1984	1980	MK IV	60	168	Helicopter
Torellbreen Vestre	Tidewater			polythermal			Yuri Macheret	Macheret and Zhuravlev, 1980	1974 1979	RV17	440	168	Helicopter

Glacier	Type	Bat.	Bor.	Therm. Struct.	Surge	Contact Person	Reference	Year	Radar	Freq. MHz	RWV	Platform
Torsfonna	Plateau			polythermal		Yuri Macheret	Macheret and Zhuravlev, 1980	1974 1979	RV17	440	168	Helicopter
Tungebreen	Valley			N.A.		Ivan Lavrentiev	Martín-Español et al., 2013	2011	VIRL6	20	168	Snowmobile
Tunnabreen	Tidewater			polythermal	1930 1970 2003	Julian Dowdeswell	Bamber, 1989	1983	MK IV	60	168	Helicopter
Tunnabreen	Tidewater			polythermal	1930 1970 2003	Julian Dowdeswell	Dowdeswell et al., 1984	1980	MK IV	60	168	Helicopter
Tunnabreen	Tidewater			polythermal	1930 1970 2003	Yuri Macheret	Macheret and Zhuravlev, 1980	1974 1979	RV17	440	168	Helicopter
Uversbreen	Valley			polythermal		Julian Dowdeswell	Bamber, 1989	1983	MK IV	60	168	Helicopter
Uversbreen	Valley			polythermal		Finnur Pálsson	Björnsson et al., 1996	1990	Time gated synthetic pulse radar	5-20	168	Snowmobile
Uversbreen	Valley			polythermal		Julian Dowdeswell	Dowdeswell et al., 1984	1980	MK IV	60	168	Helicopter
Uversbreen	Valley			polythermal		Yuri Macheret	Macheret and Zhuravlev, 1980	1974 1979	RV17	440	168	Helicopter
Valhallfonna	Plateau			N.A.		Julian Dowdeswell	Bamber, 1989	1983	MK IV	60	168	Helicopter
Valhallfonna	Plateau			N.A.		Yuri Macheret	Macheret and Zhuravlev, 1980	1974 1979	RV17	440	168	Helicopter
Vallåkrabreen	Valley			N.A.		Thorben Dunse	Internal Report	2011	RAMAC	50		
Varpbreen	Valley			N.A.		Kjetil Melvold	Melvold and Schuler, 2008	2002	PulsEkko	50-100	168	
Vestfonna	Icecap		*	polythermal		Julian Dowdeswell	Dowdeswel et al., 1986	1983	MK IV	60	168	Helicopter
Vestfonna	Icecap		*	polythermal		Yuri Macheret	Macheret and Zhuravlev, 1980	1974 1979	RV17	440	168	Helicopter
Vestfonna	Icecap		*	polythermal		Rickard Petterson	Petterson et al., 2011	2008-2009	Pulse Radar System	10	168	Snowmobile
Vestgötabreen	Part of			polythermal		Yuri Macheret	Macheret and Zhuravlev, 1980	1974 1979	RV17	440	168	Helicopter
Veteranen	Valley			N.A.		Julian Dowdeswell	Bamber, 1989	1983	MK IV	60	168	Helicopter
Veteranen	Valley			N.A.		Yuri Macheret	Macheret and Zhuravlev, 1980	1974 1979	RV17	440	168	Helicopter
Vonbreen	Valley			N.A.		Julian Dowdeswell	Bamber, 1989	1983	MK IV	60	168	Helicopter

Glacier	Type	Bat.	Bor.	Therm. Struct.	Surge	Contact Person	Reference	Year	Radar	Freq. MHz	RWV	Platform
VonPostbreen	Tidewater			polythermal	1870 1980	Julian Dowdeswell	Drewry et al., 1980	1980	MK IV	60		Helicopter
Vonpostbreen Nord	outlet			polythermal		Heidi Sevestre	Unpublished	2012	RAMAC	25		Snowmobile
Vonpostbreen south	outlet			polythermal		Heidi Sevestre	Unpublished	2012	RAMAC	25		Snowmobile
Vonpostbreen south	outlet			polythermal		Heidi Sevestre	Unpublished	2012	RAMAC	50		Snowmobile
Vøringbreen	Valley			polythermal		Yuri Macheret	Macheret and Zhuravlev, 1980	1974 1979	RV17	440	168	Helicopter
Vøringbreen	Valley			polythermal		Yuri Macheret	Macheret, 1976 Macheret and Zhuravlev, 1980	1974	RV17	430-685		Snowmobile
Vrangpeisbreen	Part of			polythermal		Yuri Macheret	Macheret and Zhuravlev, 1980	1974 1979	RV17	440	168	Helicopter
Wahlenbergbreen	Tidewater			N.A.	1908	Julian Dowdeswell	Bamber, 1989	1983	MK IV	60	168	Helicopter
Wahlenbergbreen	Tidewater			N.A.	1908	Julian Dowdeswell	Dowdeswell et al., 1984	1980	MK IV	60	168	Helicopter
Wahlenbergbreen	Tidewater			N.A.	1908	Yuri Macheret	Macheret and Zhuravlev, 1980	1974 1979	RV17	440	168	Helicopter
Werenskioldbreen	Valley			polythermal		Julian Dowdeswell	Dowdeswell et al., 1984	1980	MK IV	60	168	Helicopter
Werenskioldbreen	Valley			polythermal		Julian Dowdeswell	Drewry et al., 1980	1980	MK IV	60		Helicopter
Werenskioldbreen	Valley			polythermal		Mariusz Grabiec	IASC 2008 abstracts pp46-49	2007	RAMAC	200	164	Snowmobile
Werenskioldbreen	Valley			polythermal		Yuri Macheret	Macheret and Zhuravlev, 1980	1974 1979	RV17	440	168	Helicopter
Werenskioldbreen	Valley			polythermal		Mariusz Grabiec	Navarro et al., 2013	2008	RAMAC	25	164	Snowmobile
Werenskioldbreen	Valley			polythermal		Mariusz Grabiec	Navarro et al., 2013	2011	RAMAC	100	168	Snowmobile
Werenskioldbreen	Valley			polythermal		John Moore	Pälli et al., 2003	1998	RAMAC	50	168	Snowmobile

Bibliography

ACIA. *Arctic Climate Impact Assessment*. Cambridge University Press, 2005. 2

S. Adhikari and S. J. Marshall. Glacier volume-area relation for high-order mechanics and transient glacier states. *Geophysical Research Letters*, 39(16):L16505, 2012. 14, 22, 90, 91, 102, 104, 110, 120, 121

A. Arendt, T. Bolch, J.G. Cogley, and R. Hock G. Kaser W.T. Pfeffer G. Moholdt F. Paul V. Radi L. Andreassen S. Bajracharya M. Beedle E. Berthier R. Bhambri A. Bliss I. Brown E. Burgess D. Burgess F. Cawkwell T. Chinn L. Copland B. Davies E. Dolgova K. Filbert R. Forester A. Fountain H. Frey B. Giffen N. Glasser S. Gurney W. Hagg D. Hall U.K. Haritashya G. Hartmann C. Helm S. Herreid I. Howat G. Kapustin T. Khromova Kienholz M. Koenig J. Kohler D. Kriegel S. Kutuzov I. Lavrentiev R. LeBris J. Lund W. Manley C. Mayer X. Li B. Menounos A. Mercer N. Moelg P. Mool G. Nosenko A. Negrete C. Nuth R. Pettersson A. Racoviteanu R. Ranzi P. Rastner F. Rau J. Rich H. Rott C. Schneider Y. Seliverstov M. Sharp O. Sigursson C. Stokes R. Wheate S. Winsvold G. Wolken F. Wyatt N. Zheltyhina A. Gardner, J.-O. Hagen. Randolph glacier inventory [v1.0]: A dataset of global glacier outlines. *Global Land Ice Measurements from Space, Boulder Colorado, USA. Digital Media. Available online from http://www.glims.org/RGI/randolph.html*, 2012. 4, 10, 14, 22, 35, 91, 101, 119

K. Bælum and D. I. Benn. Thermal structure and drainage system of a small valley glacier (tellbreen, svalbard), investigated by ground penetrating radar. *The Cryosphere Discussions*, 4(4):2169–2199, 2010. 5, 44, 70, 72, 77, 83

D.B. Bahr. Width and length scaling of glaciers. *Journal of Glaciology*, 43(145):557–562, 1997. 12, 100, 110, 121

D.B. Bahr and M.F. Meier. Snowpatch and glacier size distributions. *Water Resources Research*, 36(2):495–501, 2000. 13

D.B. Bahr, M.F. Meier, and S. Peckham. The physical basis of glacier volume-area scaling. *Journal of Geophysical Research*, 102(B9):20355, 1997. 9, 10, 11, 12, 13, 23, 113

J. L. Bamber and J. A. Dowdeswell. Remote-sensing studies of kvitøyjøkulen, an ice cap on kvitya, north-east svalbard. *Journal of Glaciology*, 36:75–81, 1990. 60

J. L. Bamber, R. L. Layberry, and S. P. Gogineni. A new ice thickness and bed data set for the greenland ice sheet 1. measurement, data reduction, and errors. *Journal of Geophysical Research*, 106(D24):33773–33,780, 2001. 28

P. Bevington and D. K. Robinson. *Data reduction and error analysis for the physical sciences*. McGraw-Hill, 2003. ISBN 9780072472271. 45

N.L. Bindoff, J. Willebrand, V. Artale, A. Cazenave, J. Gregory, S. Gulev, K. Hanawa, C. Le Quéré, S. Levitus, Y. Nojiri, C.K. Shum, L.D. Talley, and A. Unnikrishnan. Observations: oceanic climate change and sea level. In S. Solomon, D. Qin, M. Manning, Z. Chen, M. Marquis, K.B. Averyt, M. Tignor, and H.L. Miller, editors, *The Physical Science Basis. Contribution of Working Group I to the Fourth Assessment Report of the Intergovernmental Panel on Climate Change*. Cambridge University Press, Cambridge, 2007. 1

H. Björnsson, Y. Gjessing, S.E. Hamran, J.O. Hagen, O. Liestøl, F. Palsson, and B. Erlingsson. The thermal regime of sub-polar glaciers mapped by multi-frequency radio-echo sounding. *Journal of Glaciology*, 42:23–32, 1996. 71, 83, 86

P. Bohorquez and S.E. Darby. The use of one- and two-dimensional hydraulic modelling to reconstruct a glacial outburst flood in a steep alpine valley. *Journal of Hydrology*, 361(3-4): 240–261, 2008. 36

J. Chen and A. Ohmura. Estimation of alpine glacier water resources and their change since the 1870s. *Hidrology in Mountainous Regions (Proceeding of two Lausanne Symposia, August,1990). IAHS Publ. no. 193*, 1990. 13, 23, 110, 121

J.P. Chils and P. Delfiner. *Geostatistics: Modeling Spatial Uncertainty*. Wiley Series in Probability and Statistics. 2008. ISBN 9780471083153, 9780470316993. 42

G. Clarke, E. Berthier, C. Schoof, and A. Jarosch. Neural networks applied to estimating subglacial topography and glacier volume. *Journal of Climate*, 22(8):2146–2160, 2009. 12, 21

J.G. Cogley. The future of the world's glaciers. In *The Future of the World's Climate*, pages 197–222. Elsevier, 2012. ISBN 9780123869173. 2, 7, 9, 22, 59, 73, 81, 89, 93, 104, 118

J.G. Cogley, R. Hock, L.A. Rasmussen, A.A. Arendt, A. Bauder, R.J. Braithwaite, P. Jansson, G. Kaser, M. Möller, L. Nicholson, and Zemp. M. Glossary of glacier mass balance and related terms. *IHP-VII Technical Documents in Hydrology No. 86, IACS Contribution No. 2, UNESCO-IHP, Parisy*, pages 96–100, 2011. 19

N. Cressie. Spatial prediction and ordinary kriging. *Mathematical Geology*, 20(4):405–421, 1988. ISSN 0882-8121. 36, 40, 42, 55

N. Cressie. The origins of kriging. *Mathematical Geology*, 22:239–252, 1990. 48

J. D'Errico. Surface fitting using gridfit. matlab central file exchange. retrieved may 18, 2012. 2006. URL http://www.mathworks.com/matlabcentral/fileexchange/8998). 36

J.C. Doornkamp and A.M. King. *Numerical Analysis in Geomorphology: An Introduction*. London: Edward Arnold, 1971. ISBN 0713155892. 33

J. A. Dowdeswell. Drainage-basin characteristics of nordaustlandet ice caps, svalbard, 1986. 84

J. A. Dowdeswell, D.J. Drewry, O. Liestøl, and O. Orheim. Airborne radio echo sounding of sub-polar glaciers in spitsbergen. Technical Report 182, Norsk Polarinstitutt, Oslo, 1984a. 4, 44, 60, 61, 62, 82, 83, 93, 118

J. A Dowdeswell, D.J. Drewry, A. P. R Cooper, M. R Gorman, O. Liestøl, and O. Orheim. Digital mapping of the nordaustlandet ice caps from airborne geophysical investigations. *Annals of Glaciology*, 8:51–58, 1986. 60, 88

J.A. Dowdeswell and J. L. Bamber. On the glaciology of edgeøya and barentsøya, svalbard. *Polar Research*, 14(2):105122, 1995. 60

J.A. Dowdeswell and T. Benham. Iceberg calving flux and mass balance of the austfonna ice cap on nordaustlandet, svalbard. *Journal of Geophysical Research- Earth Surface*, 113, 2008. 32, 71

J.A Dowdeswell, D.J. Drewry, O. Liestøl, and O. Orheim. Radio echo-sounding of spitsbergen glaciers: problems in the interpretation of layer and bottom returns. *Journal of Glaciology*, 30(104), 1984b. 12, 61, 82, 83

C.L. Driedger and P.M. Kennard. *Ice volumes on cascade volcanoes: mount rainier, mount hood, three sisters, and mount shasta.* [S.l.]. ISBN 1287012434 9781287012436. 18

Thorben Dunse. *Glacier dynamics and subsurface classification of Austfonna, Svalbard: Inferences from observations and modelling.* PhD thesis, Faculty of Mathematics and Natural Sciences, University of Oslo, 2011. 71, 88

M. B. Dyurgerov and M.F. Meier. *Glaciers and the Changing Earth System: A 2004 Snapshot.* Institute of Arctic and Alpine Research, 2005. 13, 22, 23

B. Etzelmüller, R. . Ødegård, G. Vatne, R. Mysterud, T. Tonning, and J. Sollid. Glacier characteristics and sediment transfer system of longyearbreen and larsbreen, western spitsbergen. *Norsk Geografisk Tidsskrift - Norwegian Journal of Geography*, 54(4):157–168, 2000. 77, 83

B. S. Everitt. *Cambridge Dictionary of Statistics.* Cambridge University Press, 1998. ISBN 9780521593465. 106

D. Farinotti and M. Huss. An upper-bound estimate for the accuracy of volume-area scaling. *The Cryosphere Discussions*, 7(3):2293–2331, June 2013. 4, 14, 44, 91, 93, 99, 104, 113, 119

D. Farinotti, M. Huss, A. Bauder, and M. Funk. An estimate of the glacier ice volume in the swiss alps. *Global and Planetary Change*, 68(3):225–231, 2009. 10, 14, 18, 19, 20

A. Gardner, G. Moholdt, J. G. Cogley, B. Wouters, A. Arendt, J. Wahr, E. Berthier, R. Hock, W. T. Pfeffer, G. Kaser, S. Ligtenberg, T. Bolch, M. Sharp, J. O. Hagen, M Van der Broeke, and F. Paul. A reconciled estimate of glacier contributions to sea level rise: 2003 to 2009. *Science*, 340(6134):852–857, May 2013. ISSN 0036-8075, 1095-9203. 2

S. Geisser. *Predictive inference: an introduction.* Number 55 in Monographs on statistics and applied probability. Chapman & Hall, New York, 1993. ISBN 0412034719. 99

A.F. Glazovsky, Y.Y. Macheret, M.Y. Moskalevsky, and J. Jania. Tidewater glaciers of spitsbergen. *IAHS Publication*, pages 229–240, 1991. 83

A.F. Glazovsky, I.I. Lavrentiev, Y.Y. Macheret, F.J. Navarro, and E.V. Vasilenko. Changes in geometry and hydrothermal structure of fridtjovbreen, a polythermal glacier in spitsbergen, following its surge in the 1990s. In *The Mass Budget of Arctic Glaciers. Workshop and*

GLACIODYN Meeting Group, Extended abstracts, IMAU, Utretch University, pages 39–42, 2006. 4, 31, 32

S.N. Goodman. Toward evidence-based medical statistics. 1: The p value fallacy. *Annals of Internal Medicine*, 130(2):995–1004, 1999. 106

M. Grabiec, D. Puczko, T. Budzik, and G. Gajek. Snow distribution patterns on svalbard glaciers derived from radio-echo soundings. *Polish Polar Research*, 32(4):393–421, 2011. 28

M. Grabiec, J. Jania, D. Puczko, L. Kolondra, and T. Budzik. Surface and bed morphology of hansbreen, a tidewater glacier in spitsbergen. *Polish Polar Research*, 33(2), January 2012. 5, 29, 30, 31, 32, 79, 81, 82

C. Graham and M.S. McIntyre. Hess altitudes and other morphological estimators of glacier equilibrium lines. *Arctic, Antarctic, and Alpine Research*, 35(4):482–488, 2003. 13

M. Greenwood and N. Humphrey. Glaciated valley profiles: An application of nonlinear regression. *Computing Science and Statistics*, 34:452–460, 2002. 33, 34

A. Grinsted. An estimate of global glacier volume. *The Cryosphere*, 7(1):141–151, 2013. 2, 7, 9, 10, 14, 22, 23, 59, 89, 92, 93, 99, 100, 105, 107, 109, 110, 111, 115, 118, 119, 121

W. Haeberli and M. Hoelzle. Application of inventory data for estimating characteristics of and regional climate-change effects on mountain glaciers: a pilot study with the european alps. *Annals of Glaciology*, 21:206–212, 1995. 22

J. O. Hagen and A. SæTrang. Radio-echo soundings of sub-polar glaciers with low-frequency radar. *Polar Research*, 9(1):99–107, 1991. 61, 62, 86

J. O. Hagen, K. Melvold, F. Pinglot, and J. Dowdeswell. On the net mass balance of the glaciers and ice caps in svalbard, norwegian arctic. *Arctic, Antarctic, and Alpine Research*, 35(2), 2003. 23

J.O. Hagen, O. Liestøl, E. Roland, and T. Jørgensen. Glacier atlas of svalbard and jan mayen. *Norsk Polarinstitutt Meddelelser*, 129, 1993. 3, 4, 12, 61, 62, 81, 108, 109, 110, 121

M.J. Hambrey. Structure and changing dynamics of a polythermal valley glacier on a centennial timescale: Midre lovnbreen, svalbard. *Journal of Geophysical Research*, 110(F1), 2005. 32

E. Hanna, F.J. Navarro, F. Pattyn, C.M. Domingues, X. Fettweis, E.R. Ivins, J. Nicholls, C. Ritz, B. Smith, S. Tulaczyck, P.L. Whitehouse, and H.J. Zwally. Ice sheet mass balance and climate change: a state of the science review. *Nature*, 498, 2013. 2, 9

J. Harper and J. Bradford. Snow stratigraphy over a uniform depositional surface: spatial variability and measurement tools. *Cold Regions Science and Technology*, 37(3):289–298, November 2003. 81

C Hauck and K. Christof. *Applied geophysics in periglacial environments*. Cambridge University Press, Cambridge UK New York, year = 2008. ISBN 9780521889667. 84, 87

K. Hinkelmann and O. Kempthorne. *Design and Analysis of Experiments Set.* John Wiley & Sons Inc. ISBN 9780470385517 0470385510. 105

M. Huss and D. Farinotti. Distributed ice thickness and volume of all glaciers around the globe. *Journal of Geophysical Research*, 117(F4), October 2012. 2, 9, 10, 14, 18, 19, 20, 22, 23, 59, 110, 111, 115

K. Hutter. *Theoretical Glaciology.* Reidel, Dordrecht, 1983. 11

T. Jacob, J. Wahr, W. T. Pfeffer, and . Swenson. Recent contributions of glaciers and ice caps to sea level rise. *Nature*, 482(7386):514–518, 2012. 9

L. A. James. Polynomial and power functions for glacial valley cross-section morphology. *Earth Surface Processes and Landforms*, 21(5):413432, 1996. 33

J. Jania. *Zrozumie lodowce*. Wydawnictwo Naukowe PWN, 1996. ISBN 9788301120498. 82

J. Jania, Y.Y. Macheret, F.J. Navarro, A.F. Glazovsky, E.V. Vasilenko, J. Lapazaran, P. Glowacki, K. Migala, A. Balut, and B.A. Piwowar. Temporal changes in the radiophysical properties of a polythermal glacier in spitsbergen. *Annals of Glaciology*, 42(1): 125–134, August 2005. 4, 29, 30, 31, 32

Cogleym J.G. Geodetic and direct mass-balance measurements: Comparison and joint analysis. *Annals of Glaciology*, 50:96–100, 2009. 13

M. Köning, C. Nuth, J. Kohler, G. Moholdt, and R. Pettersen. A digital glacier database for svalbard. In *Global Land Ice Measurements from Space*, Springer praxis series in geophysical sciences. Springer, New York, 1st edition, 2013. 4, 35, 54, 59, 62, 91, 94, 101, 113, 117, 119

L.M. Kulnitsky, P.A. Gofman, and M.Y. Tokarev. Matematicheskaya obrabotka dannykh georadiolokatsii i systema radexpro [mathematical processing of georadar data and radexpro system]. *Razv. Okhrana Nedr [In Russian.]*, 21:6–11, 2000. 26

N. S Lam. Spatial interpolation methods: A review. *The American Cartographer*, 10(2): 129–149, 1983. 36

J.J. Lapazaran, M. Petlicki, F. J. Navarro, F. Machío, D. Puczko, P. Glowacki, and A. Nawrot. Ice volume changes (1936-1990-2007) and ground-penetrating radar studies of ariebreen, hornsund, spitsbergen. *Polar Research*, 32, 2013. 4, 82

I. Lavrentiev, YY. Macheret, and P. Holmlund. Thermal structure and subglacial drainage system of tavlebreen, svalbard. IPY Oslo Science Conference, 2010. 83

I.I. Lavrentiev, Y.Y Macheret, and A.F. Glazovsky. Hydrothermal structure of svalbard glaciers on nordenskild land by radio-echo sounding data. In *Abstracts of conference: Integrated and interdisciplinary research in polar regions [In russian]. Sochi, Russia, 3-8 October 2011*, page 23, 2011. 75, 83

P. Lemke, J. Ren, R. B Alley, I. Allison, J. Carrasco, G. Flato, Y. Fujii, G. Kaser, P. Mote, R. H Thomas, and T. Zhang. Observations: Changes in snow, ice and frozen ground. In S. Solomon, D. Qin, M. Manning, Z. Chen, M. Marquis, K. B Averyt, M. Tignor, and H. L Miller, editors, *Climate Change 2007: The Physical Science Basis. Contribution of Working Group I to the Fourth Assessment Report of the Intergovernmental Panel on Climate Change*, pages 337–383. Cambridge University Press, Cambridge, United Kingdom and New York, NY, USA, 2007. 1

H. Li, Z. Li, M. Zhang, and W. Li. An improved method based on shallow ice approximation to calculate ice thickness along flow-line and volume of mountain glaciers. *Journal of Earth Science*, 22(4):441–448, August 2011. 18

Huilin Li, Felix Ng, Zhongqin Li, Dahe Qin, and Guodong Cheng. An extended perfect-plasticity method for estimating ice thickness along the flow line of mountain glaciers. *Journal of Geophysical Research*, 117(F1), 2012. 18

O. Liestøl. Glaciological work in 1972. *Norsk Polarinstitutt rbok.*, pages 125–135, 1974. 60

C. Lingle, L.r Lee, H. Zwally, and T. Selss. Recent elevation increase on lambert glacier,

antarctica, from orbit cross-over analysis of satellite-radar altimetry. *Annals of Glaciology*, 20(1):26–32, 1994. 28

A. Linsbauer, F. Paul, and W. Haeberli. Modeling glacier thickness distribution and bed topography over entire mountain ranges with GlabTop: application of a fast and robust approach. *Journal of Geophysical Research: Earth Surface*, 117(F3):F03007, 2012. 21

Y.Y. Macheret. Forms of glacial relief of spitsbergen glaciers. *Annals of Glaciology*, 2(1): 45–51, 1981. 12, 60, 81, 83

Y.Y. Macheret and A. B. Zhuravlev. Radio echo-sounding of svalbard glaciers. *Journal of Glaciology*, 28:295–314, 1982. 3, 4, 12, 23, 44, 60, 61, 62, 81, 82, 83, 93, 118

Y..Y. Macheret and A.B. Zhuravlev. Radilokatsiommoye zondirovanie lednikov shpitsbergea s vertolyrta [radio-echo sounding of spitsbergen glaciers from helicopter]. *Materialy Glyatsiologicheskikh Issledovaniy (Data of Glaciological Studies)*, 37:109–131, 1980. 81, 83

Y.Y. Macheret, A.B. Zhuravlev, and L.I. Bobrova. Tolshchina, podlednyy relyef i obyem lednikov shpitsbergena po dannym radiozondirovaniya. thickness, subglacial relief and volume of svalbard glaciers based on radio-echo sounding data. *Materialy Glyatsiologicheskikh Issledovaniy, Khronika, Obsuzhdeniya*, 51:49–63, 1984. 61

Y.Y. Macheret, M. Moskalevsky, and E.V. Vasilenko. Velocity of radio waves in glaciers as an indicator of their hidrothermal state, structure and regime. *Journal of Glaciology*, 39 (132):373–384, 1993. 31

Y.Y. Macheret, S.S. Kutuzov, V.V. Matskovsky, and I.I. Lavrentiev. On the estimation of ice volume of alpine glaciers. *Ice and Snow*, 121(1):5–15, 2013. 14

Jakub Malecki. *The actual state of Svenbreen (Svalbard) and changes of its physical properties after the termination of Little Ice Age*. PhD thesis, Adam Mickiewicz University, Pozna, 2013. 78, 82, 84

A. Martín-Español, E.V. Vasilenko, F. J. Navarro, J. Otero, J.J. Lapazaran, I. Lavrentiev, Y.Y. Macheret, and F. Machío. Radio-echo sounding and ice volume estimates of western nordenskild land glaciers, svalbard. *Annals of Glaciology*, 54(65):211–217, 2013. 4, 39, 64, 75, 83

G. Matheron. *The Theory of Regionalized Variables and Its Applications*. Ecole nationale suprieure des mines de Paris, 1971. 42

R.W. Mcnabb, R. Hock, S. O'Neel, L.A. and Ahn, Y. and Braun, M. and Conway, H. and Herreid, S. and Joughin, I. and Pfeffer, W.T. and Smith, B.E Rasmussen, and M. Truffer. Using surface velocities to calculate ice thickness and bed topography: a case study at columbia glacier, alaska, USA. *Journal of Glaciology*, 58(212):1451–1464, 2012. 10, 21

M. Meier, M. Dyurgerov, U. Rick, S. O'Neel, W. T. Pfeffer, R. Anderson, S. Anderson, and A. Glazovsky. Glaciers dominate eustatic sea-level rise in the 21st century. *Science*, 317 (5841):1064–1067, August 2007. 90, 91

M.F. Meier and D.B. Bahr. Counting glaciers: Use of scaling methods to estimate the number and size distribution of the glaciers of the world. *CRREL Special Reports*, 96(27):89–94, 1996. 13

K. Melvold, T. Schuler, and G. Lappegard. Ground-water intrusions in a mine beneath hoganesbreen, svalbard: assessing the possibility of evacuating water subglacially. *Annals of Glaciology*, 37(1):269274, 2004. 84, 87

M. Möller and C. Schneider. Calibration of glacier volume-area relations from surface extent fluctuations and application to future glacier change. *Journal of Glaciology*, 56(195):3340, 2010. 15

M. Möller, R. Finkelnburg, M. Braun, D. Scherer, and C. Schneider. Variability of the climatic mass balance of vestfonna ice cap (northeastern svalbard), 1979-2011. *Annals of Glaciology*, 54(63):254–264,, 2013. 123

J. C. Moore, A. Pälli, F. Ludwig, H. Blatter, J. Jania, B. Gadek, P. Glowacki, D. Mochnacki, and E. Isaksson. High-resolution hydrothermal structure of hansbreen, spitsbergen, mapped by ground-penetrating radar. *Journal of Glaciology*, 45(151):524–532, 1999. 82

M. Morlighem, E. Rignot, H. Seroussi, E. Larour, H. Ben Dhia, and D. Aubry. A mass conservation approach for mapping glacier ice thickness. *Geophysical Research Letters*, 38 (19):n/a–n/a, 2011. 21

T. Murray, D.L. Gooch, and G.W. Stuart. Structures within the surge front at bakaninbreen, svalbard, using ground-penetrating radar. *Annals of Glaciology*, 24(1):122–129, 1997. 32

T. Murray, A. Luckman, T. Strozzi, and A.M. Nuttall. The initiation of glacier surging at fridtjovbreen, svalbard. *Annals of Glaciology*, 36(1):110–116, January 2003. 83

F. J. Navarro, A. Martín-Español, J.J. Lapazaran, M. Grabiec, J. Otero, E.V. Vasilenko, and D. Puczko. Ice volume estimates from ground-penetrating radar surveys, wedel jarlsberg land glaciers, svalbard. *Arctic, Antarctic and Alpine Research, in review*, 2013. 4, 64, 80, 82

F.J. Navarro and O. Eisen. Ground pentrating radar. In P.Pellikka and W.G. Rees, editors, *Remote sensing of glaciers techniques for topographic, spatial and thematic mapping*. CRC Press, Leiden, 2010. 25, 26, 29, 82

F.J. Navarro, A.F. Glazovsky, Y.Y. Macheret, E.V. Vasilenko, M.I. Corcuera, and M.L. Cuadrado. Ice-volume changes (19361990) and structure of aldegondabreen, spitsbergen. *Annals of Glaciology*, 42(1):158–162, 2005. 4, 31, 32, 75, 81, 83

C. Nuth, J. Kohler, H.F. Aas, O. Brandt, and J.O Hagen. Glacier geometry and elevation changes on svalbard (193690): a baseline dataset. *Annals of Glaciology*, 46(1):106–116, 2007. 81

C. Nuth, G. Moholdt, J. Kohler, J. O. Hagen, and A. Kb. Svalbard glacier elevation changes and contribution to sea level rise. *Journal of Geophysical Research: Earth Surface*, 115 (F1):n/an/a, 2010. 28, 81

A.M. Nuttall. *The Quiescent Phase of Finsterwalderbreen, A Surge Type Glacier in Svalbard*. PhD thesis, School of Geographical Sciences, University of Bristol, 2001. 71

A.M. Nuttall, J.O. Hagen, and J.A. Dowdeswell. Quiescent-phase changes in velocity and geometry of finsterwalderbreen, a surge-type glacier in svalbard. *Annals of Glaciology*, 24: 249–254, 1997. 71, 79

J. F. Nye. The mechanics of glacier flow. *Journal of Glaciology*, 2:82–93, nov 1952. 18

J. F Nye. The distribution of stress and velocity in glaciers and ice-sheets. *Proceedings of the Royal Society, Ser. A*, 239(1216):113–133, 1957. 37

R. S Ødegård, J. Hagen, and S. E Hamran. Comparison of radio-echo sounding (30-1000 MHz) and high-resolution borehole-temperature measurements at finsterwalderbreen, southern spitsbergen, svalbard, 1997. 82

A. Pälli. *Polythermal glacier studies in Svalbard determined by ground-penetrating radar*. Oulun yliopisto, Oulu, 2003. ISBN 9789514271762. 82, 85

A. Pälli, J. Moore, J. Jania, and P. Glowacki. Glacier changes in southern spitsbergen, svalbard, 1901-2000. *Annals of Glaciology*, 37(1):219–225, 2003a. 32, 82, 83, 85

A. Pälli, J. Moore, J. Jania, L. Kolondra, and P. Glowacki. The drainage pattern of hansbreen and werenskioldbreen, two polythermal glaciers in svalbard. *Polar Research*, 22(2):355–371, 2003b. 29

W. S. B Paterson. *The Physics of Glaciers*. Pergamon, 3rd edition, 1994. 11

R. Pettersson, P. Christoffersen, J. Dowdeswell, Veijo A. Pohjola, A. Hubbard, and T. Strozzi. Ice thickness and basal conditions of vestfonna ice cap, eastern svalbard. *Geografiska Annaler: Series A, Physical Geography*, 93(4):311–322, 2011. 5, 32, 48, 71, 84, 88

V. Radić and R. Hock. Regional and global volumes of glaciers derived from statistical upscaling of glacier inventory data. *Journal of Geophysical Research*, 115(F1):F01010, 2010. ISSN 0148-0227. 4, 9, 10, 13, 14, 22, 23, 109, 110, 113, 122

V. Radić and R. Hock. Regionally differentiated contribution of mountain glaciers and ice caps to future sea-level rise. *Nature Geoscience*, 4(2):91–94, 2011. 2, 15, 59, 92, 115

V. Radić, R. Hock, and J. Oerlemans. Volumearea scaling vs flowline modelling in glacier volume projections. *Annals of Glaciology*, 46(1):234240, 2007. 15

V. Radić, R. Hock, and J. Oerlemans. Analysis of scaling methods in deriving future volume evolutions of valley glaciers. *Journal of glaciology*, 54(187):601–612, 2008. 15, 107, 120

V. Radić, A. Bliss, A. C. Beedlow, R. Hock, E. Miles, and J. G. Cogley. Regional and global projections of twenty-first century glacier mass changes in response to climate scenarios from global climate models. *Climate Dynamics*, April 2013. ISSN 0930-7575, 1432-0894. doi: 10.1007/s00382-013-1719-7. 2, 16, 23, 109, 110, 111, 122

S. Raper and R.J. Braithwhite. The potential for sea level rise: New estimates from glacier and ice cap area and volume distributions. *Geophysical Research Letters*, 32(5), 2005. 13, 14

L.A. Rasmussen. Bed topography and mass-balance distribution of columbia glacier, alaska, u.s.a., determined from sequential aerial photography. *Journal of Glaciology*, 34(117):208–216, 1988. 9, 21

R. Retzlaff, N. Lord, and C R Bentley. Airborne-radar studies: Ice streams a, b and c, west antarctica. *Journal Of Glaciology*, 39(133):495–506, 1993. 28

K. Riahi, A. Grbler, and N. Nakicenovic. Scenarios of long-term socio-economic and environmental development under climate stabilization. *Technological Forecasting and Social Change*, 74(7):887–935, September 2007. 123

E. Rignot, I. Velicogna, M. R. van den Broeke, A. Monaghan, and J. Lenaerts. Acceleration of the contribution of the greenland and antarctic ice sheets to sea level rise. *Geophysical Research Letters*, 38(5):L05503, 2011. 1

G. Rotschky, P. Holmlund, E. Isaksson, R. Mulvaney, H. Oerter, M. Van Den Broeke, and J. Winther. A new surface accumulation map for western dronning maud land, antarctica, from interpolation of point measurements. *Journal of Glaciology*, 53(182):385–398, 2007. 48

A. Saintenoy, J.M. Friedt, F. Tolle, E. Bernard, D. Laffly, C. Marlin, and M. Griselin. Deriving ice thickness, glacier volume and bedrock morphology of austre lovénbreen (svalbard) using GPR. *Near Surface Geophysics*, 11, 2013. 5, 32, 44, 82

A. Shepherd and 46 others. A reconciled estimate of ice-sheet mass balance. *Science*, 338 (6111):1183–1189, 2012. 1, 9

S.J. Smith and T. M.L. Wigley. Multi-gas forcing stabilization with minicam. *The Energy Journal*, Multi-Greenhouse Gas Mitigation and Climate Policy(Special Issue 3):373–392, 2006. 123

A. Songtao, E. Wang, Z.and Dongchen, K. Holmn, Z. Tan, C. Zhou, and W. Sun. Topography, ice thickness and ice volume of pedersenbreen in svalbard, using gpr and gps. *In press.* 84

G. Stuart. Characterization of englacial channels by ground-penetrating radar: An example from austre brggerbreen, svalbard. *Journal of Geophysical Research*, 108(B11), 2003. 32

E. Vasilenko, A Glazovskiy, I Lavrentiev, YY Macheret, and FJ Navarro. Change of thickness and hydrothermal structure of fridtjovbreen from 1977 to 2005. *Mat. Glyatsiol. Issled. (Data Glaciol. Studies)[In Russian.]*, 101:157–1624, 2006. 4

D. Vuuren, M. Elzen, P.L. Lucas, B. Eickhout, B.J. Strengers, B. Ruijven, S. Wonink, and R. Houdt. Stabilizing greenhouse gas concentrations at low levels: an assessment of reduction strategies and costs. *Climatic Change*, 81(2):119–159, March 2007. 123

D.A. Wheeler. Using parabolas to describe the cross-sections of glaciated valleys. *Earth Surface Processes and Landforms*, 9(4):391394, 1984. 33

J. Woodward, T. Murray, R. A. Clark, and G. W. Stuart. Glacier surge mechanisms inferred from ground-penetrating radar: Kongsvegen, svalbard. *Journal of Glaciology*, 49(167): 473–480, December 2003. 32

T. Zwinger and J. C. Moore. Diagnostic and prognostic simulations with a full stokes model accounting for superimposed ice of midtre lovénbreen, svalbard. *The Cryosphere*, 3(2): 217–229, 2009. 86